MODELING OF BLOOD FLOW IN THE MICROCIRCULATION

by

Steven D. Tessendorf

B.S., Washington University, St. Louis, 1978

A MASTER'S THESIS

submitted in partial fulfillment of the
requirements for the degree

MASTER OF SCIENCE

Department of Chemical Engineering

KANSAS STATE UNIVERSITY
Manhattan, Kansas

1985

Approved by:

Walter P Walawender

Major Professor

TABLE OF CONTENTS

Chapter page

LIST OF FIGURES

Chapter II. LITERATURE REVIEW

Chapter III. A CAPSULE FLOW MODEL FOR BLOOD FLOW IN THE MICROCIRCULATION

Chapter IV. ANALOGY BETWEEN BLOOD FLOW IN SMALL VESSELS AND THE FLOW OF OIL AND WATER IN GLASS TUBES

Chapter V. CAPSULE VELOCITY AND GEOMETRIC FEATURES FOR OIL-WATER FLOW ANALOGS TO BLOOD FLOW

page

LIST OF TABLES

Chapter II. LITERATURE REVIEW

Chapter III. A CAPSULE FLOW MODEL FOR BLOOD FLOW IN THE MICROCIRCULATION

Chapter IV. ANALOGY BETWEEN BLOOD FLOW IN SMALL VESSELS AND THE FLOW OF OIL AND WATER IN GLASS TUBES

Chapter V. CAPSULE VELOCITY AND GEOMETRIC FEATURES FOR OIL-WATER FLOW ANALOGS TO BLOOD FLOW

ACKNOWLEDGEMENTS

The author wishes to express his appreciation to Dr. Walter P. Walawender, the major professor, for his guidance, discussion, and constructive assistance in the preparation of the text.

The author also wishes to thank the members of the supervisory committee, Dr. Erickson, Dr. Fan and Dr. Walawender for their suggestions and comments.

Special thanks are extended to the Department of Chemical Engineering for the opportunity it has provided to me at several points in my education.

This work was supported in part by a grant from the American Heart Association, Kansas Affiliate.

Chapter I

INTRODUCTION

Tbere have been many studies on blood flow in the arterioles, venules and capillaries of the microcirculation. The earliest attempts considered only tbe analysis of homogeneous non-Newtonian flow in large cylindrical vessels. Tbe arterioles and venules (20 - 400 microns in diameter) have been of interest since they are believed to be responsible in part for the local regulation of blood flow in vascular beds. The flow in the arterioles is affected by vessel geometry (taper), small vessel diameter (tbe Fahraeus effect), and the rheology of blood. For small vessels, blood is no longer a homogeneous fluid. The flow can be visualized as a core of whole blood surrounded by a plasma layer. The concept of concentric annular flow (CAF) has been investigated by Tbomas (1962), Cbarm et al. (1968), Gazley (1972), Ware et al. (1974), and Prasassarakich and Walawender (1980). The CAF model has accounted for the Fahraeus-Lindqvist effect and the influence of the non-Newtonian rheology of blood.

Microscopic observations of blood flow (in vivo) have been made by Bloch (1962). He observed the existence of a plasma layer at the vessel wall which often reacbed tbe center of the vessel. His work, and other studies by Krogh (1922), Jeffords and Knisely (1956), Palmer (1959), Monro (1963), Branemark (1968), and Barbee (1971), bave suggested tbat blood flow in microvessels can be described as a continuous phase of plasma witb the intermittent passage of bulk masses of red cells. This type of flow is similar to the flow of oil and

water in pipes observed by Charles et al. (1961). Prasassarakich (1979) ohserved the same type of flow patterns reported hy Charles in her work on oil and water flow in glass tubes witb diameters less than 1 cm. These two systems exhihited the feature that the in situ volume concentration was less than the input concentration. This apparent similarity to microcirculatory hlood flow stimulated the modeling of blood flow by an oil and water system in the research of Prasassarakich (1979).

Tbe CAF model is physically more realistic if it is adapted to the intermittent nature of hlood flow. The ohjective of the theoretical work in tbis tbesis was to develop a Capsule flow model that considers the intermittent nature of blood flow in tbe microvessels.

Tbe oil and water systems investigated exhihited capsule flow behavior at pseudoshear rates less than 10 sec^{-1}. The objective of the experimental work presented in this thesis was to study an oil-water flow analog that exhihited capsule flow. Comparisons of the oil-water flow analog to in vivo microvascular flow and in vitro blood flow data was also made.

Chapter 2 reviews various aspects of hemorheology. It first considers the properties of whole blood and its rheology. A review of the flow hehavior follows, including some of the works on blood flow in large and small diameter tuhes. For flow in large tubes where the flow is homogeneous, models are reviewed that describe the flow under Newtonian conditions. In small tubes where hlood flow is considered to be heterogeneous, concentric annular flow models that describe the pressure-flow behavior and predict the Fahraeus-Lindqvist effect are discussed. Next, the phenomena of capillary flow is considered. The proposed models have heen reviewed with special attention given to those works which consider pressure-flow comparisons, in-tube

hematocrit, and marginal layer thickness. Many of these works have also investigated cell velocity, mean velocity, and the velocity profiles in capillaries that are slightly greater in diameter tban the red cell or model red cells. Finally, a review of experimentally measured velocity profiles in vessels of arteriole and capillary size is presented.

Chapter 3 reviews the concentric annular flow (CAF) model as developed by Prasassarakicb (1979). Consideration is tben given to capsule flow in an attempt to develop a flow model that is physically more realistic. The model first considers flow with blood capsules that are cylindrical in shape with gaps of plasma in between. Its ability to describe the in vitro pressure-flow data of Barbee (1971) is not as good as tbat of tbe CAF model. A modification is tben considered in which the blood capsules are capped on each end by bemispheres. In tbis model a dimensionless pressure ratio ($\bar{R}$) is used to compare the capsule and CAF models. It depends explicitly on the ratio of the end cap radius to the capsule length. The value of the ratio of end cap radius to the capsule length is adjusted to force tbe value of $\bar{R}$ to lie between 0.95 and 1.00. Values of the ratio of tbe end cap radius to capsule lengtb from observation in the microcirculation compare favorably with the forcing.

In Chapter 4, a comparative analysis of the flow of oil and water mixtures in glass tubes with blood flow in microvessels is presented. Comparisons are made in terms of the wall shear stress-pseudoshear rate curves and their dependence on the input concentration. Two flow systems, System I (Reynolds numbers greater than 1) and System II (Reynolds numbers less than 1), have given capsule flow patterns similar to those observed for in vivo and in vitro blood. Tbe apparent viscosity of both oil-water systems decreased with increasing pseudoshear rate. This trend is analogous to the apparent viscosity

versus pseudoshear rate behavior of blood that has been observed by Merrill et al. (1963), Dintenfass (1963), Goldstone et al. (1970), Schmid-Schonbein et al. (1973), and Bate (1977). The data for both oil-water systems were correlated by the generalized friction factor correlation of Metzner and Reed (1955) and the nonlinear correlation, $D^m Tw = A\ U^s$, of Prasassarakich (1979).

Chapter 5 further examines the comparison between the flow of oil and water mixtures and blood flow in small tubes. Experimental measurements of oil capsule geometry and velocity are presented for the capsule flow of System II (Reynolds number less than 1). Capsule velocities, velocity profiles, and various geometric ratios for the oil-water system are compared with physiological observations. The comparisons show similar features for both systems.

Chapter 6 summarizes the major conclusions of this thesis and presents recommendations for future research.

Chapter II

LITERATURE REVIEW

2.1 INTRODUCTION

A knowledge of the microrheology of blood is essential for the physiologist to understand the functional behavior of normal and abnormal microcirculation. As early as the sixth century B.C. Alcmeon of Croton, the first Greek known to have practiced dissection, distinguished two types of blood vessels (phlebos) originating in the heart which were responsible for blood transport in the body (Sarton (1927), Sarton (1952), and Wiberg (1937)). For a long period of time, it was known that the motion of the blood occurred throughout the body but, the concept of a closed loop in the mammalian circulation was not established until the work of William Harvey (1578-1657). Harvey abandoned the old concept that blood passed through the wall between the left and right side of the heart (Noodergraaf, 1978). He was able to prove the existence of a closed system of conduits through which blood flowed without the aid of a microscope. It was not until 1661 that Marcello Malpighi discovered the invisible link between the arteries and veins, the microcirculation (arterioles, venules, and capillaries). This discovery led to the elucidation of the primary function of the blood, which is perfusion of the body tissues with nutrients, the elimination of wastes, and the distribution of thermal energy to the peripheral tissues.

Microrheology is the study of the heterogeneous nature of blood as it exists and functions in the microcirculation. The total resistance encountered

by the heart depends on the microrheology at the three levels of the microcirculation. The physiologist recognizes favorable and unfavorable flow conditions that enhance or inhibit the effectiveness of the heart in perfusing all of the body tissues.

A review of the hemorheology of the microcirculation is presented in this chapter. Initially, the properties of whole blood and its rheology are considered. Blood is a heterogeneous fluid that is composed of plasma and cells. The special properties of the red cell include its ability to transport oxygen and carbon dioxide and to deform isochorically (without change in total cell surface area or volume). The red cell is capable of forming rouleaux (chains of cells). The rouleaux form the three dimensional networks that give whole blood a yield stress and its non-Newtonian rheology. Several constitutive equations are reviewed including the widely used Casson equation.

A review of the flow behavior in the microcirculation is then presented. Three flow regimes, pseudohomogeneous, multi-cell heterogeneous, and single cell heterogeneous describe the basic flow patterns that have been observed in vivo and in vitro. The Fahraeus and Fahraeus-Lindqvist phenomena are discussed along with the major flow models which have been used to describe them. They include the Sigma, Radial Distribution, and Concentric Annular flow models.

The mathematical and physical modeling of capillary flow is reviewed next. Special attention has been given to those works that focus on the prediction of pressure-flow behavior, cell or model cell velocity, in situ hematocrit, and marginal layer thickness. A review of of the experimental techniques for the measurement of velocity profile for flow in arterioles and capillaries is presented. Finally, a review of some studies on the flow of oil and water in pipes and tubes is given. The studies indicate an analogy of the flow of oil and water to the flow of blood in the microcirculation.

2.2 BLOOD PROPERTIES AND RHEOLOGY

2.2.1 Blood Constituents

In man, blood is a heterogeneous fluid which is composed of two distinct phases. Blood is a suspenaion of approximately 45% (by volume) cellular elements in an aqueous solution of proteins and salts (plasma). The cellular elements include: the erythrocytes (red cells, D = 8 microns), leucocytes (white cells, D = 6-9 microns), and platelets (clotting cells, D = 2.5 microns). The respective functions of the cellular elements are oxygen and carbon dioxide transfer, control of infectious disease, and clotting of blood when injury occurs. In men the average red cell count is about 5.4 million cells per mm^3 while in women it is about 4.8 million cells per mm^3. The leucocytes are divided into two categories, granular and non-granular, and they normally exist at a number density of between 5 and 10 thousand cells per mm^3. They increase in number when the body is fighting disease. Platelets have a cell count of 250,000 to 500,000 per mm^3. Since they have a small diameter relative to the red cells they occupy only a small percentage of the total blood volume. The rheology of blood depends primarily on the red cells because they are the dominant cellular element.

The hematocrit (H) is defined as the percent of the total blood volume occupied by the cells. The normal human hematocrit of 45-50% represents a very close packing of the cells when no pathology exists. In polycythemia, where the number of erythrocytes is excessively high, hematocrits of 60-70% exist and the viscosity of blood may be affected significantly.

The blood plasma occupies the remaining 55% of the volume of whole blood. It is composed of water, proteins, carbohydrates, lipids, electrolytes, salts, hormones, antibodies and enzymes. Plasma is about 90% water by weight with the

remainder being plasma proteins (7%), inorganics (1%), and organics (1%). The plasma proteins are separable by ultracentrifugation and electrophoresis. The major proteins are listed along with some of their properties in Tahle 1. In flow, the eliptical proteins orient themselves so that the major axis is parallel to the flow. This hehavior prevents the leakage of proteins from the blood stream through large pores in the capillaries. Plasma is called blood serum when the fibrinogen is removed from clotted hlood. The serum contains cations (Na^{+1}, K^{+1}, Ca^{+2}, Mg^{+2}) and anions (Cl^{-1}, HCO_3^{-1}, PO_4^{-2}, SO_4^{-2}). The total milliequivalents per liter of the cations must equal the total milliequivalents per liter of the anions with a typical numerical value of 155.6.

In mammals the vascular network through which hlood flows is called the circulatory system. It is a closed loop system, as illustrated in Figure 1, which is divided into the left heart, systemic circulation, right heart, and pulmonary circulation. Blood is pumped by the left heart into the systemic circulation which includes all the organs and tissues. It is returned to the right heart which then pumps it to the pulmonary circulation for the exchange of blood gases in the lungs. In hoth of these suhsystema, hlood passes through a series of vessels which decrease in diameter with distance from the heart and then increase in diameter returning to the heart. Tahle 2 presents the size distribution of the hlood vessels in the mesenteric vasculature of the dog, based upon the work of Mall (1887). In man, blood pressure in the systemic arteries is maintained hy the left atrium of the heart at 80-120 mm Hg. For the pulmonary artery it is maintained at 10-20 mm Hg. These pressures are adequate to force the blood through the arterial network to the capillaries and then hack through the venous side for return to the left and right ventricles of the heart._

TABLE 1

Some properties of the major plasma proteins

Protein	Molecular Weight	Isoelectric Point (pI)	Dimension (Angstroms)
Fibrinogen	400,000	5.3	700 x 38
γ-globulin	156,000	6.3	235 x 44
β_1-globulin	1,300,000	5.4	185 x 185
β_2-globulin	150,000	6.3	-
α_1-globulin	200,000	5.2	300 x 50
Albumin	69,000	4.9	150 x 38

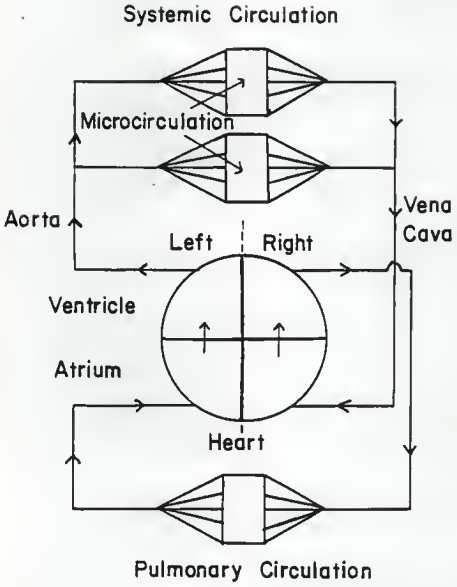

Figure 1: Schematic of the circulatory system

TABLE 2

Mesenteric vascular bed of the dog

Vessel Type	Diameter (mm)	Number	Length (cm)
Aorta	10	1	40
Large arteries	3	40	20
Main artery branches	1	600	10
Terminal branches	0.6	1,800	1
Arterioles	0.02	40,000,000	0.2
Capillaries	0.008	1,200,000,000	0.1
Venules	0.03	80,000,000	0.2
Terminal veins	1.5	1,800	1
Main venous branches	2.4	600	10
Large veins	6.0	40	20
Vena cava	12.5	1	40

2.2.2 The Red Blood Cell

A variety of in vivo studies have been conducted on the properties of the red blood cell with mammals other than humans and with non-mammals. Waugh and Evans (1976) made equilibrium and relaxation measurements on micropipet-aspirated cell membrane projections. They determined "shear" moduli and surface viscosity coefficients for the erythrocyte membranes from Congo eel (Amphiuma), frog, turkey, toadfisb, snake, turtle, iguana, opossum, tree shrew, and human red cells. The elastic shear moduli ranged from a low value of 0.0153 dynes/cm for tbe opossum to a high value of 0.240 dynes/cm for pond turtle. The surface viscosity varied from 0.00034 dyne-sec/cm in the opossum to 0.091 dyne-sec/cm in the frog. Chien et al. (1971) conducted a study on the comparative hemorheology of five mammalian (man, dog, elepbant, sheep and goat) and four non-mammalian (turkey, box turtle, frog and amphiuma) species. Relative viscosity increased with cell percentage in both Ringers solution and plasma for all species. With cell percentage constant, the relative viscosity decreased with increasing shear rate for all species. They also surveyed the differences of key hematological parameters including in vivo hematocrit, red cell dimensions, red cell surface area, and red cell volume. These parameters are summarized in Table 3.

In tbe microvasculature the red blood cell is responsible for delivering oxygen to and removing carbon dioxide from the capillary beds. Its unusual physical properties play an important role in determining the viscosity of blood and the flow behavior in the different flow regimes which are encountered in tbe microvasculature. Dintenfass (1967) has observed that the flow behavior of amphiuma blood is very similar to that of human blood even thougb the red cell size is much larger for ampbiuma blood (68 x 42 microns),

TABLE 3

Dimensions of erythrocytes and in vivo hematocrit (from Chien et al., 1971)

	H (%)	RBC Conc. (10^6/mm^3)	D x D x Thickness (microns x microns x microns)	Surface area (square microns)	Volume (cubic microns) Measured
Mammals					
Goat	28.9	16.1	3.0-4.5 x 1.6	42	18
Sheep	37.0	10.6	4.8 x 4.8 x 1.7	60	37
Dog	44.1	5.95	7.5 x 7.5 x 1.6	126	74
Man	44.0	4.99	8.4 x 8.4 x 1.6	152	90
Elephant	35.9	3.19	9.2 x 9.2 x 1.7	181	112
Non-mammals					
Turkey	36.8	2.72	13.9 x 8.0 x 2.5	249	136
Turtle	20.6	0.520	19.7 x 12.7 x 3.5	513	394
Frog	24.7	0.296	28.0 x 15.6 x 6.0	1102	823
Amphiuma	29.1	0.027	65.0 x 30.0 x 13.5	6605	10,800

than for the buman blood (8 X 2 microns). His observation illustrates the significance that the erytbrocyte flexibility and the large ratio of cell surface area to volume play in adapting to flow geometry.

Hartert (1975) has postulated tbat red blood cells are flexible because tbey are not completely filled with intracellular fluid. He has demonstrated this flexibility using a plastic bag partially filled witb water and sealed without air trapped in the bag. The human red cell in its rigid state is a biconcave disc as is illustrated in Figure 2. This particular shape allows an incomplete filling of tbe membrane shell and because of this the red cell may be deformed isochorically, tbat is, without a change in the total surface area or volume. A variety of parachute shapes are possible both in normal and pathological blood. These are illustrated in Figure 3. Each shape is determined by the aggregating capabilities of the cells and the shear rate in a given flow situation.

Schmid-Schonbein and Wells (1969) worked witb human red cells dispersed in Dextran solutions and found that the cells possessed the flow properties of fluid drops when viewed through their transparent cone and plate viscometer (rheoscope). They found identical results for three different anticoagulants Citrate-Phosphate-Dextrose (CPD), heparin, and ethylenediaminetetractetate (EDTA). In their work, sbear rates from 0.1 to 200 sec^{-1} in both a GDM viscometer and Wells-Brookfield microviscometer. Their observations have suggested tbat the erytbrocyte:

1. is a flexible shell.
2. is incompletely filled with an incompressible viscous fluid.
3. is bighly bendable.
4. has considerable extensional rigidity.

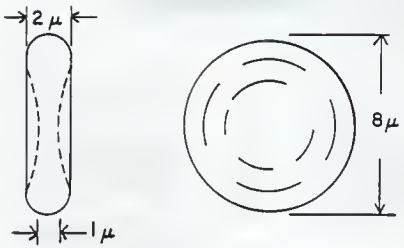

Figure 2: The human red cell (from Barbee, 1971).

Figure 3: Parachute shapes of erythrocytes (from Guest et al., 1971)

A) Characteristic Parachute-like shapes of normal erythrocytes traversing a capillary

B) Erythrocytes of patient with acquired hemolytic anemia as they appeared while traversing a capillary

5. can be deformed isochorically, that is, without a change in surface area or volume into a variety of shapes.

6. can be deformed into a prolate ellipsoid when suhjected to a uniform sbear field, and that tbis deformation is accompanied hy botb an orientation of the cell in tbe shear field and a rotstional motion of the cell membrane around its contents resemhling the rotation of the tread of a tank around its wheels.

An important consequence of the final ohservation is that it is possible for the transmission of external shear stresses across tbe memhrane to occur, resulting in inner circulation of the hemoglohin so that tbe erythrocyte participates in flow rather than just distorting it. For tbis reason the viscosity of the fluid inside the membrane affects the overall viscosity of the blood.

2.2.3 Factors Influencing the Rheology of Blood

In many species, hlood can exhibit a yield stress which influences the hlood viscosity in a given flow situation. This is due to the tendency of tbe red cells to form rouleaux (chains of erythrocytes) in the presence of fihrinogen and other serum proteins.

Merrill (1963) et al., sbowed that buman blood viscosity at pseudoshear rates (U) less than 10 sec^{-1} is reduced by the in vitro removal of fihrinogen from the blood. Ehrly and Lange (1971) demonstrated a clear reduction in human blood and plasma viscosity and erythrocyte aggregation after the addition of Streptokinase to human blood in vitro. Ehrly (1973) used Arwin, a fihrinogen-lowering anticoagulant, in vivo with twelve humans experiencing peripheral arterial arteriosclerosis and was ahle to lower the hlood viscosity relative to that of water from 4.74 to 4.41 and the plasma viscosity relative to water from 1.68 to 1.57 within 24 hours after starting treatment. Using microscopic examination, he found no aggregation in any of the twelve patients

that previously exhibited rouleaux formation. Ehrly's work indicated that a reduction in fibrinogen reduced the viscosity of human blood through both aggregation and plasma viscosity reduction.

In human blood, anticoagulated with EDTA, CPD, or ACD (acid-citrate-dextrose), Goldstone et al. (1970) agreed that aggregation and disaggregation of red blood cells was a critical variable in the rheology of blood in both physiologic and pathologic conditions. They used a direct visualizing viscometer (modified Wells-Brookfield viscometer with transparent cone and plate) to analyze the formation, dispersion, and flow behavior of red cell aggregates under well defined flow conditions. Pathologic aggregates differed from normal aggregates in that they were considerably more resistant to shear and settled more rapidly. Red cells from ill patients also formed aggregates in serum indicating that serum proteins as well as fibrinogen were involved in aggregate formation.

Goldstone et al. (1970) described their observations of rouleaux and their behavior over a range of shear rates from 2.3 to 46 sec^{-1}. For steady shear rates less than 46 sec^{-1}, aggregates were composed of rouleaux which aligned themselves so that secondary three dimensional structures were maintained. As long as steady shear was maintained an equilibrium condition existed in which the aggregates remained constant in size and the secondary structures remained essentially undisturbed. Large three dimensional structures composed of many interconnected rouleaux moved as units and remained undeformed despite shearing stresses of up to 3 dynes/cm^2 for a shear rate of 46 sec^{-1}. At times small rouleaux (from two to five cells) were separated from the edges of one three dimensional structure and subsequently incorporated into another three dimensional structure.

In the higher shear rate range of 230-460 sec^{-1}, three dimensional structures were broken apart, forming independent rouleaux. They observed that short chain rouleaux (4 to 10 cells) were quite resistant to shear under both normal and pathologic conditions. Their work supported Merrill's (1969) hypothesis that Casson behavior is a consequence of reversible red cell aggregation. Based on the observations of the structure of blood in flow, models have been developed to describe the rheology of blood. These models will be briefly reviewed in the next section.

2.2.4 Constitutive Equations

Scott Blair (1959) first applied the Casson equation to the rheology of blood. The Casson (1958) model was initially developed to describe the flow behavior of printing inks and lithographic varnishes. The model postulated a linear relationship between the square root of the shear rate and the square root of the shear stress. It is the most popular equation to describe the rheology of blood under non-Newtonian conditions. It predicts Newtonian behavior at shear rates greater than 200 sec^{-1}. The actual transition point depends on the type of blood, suspending fluid, and anticoagulant as shown in Table 4. In mathematical notation the constitutive relation is:

$$Tw^{1/2} = Ty^{1/2} + S\dot{\gamma}^{1/2} \qquad (1)$$

where

Ty = yield stress

S = Casson viscosity

The shear stress - shear rate behavior of blood can be described by the Casson equation over a wide range of hematocrit and shear rates from 1 to 100,000 sec^{-1} (Charm and Kurland (1962),(1965)) and 0.1 to 20 sec^{-1} (Merrill et al. (1965), Cokelet et al. (1963)).

TABLE 4

Non-Newtonian behavior of blood

Investigator	Instrument	Mammal	Suspending Fluid	Anti-coagulant	Rate of shear above which non-Newtonian behavior disappears (sec^{-1})
Brundage (1934)	Rotating-cylinder	Cat Rabbit	Plasma	Oxalate	50
Muller (1948)	Capillary-tube	Bovine	Serum	---	300*
Kumin (1949)	Capillary-tube	Bovine	Serum	---	300*
Coulter and Pappinbeimer (1949)	Capillary-tube	Bovine			250*
Bayliss (1960)	Capillary-tube	Dog	Serum	---	450*
Cerny (1963)	Capillary-tube	Dog	Plasma	Heparin	300-400*
Cokelet et al. (1963)	Rotating-cylinder	Human	Plasma	Citrate	50
Merrill and Wells (1965)	Cone-and-plate	Human	Plasma	None	100
Brooks et al.(1970)	Rotating-cylinder	Human	Plasma	ACD	100
Goldstone et al.(1970)	Couette	Human	Plasma	EDTA,CPD,ACD	50

* At the tube wall

Walawender et al. (1975a) proposed an approximate Casson model for tube flow of blood based on order of magnitude considerations. Their model is given below:

$$Tw^{1/2} = \frac{8}{7} Ty^{1/2} + 2\sqrt{2}\, S\, U^{1/2} \qquad (2)$$

where

$$Tw = \text{wall shear stress} = \frac{R\Delta P}{2L}$$

$$U = \text{pseudoshear rate} = \frac{Q}{2\pi R^3}$$

Their equation was found to be in good agreement with experimental data from a coiled capillary viscometer using heparinized bovine blood and silica gel suspensions as test fluids.

Other researchers (e.g. Charm and Kurland (1962) and Hershey (1966)) have suggested the power law model to characterize blood rheology:

$$T = b\, \dot{\gamma}^{a} \qquad (3)$$

where a and b are constant. Charm and Kurland (1962) presented data indicating that the shear stress-shear rate behavior of canine blood in a cone and plate viscometer can be described by the power law model with the exponent (a) in the range of 0.76-0.84. However, power law behavior is only applicable for a limited range of shear rate.

The above constitutive equations adequately describe the flow of blood under pseudohomogeneous flow conditions. Pseudohomogeneous flow exists in blood when either the ratio of vessel to red cell diameter or the shear rate is large. Not all flow situations can be described by pseudohomogeneous flow models; consequently it is necessary to consider other flow regimes.

2.3 FLOW BEHAVIOR

2.3.1 Flow Regimes

In the microvasculature, blood flow may be classified into three types according to the ratio of vessel diameter to erythrocyte diameter. These types are; pseudohomogeneous, multi-cell heterogeneous, and single cell heterogeneous. They are illustrated in Figure 4.

2.3.1.1 Pseudohomogenous Flow

When the ratio of the vessel diameter to the red cell diameter is greater than 50, the rouleaux yield to the existing shear stresses. Under this condition, blood can be treated as a homogeneous fluid for fluid mechanical purposes. For pseudohomogeneous flow the rheology may be either Newtonian or non-Newtonian. For shear rates greater than 200 sec^{-1}, non-Newtonian behavior may be neglected and the dependence of blood viscosity (μb) on hematocrit (H) is of the form

$$\mu b = \frac{\mu p}{(1 - KH)} \qquad (4)$$

where

μp = plasma viscosity

K = constant

The constant K varies between 1.5 and 2.5, depending upon the size, shape and flexibility of the erythrocytes (e.g. human, dog, bovine, or rat), the suspending fluid (plasma, serum or A.C.D.) and anticoagulant (citrate, heparin, EDTA or arwin). For shear rates less than 200 sec^{-1} the behavior of blood is non-Newtonian and is best described by the Casson model.

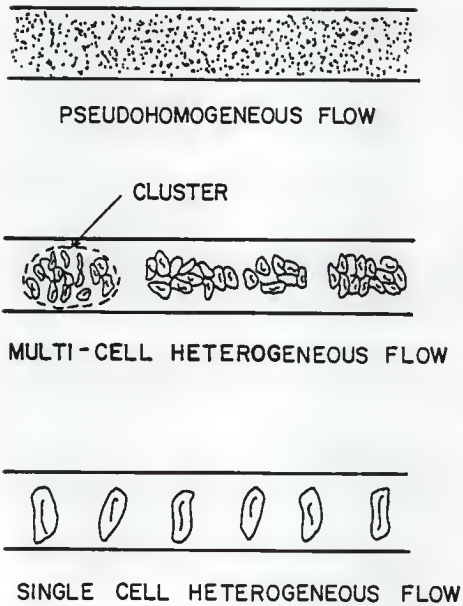

Figure 4: Flow regimes of blood.

2.3.1.2 Multi-cell Heterogeneous Flow

When the vessel to red cell diameter ratio is in tbe range of 4-50, blood flow is beterogeneous. It flows as clusters of red cells and entrapped plasma surrounded by an annulus of plasma witb plasma filling the gaps between tbe clusters. This type of flow has been observed by various researchers (e.g. Krogb (1922), Jeffords and Knisely (1956), Palmer (1959), Bloch (1962), Monro (1963), Branemark (1968), and Barbee (1971)). If shear rates are high enougb, tbe plasma gaps can disappear and tbe flow can be described as a continuous core of cells surrounded by an annulus of plasma. Tbis type of flow is called concentric annular flow (CAF). Prasassarakich and Walawender (1980) have been able to quantitatively model the in vitro data of Barbee and Cokelet using a CAF model.

When sbear rates are less 1 sec^{-1} or tbe tube diameter to cell diameter ratio approaches 4, gaps are present between tbe cell clusters and the concentric annular flow model does not completely characterize the flow. In this situation, prediction of pressure drop for a given feed hematocrit and flow rate is possible but tbe predicted in-tube bematocrit (the bematocrit obtained by suddenly stopping flow and then measuring tbe cell fraction of the fluid in the vessel) only qualitatively approximates tbe observed in-tube hematocrit. Tbe error in tbe predicted hematocrit increases as the tube diameter decreases.

2.3.1.3 Single Cell Heterogeneous Flow

When tbe ratio of tbe vessel to cell diameter is in the range of 1-4, tbe cells pass tbrough tbe vessels individually. In this regime, individual red blood cells can exhibit different types of flow behavior.

1. They may travel edgewise, thus reducing their cross-sectional area relative to the flow stream, and occasionally tumhle end over end.

2. They may hegin to deform and assume the shape of prolate ellipsoids (normally they are hiconcave disks) with their long axes parallel to the direction of flow.

3. The red cell memhrane may hegin to "track" around the memhrane resemhling the rotation of the tread on a tank.

When the ratio of vessel to red cell is approximately unity, cells generally travel through the vessels in single file and occupy the entire cross-section of the vessel. Each cell may be deformed extensively and is separated from its leading and trailing partners by gaps of plasma. The actual shape of the deformed cells depends on the rate of shear and the vessel diameter. In this type of flow, nutrients and waste products are effectively exchanged hetween the hlood and local body tissue.

2.3.2 The Plasma Layer

Sufficient evidence has heen provided hy various researchers confirming the existence of a plasma layer in the microcirculation. In 1835 Poiseuille (Charm and Kurland (1974)) ohserved a marginal layer of plasma in the flow of blood through capillaries. He noted that the peripheral cell free zone increased in thickness as the flow rate increased. Bloch (1962) observed in vivo that the magnitude of the peripheral plasma layer varied with the diameter of the vessel and the linear flow velocity. Photographing at 16-24 frames per second, he ohtained measurements of the thickness of the marginal plasma layer in the frog mesentery and calculated δ/D for three capillary sizes. He found that the plasma layer thickness (δ) extended in an irregular manner toward the center of the vessel and, at times, ohserved cell free spaces between the slugs of cells passing through the vessels.

Monro (1963), in repeated observations of the microvessels in the rabbit ear chamber, observed axial streaming (plasma layer) and plasmatic gaps between groups of cells. The plasmatic gaps increased in length as the flow stream divided into smaller branches. This was attributed to the effects of plasma skimming (the preferential flow of plasma to branching vessels from the cell free marginal layer that exists at the wall of the vessel). An interesting characteristic regarding rabbit erythrocytes is that they do not form rouleaux as do those of other mammals.

Bugliarello and Hayden (1963) conducted an in vitro study to measure velocity profiles using acid-citrate-dextrose (ACD) treated human blood in tubes between 40 and 84 microns in diameter. Shear rates ranged between 12.8 and 64 sec^{-1}. They observed a peripheral plasma layer and concluded that the hematocrit influenced the peripheral layer thickness and that relatively large velocity changes did not affect the thickness. As Bloch observed in vivo, they observed in vitro a fluctuating plasma layer which sometimes extended to the center of the tube. Even though their shear stresses were low (between 0.2 and 5 dynes/cm^2), they did not report the existence of rouleaux for their flow system as Goldstone et al. (1970) observed using the rheoscope. Bugliarello and Hayden stated that the basic flow behavior was not altered by the ACD anticoagulant, but that they did not systematically study the effects of addition of the anticoagulant or the removal of fibrinogen.

Barbee and Cokelet (1971) noted the existence of a peripheral plasma layer in tubes as small as 29 microns and observed that the peripheral layer sometimes extended to the center of the tube for periods of time sufficient in length to conclude that a capsule flow phenomena existed.

Schmid-Schonbein and Zweifach (1975) in their study of in vivo erythrocyte velocity profiles for arterioles and venules in the rabbit found a peripheral plasma layer and observed that the width did not appear to be related to the flow rate. They also concluded that the peripheral plasma layer thickness was influenced by the hematocrit.

As indicated by the above discussion, researchers that have observed the peripheral plasma layer, have also found that it can extend to the center of the vessel.

2.3.3 The Fahraeus and Fahraeus-Lindqvist Effects

The phenomena of the reduction of in tube hematocrit as tube diameter decreases for the flow of blood in small tubes is referred to as the Fahraeus (1929) effect. The simultaneous reduction of apparent viscosity with decreasing tube diameter is termed the Fahraeus-Lindqvist (1931) effect. In tubes less than 400 microns in diameter the pressure drop that is required to produce a given flow rate for blood is considerably less than that calculated for Newtonian flow. Modeling of both of these phenomena have been the goals of several researchers.

Charm et al. (1968), Lih (1969), and Baker (1972) have attempted to explain these effects by assuming models with radial cellular concentration profiles. As mentioned previously, substantial evidence exists to suggest that a peripheral plasma layer surrounds a core of fluid which contains the erythrocytes. The Concentric Annular flow (CAF) model acknowledges the plasma layer and variations of the model have been applied by Thomas (1962), Charm et al. (1968), Gazley (1972), Ware et al. (1974), and Prasassarakich and Walawender (1980).

2.3.3.1 The Sigma Model

Dix and Scott-Blair (1940) proposed the sigma model and found that it quantitatively explained the Fahraeus-Lindqvist effect in the flow of clay suspensions. This model assumed a finite numher of concentric, homogeneous, laminae of equal thickness making it different from the Hagen-Poiseuille model which assumes an infinite numher of laminae. The sigma model effectively described the experimental data of Haynes and Burton (1959) and Kumin's (1949) ox hlood data. Figure 5 presents a schematic representation of the concept of the sigma model.

2.3.3.2 The Radial Distribution Model

Several researchers have assumed the cell concentration profile to he non-uniform as a function of tuhe radius. Charm et al. (1968), Lih (1969), and Baker (1972) have developed models for the radial cell distribution with a maximum concentration at the center and a finite concentration at the wall. Charm et al. (1968) considered a model of hlood flow with a linear decrease in cell concentration from the center to the tuhe wall. They found that their radial distrihution model could he approximated hy a model with a plasma layer surrounding a core of whole hlood. Lih (1969) and Baker (1972) used power functions to describe the concentration profile. They ohtained pressure flow relationships, velocity profiles, and tuhe hematocrits from their models. Baker also made experimental ohservations of the velocity profile, tuhe hematocrit, and shear rate. From these ohservations it has heen determined that a model with a constant hematocrit across the core with an immediate drop of hematocrit near the wall hest describes the experimental data.

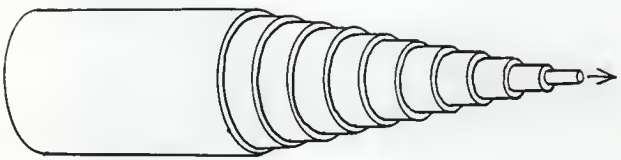

Figure 5: The Sigma flow model

2.3.3.3 The Concentric Annular Flow Model

Thomas (1962) developed a two phase flow model with a Newtonian core of uniform hematocrit surrounded hy a Newtonian plasma layer. Using the pressure-flow data of Kumin's ox hlood experiments (1949) he calculated the plasma layer thickness and predicted the tuhe (volume average) hematocrit from the model. Kumin's data did not contain measurements of the tuhe hematocrit for comparison. Thomas indicated that the thickness of the plasma layer was hetween 1.5 and 5.0 microns, increasing with increasing wall shear stress and decreasing tuhe diameter.

Charm et al. (1968) assumed a linear decrease in hematocrit from the center to the tuhe wall in their model. They found that the flow could he approximated without significant error hy a model with a cell free Newtonian plasma layer at the wall and a core of whole hlood exhihiting Casson fluid hehavior. They derived a pressure-flow relation containing the plasma layer thickness (δ) as a parameter. This parameter was then adjusted to match the model predictions with their experimental data. The calculated plasma layer thickness ranged from 1-10 microns and depended on the wall shear stress, tuhe diameter, and feed hematocrit.

Ware et al. (1974) used the data of Charm et al. (1968) to develop an expression for the plasma layer thickness as a function of Reynold's numher, Bingham numher, and feed hematocrit. They calculated velocity profiles from their model and found that they agreed with the in vitro experimental data of Bugliarello and Sevilla (1970). They were ahle to show that the two layer model could qualitatively predict the Fahraeus-Lindqvist effect and the shear thinning hehavior of hlood.

Barbee and Cokelet (1971) conducted blood flow experiments in small glass tuhes. They collected hlood from healthy human donors and anticoagulated the samples with an ACD solution using routine blood hank procedures. They recorded pressure drop-flow rate data at constant feed reservoir hematocrits ranging from 15.1% to 55.9% for a number of different tuhe diameters ranging from 29 to 811 microns. They developed an empirical model to relate the wall shear stress to the pseudoshear rate. Their model is given below:

$$Tw = 8\ \mu p\ U\ \exp\left(\frac{4.2\ Ht}{U^{c}}\right) \qquad (5)$$

where Ht = measured tube hematocrit

c = an adjustable constant that changes with shear rate and is a function of hematocrit

Gazley (1972) proposed a two phase model with a uniform hematocrit equal to the feed hematocrit. He calculated the marginal layer thickness associated with Barbee´s (1971) in vitro experimental data for human blood. Barbee´s data included the variation of both feed hematocrit and tube diameter. The marginal layer thickness was calculated to be 4.45 microns and found to be independent of shear stress, tuhe diameter, and feed hematocrit.

Gupta and Seshadri (1977) conducted in vitro studies for human red blood cells in vessels ranging from 86 to 444 microns in diameter. They measured flow rates, pressure drops, feed reservoir hematocrits, and cup-mixing and tuhe hematocrits. They studied plasma, whole blood, and red cells suspended in saline and were ahle to confirm and quantify the Fahraeus-Lindqvist and Fahraeus effects. They also determined the marginal layer thickness and velocity profiles. They found that the marginal layer thickness increased with decreasing tuhe diameter at a given hematocrit and decreased with increasing hematocrit at a given tuhe diameter.

Gaehtgens et al. (1978) conducted in vitro studies with glass capillaries (15-95 micron I.D.) which verified the Fahraeus effect and also quantified cell screening as a function of reduced flow rate and suspension medium (Ringers solution versus Ringers solution with high molecular weight dextran). They found that cell screening increased with decreasing flow rate and the addition of dextran.

Prasassarakich (1979) developed a CAF model using a marginal plasma layer having a Newtonian fluid behavior and a core of uniform hematocrit having Casson fluid behavior. She used a constant marginal plasma layer of 1.2 microns based on estimations from the work of Thomas (1962) and Ponder (1948). Figure 6 schematically illustrates the concept of the CAF model of Prasassarakich (1979). Newtonian behavior was assumed for the plasma layer and Casson behavior was assumed for the core. The plug flow region of the core was neglected.

The following relationship between the wall shear stress and pseudoshear rate was developed.

$$Tw = \frac{\frac{188}{147} Ty \frac{R}{Ro} + \frac{32}{7}\sqrt{2Ty\, S\, U\left[\frac{R}{Ro}\right]^5}\sqrt{1+E} + 8S\, U\left[\frac{R}{Ro}\right]^4 (1+E)}{(1+E)^2} \qquad (6)$$

where

$$E = \frac{S^2}{\mu p}\left(\left[\frac{R}{Ro}\right]^4 - 1\right)$$

For equation (6) to he applicahle, it is required that Tw he greater than 20 times Ty and that U he greater than 3 sec^{-1}. Equation (6) hecomes approximately equal to the Casson equation (equation 2) presented hy Walawender et al. (1975) in the limit of Ro-->R and E—>0.

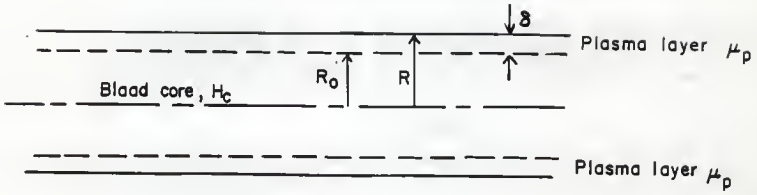

Figure 6: The Concentric Annular flow model (CAF) (from Prasassarakich, 1979)

The model developed by Prasassarakich may be used when the peripheral plasma layer viscosity and thickness are specified. A mass balance on the red cells in the core and the Casson parameter correlations of Ware et al. (1974) are used in a trial and error procedure to determine the Casson parameters (Ty and S) for a given feed hematocrit. These parameters are then used in equation (6) to predict the dependence of the wall shear stress on the pseudoshear rate. Predictions of the wall shear stress - pseudoshear rate data of Barbee by the CAF model are shown in Figure 7 for a 29 micron tube and in Figure 8 for a 99 micron tube. Inspection of the curves for the two tube diameters but similar hematocrits show that as the tube diameter decreases, the wall shear stress decreases for a given pseudoshear rate. This is the Fahraeus-Lindqvist effect.

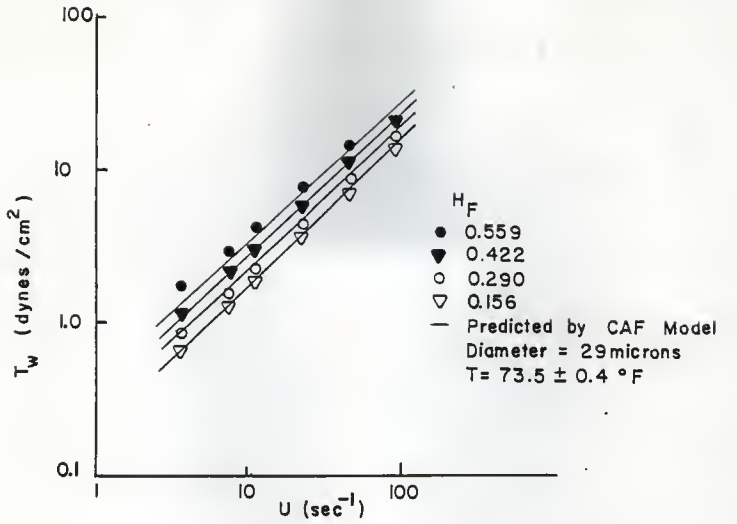

Figure 7: Comparison of Barbee's data with predicted behavior by CAF (from Prasassarakich, 1979)

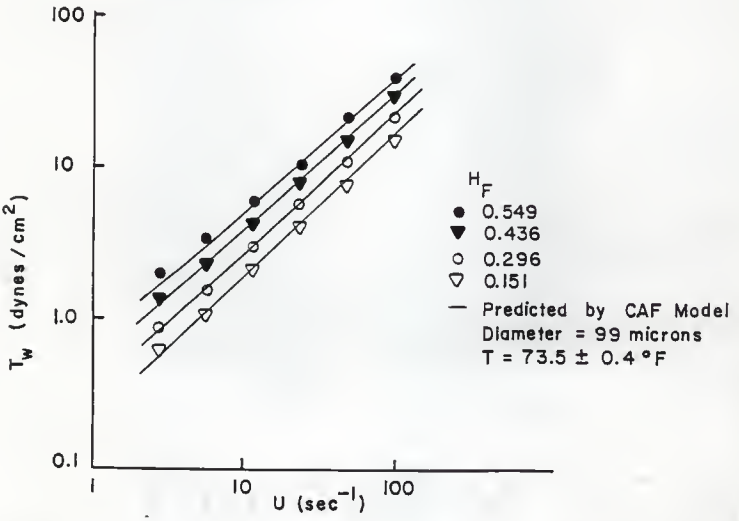

Figure 8: Comparison of Barbee's data with predicted behavior by CAF (from Prasassarakich, 1979)

2.3.4 Inversion of the Fahraeus and Fahraeus-Lindqvist Effects

When the diameter of the vessel approaches that of an individual erythrocyte an inversion of both the Fahraeus (e.g. Cokelet (1976), Alhrecht (1979), Gaehtgens (1980), and Oda et al. (1983)) and Fahraeus-Lindqvist (e.g. Dintenfass (1967), Lingard (1977), and Gaehtgens (1980)) effects occur and both tuhe relative hematocrit and apparent viscosity at a given shear rate hegin to incresse as the vessel diameter approaches the red cell diameter. The incresse in apparent viscosity occurs at a critical diameter of 5-7 microns for normal human blood. The critical radius at which the inversion phenomena takes place is not unique for a given species. It depends on hematocrit, temperature, pH, and internal viscosity of the red cells. In the presence of platelet aggregates, neither blood pH nor the hemstocrit are important and the size of the platelet aggregates hecome the dominate factor. This is due to the high internal viscosity of the platelet aggregates. When plstelet aggregates are not a factor, the critical radius of the inversion phenomena is only slightly affected by the hematocrit. However, it is significantly affected hy the pH because of its influence on the flexibility of the erythrocyte membrane. In human hlood the critical radius is as low as 2 microns (pH = 7.35) while in low pH blood (pH = 6.0) it can be as high as 50 microns (Dintenfass, 1976).

2.4 THE CAPILLARY FLOW REGION

The single cell flow regime consists of several flow types depending on spacing of red hlood cells, flow rate, and ratio of cell to vessel diameter. The cells may pass through the capillaries in axial train fashion if the spacing is small. At low shear rstes no deformation of the erthrocytes occurs and the cells flow in their rigid hiconcave discoid form as shown in Figure 2.

At higher shear rates the red cells begin to deform into their parachute shaped forms (Figure 3) while still maintaining close spacing.

Single cell holus flow occurs when the hematocrit decreases and the spacing between cells increases. In this situation, the deformation of the cell and the velocity profile that develops in the holus depends on the shear rate. Both the axial train and single cell holus flow patterns occur when the vessel diameter is just slightly greater than the cell diameter.

If the vessel diameter is less than the cell diameter the red cells are limited to passage in a single file fashion. Here the erythrocytes must deform extensively as has been observed by Hochmuth et al. (1970).

2.5 TWO PHASE MODELING IN THE CAPILLARIES

The first attempt to model the flow of blood in capillaries resulted in the well known Poiseuille equation. It is valid for incompressible Newtonian fluids in laminar flow. In 1668 Leeunhoek (Skalak and Chien, 1981), first reported the single file flow of red blood cells in capillaries. He distinguished individual cells separated by regions of clear plasma and remarked on the elongation of the cells as they passed through the narrowest capillaries in the tail of a live tadpole.

The quantitative description of the pressure drop and flow behavior of blood flow in the capillaries lagged behind observations until very recently. In the interim, the anatomy of various capillary beds and the laws of transport across capillary walls were extensively developed. August Krogh (1922) summarized the early knowledge of the anatomy and physiology of the capillaries. He noted that

1. Capillary diameters usually appeared fixed but variations in flow velocity could often be distinguished.

2. Plasma skimming was responsible for the effect of reduction in hematocrit in certain capillaries due to the sweeping of cells past their entrances.

3. Red blood cells were very deformable.

4. In the smallest capillaries the red blood cells were narrowed in width and increased in length.

Prothero and Burton (1961) conducted a theoretical and experimental study on the nature of cell motion in capillaries by examining the flow of air bubbles in short columns of liquid. The bolus flow pattern observed in the capillaries was the subject of their experiments. They noted that the plasma that filled the gaps betweeen individual red cells did not move in simple laminar flow, but exhibited an eddy motion which circulated the plasma between the cells. They developed a model for bolus flow and used it to estimate the flow rate of blood in capillaries and to estimate transport coefficients in holus flow.

Whitmore (1967) developed an axial train model for single cell flow in vessels with diameters slightly larger than the red blood cell. His analysis assumed an axial train containing red cells and the suspending fluid, surrounded by an annulus of the suspending fluid. The train of cells and suspending fluid traveled as a single cylindrical unit with an infinite viscosity. His analysis did not consider secondary, or holus flow, in the region between the cells. His model predicted that the axial train moved at a constant velocity, V, given by

$$V = \frac{2Vm}{(1 + X)} \tag{7}$$

where

Vm = the mean velocity of the suspension as a whole

X = the ratio of the diameter of the axial train to the tube diameter

The axial train model also yielded a simple predictive equation for the core hematocrit, with constants as functions of shear rate.

Sutera and Hochmuth (1968) conducted large scale modeling studies on blood flow in capillaries using a 1 cm glass tube and large, rigid, neutrally buoyant discoids. Four shapes, approximating different possible red cell deformations were used. Pressure drop measurements revealed that the size (diameter and thickness), spacing, and orientation were the principal factors that determined the additional pressure drop (in excess of the Poiseuille flow) associated with the cells. For discoids normal to the flow, the additional pressure drop was sensitive to the diameter of the discoids. They compared their experimental pressure drops with the in vivo data of Landis for capillary blood flow in humans (1930) and frogs (1926). Their comparisons, based on geometric scaling, showed good agreement between the model predictions and the in vivo observations.

Barnard et al. (1968) formulated a mathematical model for a single flexible solid object suspended in a fluid flowing in a conduit. Their work was based on the Navier Stokes and continuity equations for the fluid and a force balance on the cell. They solved their nonlinear boundary value problem by numerical methods for velocities similar to those of physiological interest (1 mm/sec). Their analysis predicted parachute shape cells whose sides did not touch the capillary wall. The predictions were in agreement with the in vivo observations of Bloch (1962), Branemark and Lindstrom (1963), and Guest et al. (1963). Their analysis tended to discredit the general approach of the holus flow model which assumed no plasma layer. When the cell diameter equaled the capillary diameter the ratio of the cell velocity to the mean plasma velocity was found to be 1.67.

Lew and Fung (1969) used the Navier-Stokes and continuity equations as the basis for a theoretical analysis of bolus flow. They developed velocity and pressure profiles for the plasma between two cells moving slowly through a capillary. In their model, the red cells were approximated by cylindrical pill boxes whose radii were the same as the vessel. They found that for small spacing, the plasma in the bolus was unable to develop the Poiseuille velocity profile. When the ratio of the bolus length to vessel diameter approached unity, a parabolic velocity profile developed midway between the cells.

Lee and Fung (1969) also conducted modeling experiments using flexible thin-walled rubber model cells filled with liquid (geometrically similar to human red cells). Reynolds numbers ranged from 0.0004 to 0.04. They found that the cells deformed extensively when the cell to tube diameter ratio (Dc/Dt) was greater than 0.98. For larger model cells (Dc/Dt greater than 1.36), indentations of the trailing edges of the cells occurred at higher velocities. The model cells resembled the deformed red blood cells observed in vivo by Palmer (1959), Bloch (1962), Branemark and Johnson (1963), Branemark and Lindstrom (1963), and Guest et al. (1963). They related the model cell velocity, Vc, to the mean flow velocity, Vm, by

$$Vc = k(Vm - \alpha) \tag{8}$$

where

k = slope of the regression line derived from their data

α = intercept of the Vm axis

The value of k varied from 1.00 (Dc/Dt = 1.69) to 1.26 (Dc/Dt = 0.98) and alpha varied from 0 to .015 cm/sec. They computed the pressure drop for capillary blood flow in vivo from the model data. Their results compared favorably with the in vivo measurements of Zweifach and Intaglietta (1968) for the mesentary of the rabbit.

Hochmuth et al. (1970) used high speed photography in their in vitro studies of human red cells passing through capillaries ranging in diameter from 4.5 to 10.7 microns. They observed that the red cells tended to move in an edge-on orientation with the cell shape becoming more axisymmetric at high velocities. They also observed that the apparent thickness of the peripheral plasma layer increased with increasing velocity in the range of 0-1 mm/sec and that it remained essentially constant for velocities greater than 1 mm/sec. They plotted the red cell length (in the tube) versus the red cell velocity with capillary diameter as a parameter. The cell lengths did not depend strongly on cell velocity but, they did depend on capillary diameter. Average values for the cell lengths ranged from 8.5-9.0 microns for the 4.5 micron capillary to 6.5 microns for capillaries with diameters greater than 7.6 microns.

Sutera et al. (1970) studied capillary flow with large-scale deformable model cells having undeformed Dc/Dt ratios of 1.0, 1.3, and 2.0 in a 1.974 cm diameter glass tube. They observed the cell orientation and stability, cell velocity, and pressure drop. They conducted dimensionless analyses which revealed that

$$\frac{Vc}{Vm} = f1\left(\frac{\mu f\, Vm}{Dt\, Ec}, \frac{Dc}{Dt}, \frac{tc}{Dc}\right) \tag{9}$$

and

$$\frac{\Delta Pc}{\mu f\,[Vm/Dt]} = f2\left(\frac{\mu f\, Vm}{Dt\, Ec}, \frac{Dc}{Dt}, \frac{tc}{Dc}\right) \tag{10}$$

wbere

ΔPc = the additional pressure drop due to a single cell

Ec = the elastic constant of tbe cell membrane

Dc = the diameter of the undeformed cell

Dt = the internal diameter of the tube

tc = the thickness of the cell membrane

μf = the viscosity of the suspending fluid

They plotted these dimensionless variables using tbeir model cell data and the model cell data of Lee and Fung (1969). Tbey found similar trends for hoth dimensionless velocity and dimensionless additional pressure drop versus dimensionless diameter. However, tbe dimensionless additional pressure drop curves were lower for their data than for Lee and Fung's data because their model cells bad thinner membranes.

Skalak et al. (1972) analyzed the flow of rouleaux (with chain lengths of 1, 3, and 5 cells) in tubes witb tbe ratio of cell to tube diameter ranging from 0.6 to 1.0. They considered non-deforming, red cell shaped particles suspended in a Newtonian fluid. Tbe cells were assumed to he axisymmetricaly located in a circular tube and to he spaced evenly along tbe axis. Their solutions were obtained with a finite element method based upon a variational theorem for slow viscous flow (Stokes flow). Tbe major effect of increasing rouleaux length was to slightly decrease the apparent viscosity. Tbe most important parameter in determining tbe apparent viscosity was found to he the red cell to capillary diameter ratio.

Lingard (1974) used human erythrocytes suspended in bovine serum albumin for flow experiments in nucleopore filters (pore sizes of 4.9 and 6.9 microns).

Figure 9 illustrates the similarity of the 4.9 and 6.9 micron pore relative resistance. The relative apparent viscosity was constant up to a velocity of 0.25 mm/sec, beyond which lubrication forces produced deformation and reduced resistances with increasing cell velocity. They calculated an effective fluid film thickness (h) for their data (Reynolds numbers between 0.0001 and 0.001) and found it to he 2-4% of the capillary radius and to increase with cell velocity. The increase in film thickness with cell velocity implied a difference between red cell (Vc) and mean (Vm) fluid velocities in a pore. They derived an equation for the effective plasma film thickness based on the drag per unit area on a red cell of cylindrical shape of length (Lc) moving in a pore under the total measured pressure drop across the pore (ΔPt) as

$$2R\,h - 3h^2 = \frac{4\,\mu p\,Vm}{(\Delta Pc/Lc)} \qquad (11)$$

where

$$\Delta Pc = \frac{\Delta Pt - (1 - C)\Delta Ppl}{Nc} \qquad (12)$$

and

R = the radius of the pore

Vm = the mean velocity in the pore

μp = the viscosity of the plasma

C = volumetric fraction of red cells in a pore

Lc = effective length of a red cell = $Vrhc/\pi R^2$

ΔPt = total pressure drop across a pore

ΔPc = the additional pressure drop per cell

ΔPpl = pressure drop across a pore for plasma alone at the total flow rate

Nc = number of red cells per pore

They also plotted the measured pressure gradient versus the bulk velocity at a hematocrit of 40% with pore size as a parameter. Their data formed two linear regions corresponding to flow before and after extensive cell deformation. Figure 10 illustrates these relationships.

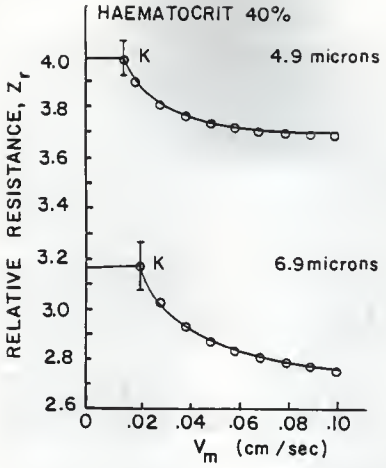

Figure 9: Relative resistance versus mean velocity for pore filter flow (from Lingard, 1977)

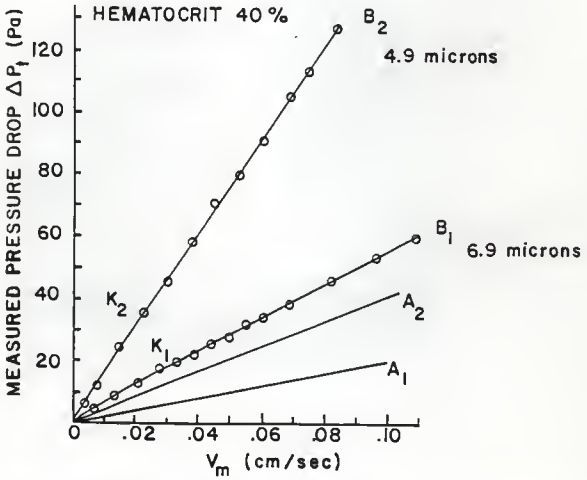

Figure 10: Pressure gradient versus mean velocity for pore filter flow (from Lingard, 1977)

2.6 VELOCITY PROFILES AND THEIR MEASUREMENT

2.6.1 Measurement Techniques

Red blood cell velocity and vessel hematocrit are as important as pressure gradient and hulk flow measurements in characterizing the Fahraeus and Fahraeus-Lindqvist effects. Velocity is determined through analysis of photographic and video measurements. Collection of data with phase contrast microscopes connected to a high speed camera (up to 3000 frames per second) is known as high speed microcinematography. This method is used for hoth in vivo and in vitro flow measurements. The magnified image of the glass tuhe or living vessel is projected onto a viewing screen and the motion of selected cells is analyzed using a frame by frame technique or a photometric double slit technque. In the frame hy frame technique (Bugliarello and Hayden (1963)), the images are projected on the viewing screen one at a time. A specific cell is identified and its motion is traced across the viewing screen. Lengths of travel and time of travel are determined from one frame to the next to determine the velocity of the red cell. In the double slit method (Wayland and Johnson (1967)), images of the red cells in the vessel pass through two slits (having a specific separation distance) in the viewing screen and activate two photomultiplier tubes which lie beneath the surface of the viewing screen. Each photomultiplier tube provides similar waveforms that are separated by the time required for a red cell image to pass between the photomultipliers. The signals are cross-correlated to determine the time delay. The time delay, when divided into the corrected separation distance of the photomultiplier tuhes, determines the velocity. Velocity profiles are ohtained from either technique by scanning the vessel diameter.

Noninvasive television microscopy (Butti et al. (1975)) produces signals for in vitro and in vivo flow that are analyzed in three different ways: 1) By a frame by frame determination of the position of a plasma gap in the capillary. 2) By using a two-channel video densitometer which provides signals proportional to the average light level in two windows positioned at an upstream and a downstream site in the televised capillary. The time delay between similar characteristic features in the recorded upstream and downstream signals produced by the passage of plasma gaps and erythrocytes is measured manually. 3) By direct on-line cross-correlation of the densitometer signals from the upstream and downstream windows.

Laser Doppler anemometry (Einav et al. (1975)) is another noninvasive technique that is used to measure velocity in glass tubes and living vessels. This technique detects the Doppler shift of laser light that is scattered by the flow of the red blood cells. The amplitude of the Doppler signal is related to the number density of the scattering particles.

2.6.2 Experimental Studies of Velocity Profiles

On the basis of viscosity and hematocrit considerations, Fahraeus (1931) deduced that red cells move faster through narrow glass tubes than the plasma does. Gaehtgens et al. (1976) have confirmed the Fahraeus and Lindqvist deductions by direct measurement of plasma and RBC velocities in glass capillary tubes. They reported that the RBC velocity is always higher than the plasma velocity by as much as 2.4 times. While in vitro studies with glass capillaries have consistently shown the RBC velocity to be higher than the plasma velocity, in vivo studies on the intact circulation have produced a variety of results.

Bugliarello and Hayden (1963) studied the flow of ACD anticoagulated buman blood in vitro using 40, 67, and 84 micron tubes with a phase contrast microscope connected to a high speed camera. They were able to determine velocity profiles, cell orientation and drift, and the thickness of the peripberal plasma layer. Their velocity profiles, measured for hematocrits from 6-40%, were expressed as fractions of the measured centerline velocity. In all cases, tbe profiles deviated from tbe Newtonian paraholic shape. They found that

1. Cell velocities increased from the wall to the centerline and only at the lowest velocity and higbest bematocrit in tbe 40 micron tuhe was plug flow approached in the core.
2. Profiles were asymmetric due to settling and usually blunter in the lower section of a horizontal tube.
3. The profiles were blunter tban Newtonian profiles, particularly in smaller tubes and in the lower portion of the horizontal tuhe.

Greenwald (1969) used a fiber optic technique to directly measure erythrocyte velocities in tbe capillaries of the retrolingual membrane of the frog. Two fiher optic probes, mounted in a single holding device, were positioned witb a micromanipulator adjacent to a capillary wall so that two signals were detected whenever a single red hlood cell passed hy. Cross-correlation of the signals gave a time delay which when divided into the distance between tbe probes yielded the erytbrocyte velocity. They observed 468 different red blood cells and obtained an average velocity of 1.01 mm/sec.

Gaehtgens et al. (1970) used a pbotometric douhle slit technique to study human hlood flowing in vertical glass tubes witb diameters ranging from 25.0 to 127.4 microns. Their pseudoshear rates ranged from 1 to 300 sec^{-1} and bematocrits ranged from 30.5 to 45 %. They ohserved non-paraholic velocity profiles with the greateat deviation in the smallest tubes at low flow rates

and high hematocrits. The effect of flow rate on the velocity profiles was most pronounced in small tubes. The effect of hematocrit and flow rate on the shape of the velocity profiles predicted by the Casson model showed good agreement with their experimental data when a cell-free plasma layer of less than 1 micron was assumed for the Casson model. Qualitatively, their observations agreed with those of Bugliarello and Hayden (1963).

Bugliarello and Sevilla (1970) used high speed microcinematography to study ACD-treated human blood flowing through tubes with diameters of 40 and 70 microns. Hematocrits studied ranged from 5 to 40 % and flow velocities ranged from 5 to 15 mm/sec (Reynolds numbers betweeen 0.01 and 0.1). Their films of in vitro flow extended the observations of Bugliarello and Hayden (1963) and allowed them to directly measure angular velocities of the cells. They were able to measure the peripheral plasma layer thickness which was not significantly or consistently influenced by flow velocity or tube diameter. The peripheral plasma layer thickness varied from 4 to 8 microns. Their shear stress versus shear rate data fit the Casson equation well.

Gaehtgens et al. (1970) used a photometric dual slit technique to measure erythrocyte (Dc = 5.6 microns) flow velocities in vessels of the cat mesentery. Figure 11 illustrates the variations in the cell velocity as a function of vessel diameter. The mean and standard deviation of the RBC velocities in 37 arterioles and 38 venules were 7.04 + 1.03 mm/sec and 3.93 + .41 mm/sec respectively. In capillaries, the RBC velocities were 1.7 mm/sec and less. Their work did not determine velocity profiles in the arterioles or venules and they did not measure hematocrits or the peripheral plasma layer thickness.

Richardson et al. (1971) used the cross-correlation of signals derived from a magnified image of flow in vessels to obtain cell velocities. They

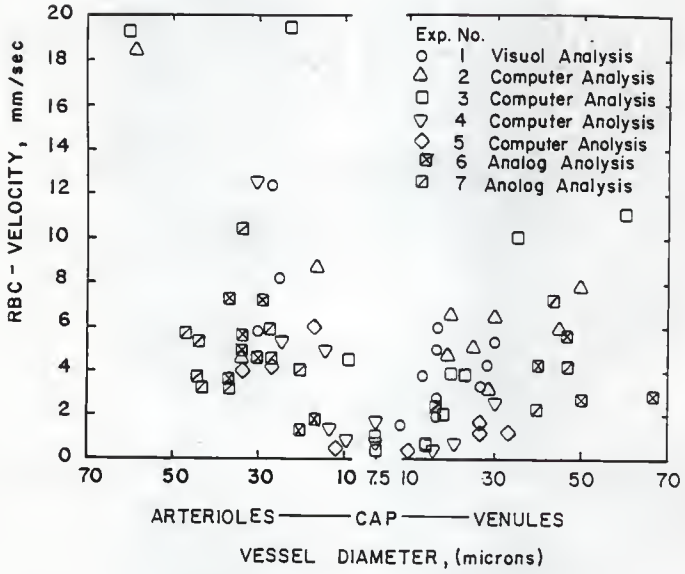

Figure 11: RBC velocities in the microvessels of the cat mesentery (from Gaehtgens et al., 1970)

studied arterioles and venules with diameters hetween 20 and 80 microns in the omentum of both dogs and cats. Their studies yielded velocities ranging from 1.0 to 23.8 mm/sec.

Cokelet (1971) determined the tube hematocrit (Ht) by microphotography for the flow of blood in glass tubes witb diameters between 8.1 and 23 microns. Tbey observed the Fahraeus effect (decreasing tube relative hematocrit with decreasing diameter) down to 10-20 microns, beyond which an inversion of the Fahraeus effect occurred.

Rosenhlum (1972) used higb speed microcinematography to measure cell velocities near tbe wall and at the centerline of cerebral surface vessels in mice. Most of the vessel diameters were between 15 and 35 microns, arterioles averaged 27 + 2 microns and venules 24 + 2 microns. They did not measure velocity profiles or tuhe hematocrits. In normal mice, the erythrocyte velocity at the center was 30% greater than the velocity at the wall for centerline velocities ranging from 1.0 to 13.0 mm/sec. When the blood viscosity was increased by the addition of bigh molecular weight dextrans the velocity at the center was only 6% greater tban tbe velocity at the wall for centerline velocities ranging from 1.0 to 17.0 mm/sec.

Johnson et al. (1973) measured capillary hematocrits in tbe microcirculation of anesthesized cats, using a dual slit photometric technique. They measured tbe average red cell velocity by cross-correlation and the red cell flux with a 4-bit counter. The flux (cells/sec) divided hy the velocity (mm/sec) yielded a hematocrit index (cells/mm). The bematocrit index represented the average numher of red cells per unit length of column flow passing the photosensors. Their red cell velocities ranged from 0.3 to 1.1 mm/sec and their hematocrit index ranged from 10 to 133 cells/mm. The red cell velocity was correlated with tbe hematocrit index.

Jendrucko and Lee (1973) conducted studies with glass tuhes (diameters ranging from 37 to 116 microns) which were very similar to in vivo studies of Johnson et al. (1973) for a hematocrit range of 14 to 50%. Magnified images of red cells were projected onto a viewing screen. Using a fiher optic probe and a photomultiplier module, they detected and recorded the optical density of the red cell images. They determined the optical density as a function of hematocrit and tuhe size. They found that the flow rate had a negligihle effect on the calihration of the optical density curves. This enahled them to estahlish the optical density for a given hematocrit as the average of the optical density for several different flow rates. They verified the Fahraeus effect with their system.

Schmid-Schonbein and Zweifach (1975) used high speed cinematography to measure velocity profiles in the arterioles and venules of the rahhit omentum. The diameters ranged from 16 to 54 microns and the maximum velocities ohserved ranged from 1.1 mm/sec to 9.7 mm/sec. The velocity profiles were time variant and more hlunted than the profiles of Poiseuille flow. As the vessel diameter decreased, the blunted nature of the profile was more pronounced.

Einav et al. (1975) measured velocity profiles in the hamster cheek pouch in vivo by noninvasive techniques. Arterioles with diameters hetween 65 and 98 microns were studied using Laser Doppler Anemometry. The maximum velocities had values of 6-7 mm/sec and the profiles were blunted parabolas. Their profiles were similar to the in vitro studies of Bugliarello and Hayden (1970), Gaehtgens (1970), and Bugliarello and Sevilla (1970). They noted that the amplitude of the Doppler signal was related to the number density of the scattering particles. The Doppler signal qualitatively exhihited higher hematocrits in the center of each tuhe.

Fronek and Zweifach (1977) studied flow and pressure distribution in the arterioles of the cat tenuissimus muscle hy intravital microscopy. They obtained centerline velocities by cross-correlation which ranged from 3.8 to 11.7 mm/sec in arterioles and precapillaries with diameters from 9 to 50 microns. They also measured ahsolute pressures for the vessels hut did not report pressure gradients. Figure 12 illustrates the pressure distribution in the mesenteric vessels.

Butti et al. (1978) used a noninvasive television microscope to evaluate cell velocities in the capillaries of the human nailfold. The maximum ohserved erythrocyte velocity was 2.5 mm/sec hut in most cases the values were 1-2 mm/sec. The diameter of the capillaries increased from a range of 9-12 microns at the arteriole end of the capillary to 12-18 microns at the venule end of the capillary. They ohserved that plasma gaps were easily discernible and maintained their spatial relationship over a comparatively long distance while in the arterioles. Conversely, in the venous limh, since the greater diameter allowed the red cells to pass side hy side, there was considerahle mixing in the flow with a decrease in the correlation length.

Alhrecht et al. (1979) demonstrated the inversion of the Fahraeus effect for the flow of red blood cells in glass tubes. Their tubes ranged in diameter from 3.3 to 11.0 microns and they used three feed hematocrits (10%, 35%, and 60%) and a range of velocities up to 3 mm/sec. The tuhe relative hematocrit increased from 0.7 at 11.0 microns to 0.94 at 3.3 microns. The ratio of cell velocity to plasma velocity decreased from 1.6 at 11.0 microns to 1.0 at 3.3 microns.

Cohen and March (1980) developed a video-based douhle slit method for measuring mean blood velocity in vivo in the kidney medulla. Initial work was

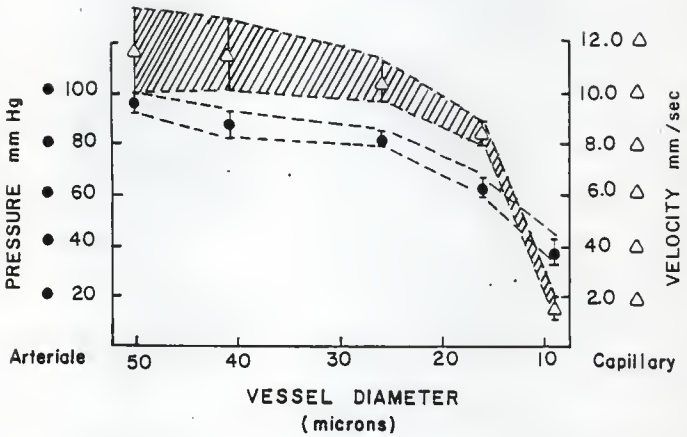

Figure 12: Pressure and flow velocity distribution in cat tenuissimus muscle (from Fronek and Zweifach, 1977)

done in vitro using glass capillaries ranging in diameter from 16 to 28 microns with dog blood. They used a fast Fourier transform routine to find the mean erythrocyte velocity as a function of hematocrit, vessel diameter, plasma osmolality and mean blood velocity. The ratio of erythrocyte velocity to mean velocity increased from 1.3 to 1.6 as tube diameter increased from 16 to 28 microns. The novelty of their technique was that it could handle normal body respiratory motion for in vivo measurements. They also presented normalized power spectral densities and phase differences for the two window signals as a function of system frequency.

2.7 TWO PHASE OIL-WATER FLOW STUDIES

Charles et al. (1961) studied the flow of neutrally buoyant oils (viscosity 6.9 and 16.8 centipoises) and water in 2.65 cm diameter pipes. In the laminar flow region, they observed both bubble and capsule flow with uniform spacing. At superficial water velocities of 3.05 cm/sec, the introduction of small quantities of oil resulted in a symmetrically dispersed bubble flow pattern. The oil bubbles were widely separated and nearly spherical. The size and spacing of the bubbles was not totally determined by the fluid properties, flow rates, and pipe geometry, but within limits, depended on the mode of introduction of the two fluids. With an increase in the superficial oil velocity to 6.09 cm/sec the oil bubbles moved closer together and agglomeration occurred to form a pattern of cylindrical capsules with diameters nearly equal to the tube diameter. A continuous central core of oil flowing inside a film was formed as the oil velocity was further increased.

The observed flow patterns were defined by separate regions on a superficial oil velocity versus superficial water velocity flow map. For a

constant superficial water velocity of 3.05 cm/sec the bubble region of flow began and ended at superficial oil velocities of 1.52 and 2.13 cm/sec respectively. The capsule flow region began and ended at superficial oil velocities of 1.52 and 10.7 cm/sec respectively, and concentric annular flow began at 10.7 cm/sec respectively. For a constant superficial water velocity of 60.96 cm/sec the bubble flow region began and ended at superficial oil velocities of 12.2 and 27.4 cm/sec respectively. The capsule flow region began and ended at 27.4 and 39.6 cm/sec respectively, after which the concentric annular flow region was observed.

At higher superficial velocities of both phases, oil droplet flow was observed and the in situ volume fraction of oil was less than the input fraction which is analogous to the Fahraeus effect for blood.

Greenkorn et al. (1974) studied the two-phase flow of oil and water mixtures with several different pipe diameters. They suggested a concentric annular flow model to describe the pressure-flow data. Their model was based on the assumption of two-phase annular flow and employed an overall two-phase momentum transfer coefficient. They measured concentration and velocity profiles and found that the annular flow assumption provided a good approximation to the real flow pattern (discontinuous core). The pressure drop for the flow of oil was predicted from the momentum transfer coefficient, flow rate, pipe diameter, and oil concentration.

Prasassarakich (1979) studied the laminar flow of oil and water mixtures in glass tubes with inside diameters of 0.26, 0.339, and 0.5 cm with respective volumetric flow rate ranges of 20-40, 40-60, and 75-340 cc/min, corresponding to 6.27-12.55, 7.38-11.07, and 6.36-28.86 cm/sec mean velocity. The input oil percentages ranged from 10% to 75%. She observed bubble flow patterns for 10%

and 25% oil and capsule flow patterns for 50% and 75% oil. The nature of the bubble flow and capsule flow patterns depended upon the flow rate. At the low flow rates botb the bubbles and capsules travelled as individuals. At the high flow rates botb tbe bubbles and capsules travelled in groups of 2, 3, and 4.

She applied the Metzner Reed friction factor correlation to her oil-water data and found that it conformed to tbe correlation reasonably well (all of ber data fell within ±20% of the correlation). She used a non-linear parameter estimation method by Bard (1967) to fit the data to the following semi-empirical relation

$$D^{m}Tw = A\ U^{s} \qquad (13)$$

She also fit tbe in vitro blood flow data of Barbee (1971) to this equation. Botb flow systems were adequately described by tbis correlation.

Sbe found that her laminar oil-water system exhibited some analogous flow behavior to tbe in vitro blood flow of Barbee (1971). These analogies included:

1. For a given tube diameter tbe log-log plots of wall shear stress (Tw) versus pseudosbear rate (U) shift downward as the feed hematocrit or input oil concentration decreases.

2. For a given feed hematocrit or input oil concentration the log-log plots of Tw versus U shift downward as tube diameter decreases. Tbis pbenomena, for the case of blood flow has been called the Fahraeus-Lindqvist effect.

3. Both the oil-water system and blood flow in small tubes can be correlated by equation (13).

Her work (whicb was conducted for Reynolds numbers between 30 and 1000) suggested that oil-water flow at Reynolds numbers less than 30 would provide furtber insigbts into the analogies between oil-water and blood flow because of low Reynolds numbers encountered in tbe microcirculation.

2.8 NOMENCLATURE

a	:	power law exponent
A	:	nonlinear equation viscosity coefficient
b	:	power law coefficient
c	:	an adjustable constant of Barbee's (1971) empirical model
C	:	volumetric fraction of red cells in a pore
D	:	diameter (cm)
Dc	:	major diameter of a red cell (microns)
Dt	:	diameter of tube (microns)
Ec	:	Young's modulus of a red cell membrane (dynes/cm^2)
H	:	hematocrit (%)
Ht	:	tube hematocrit (%)
h	:	fluid film thickness (cm)
k	:	dimensionless slope of the regression line of cell velocity versus mean velocity
K	:	hematocrit multiplier for Newtonian expression of blood viscosity
Lc	:	effective length of a red cell in a pore (cm)
m	:	nonlinear exponent for dependence on tube diameter
Nc	:	number of red cells per pore
ΔPpl	:	pressure drop across a pore for plasma alone at the total flow rate (dynes/cm^2)
ΔPt	:	total pressure drop across a pore (dynes/cm^2)
ΔPc	:	pressure drop per red cell (dynes/cm^2)
R	:	radius of vessel (cm)
Rp	:	region of plug flow in the Casson core (cm)

s	:	nonlinear exponent for dependence on U
S	:	Casson constant ($dyne^{1/2}sec^{1/2}/cm$)
T	:	shear stress ($dynes/cm^2$)
Tw	:	wall shear stress ($dynes/cm^2$)
Ty	:	yield stress ($dynes/cm^2$)
tc	:	red cell membrane thickness (cm)
U	:	pseudoshear rate (sec^{-1})
V	:	velocity (cm/sec)
Vc	:	cell velocity (cm/sec)
Vrbc	:	volume of a red blood cell (cm^3)
Vm	:	mean flow velocity (cm/sec)
X	:	dimensionless ratio of the diameter of the axial train to the diameter of the tube
Zr	:	dimensionless relative resistance
α	:	intercept of Vc axis (cm/sec)
δ	:	marginal plasma layer thickness (cm)
γ	:	average shear rate (cm-1)
μb	:	blood viscosity (poise)
μp	:	plasma viscosity (poise)
μf	:	carrier fluid viscosity (poise)

Chapter III

A CAPSULE FLOW MODEL FOR BLOOD FLOW IN THE MICROCIRCULATION

3.1 INTRODUCTION

In tbe microcirculation, the vessel to red cell diameter ratio ranges from 4-50 and blood flow is beterogeneous in nature. The flow pattern can be described as clusters of red cells and entrapped plasma surrounded by an annulus of plasma witb plasma filling the gaps between the clusters (multi-cell heterogeneous flow). This type of flow has been observed in vivo by Krogh (1922), Jeffords and Knisely (1956), Palmer (1959), Blocb (1962), Monro (1963), and Branemark (1968) and in vitro by Barbee (1971). If the shear rate is high enougb, the plasma gaps can disappear and the flow can be described by a continuous core of cells surrounded by an annulus of plasma. Tbis type of flow is termed concentric annular flow. When plasma gaps are present between the cell clusters tbe concentric annular flow model does not completely characterize the flow, although it can describe the pressure-flow bebavior. This type of flow can be termed capsule flow.

Microcirculatory flow is also characterized by the fact that tbe Fahraeus effect occurs. Tbe Fahraeus effect refers to the decrease in tbe tube relative bematocrit with decreasing tube diameter down to tube diameters of about 20 microns (Fahraeus, 1929). This phenomena has been confirmed by the work of several investigators (e.g. Hochmuth and Davis (1969), Barbee and Cokelet (1971), Azelvandre and Oiknine (1976), and Gaehtgens et al. (1978)).

Multi-cell heterogeneous flow in the arterioles (diameter greater than 30 microns) has a parallel to single cell heterogeneous flow in the capillaries (diameter less than 30 microns). The main difference is that cell clusters rather than single cells are present, however plasma gaps exist in hoth cases. Heterogeneous flow in the capillaries has heen ohserved in vivo by Palmer (1959), Bloch (1962), Monro (1963), and Branemark (1968) and in vitro hy Hochmuth et al. (1970), Albrecht (1979), and Gaehtgens (1980). In the capillaries, single file or multi-file (Gaehtgens, 1980) flow takes place in which the individual cells deform under sufficient shear rates (greater than 1 sec^{-1}). The deformed cells are parachute or capsule shaped (Branemark (1968), Guest et al. (1971), and Gaehtgens (1980)) and gaps of plasma exist hetween the individual cells for hoth the single and multi-file cases. Gaehtgens (1980) found that single file flow occurred when the vessel diameter was less than 8 microns. In this case, the cells passed through the vessel one hy one. For vessel sizes greater than 8 microns he found that the cells formed side hy side multiple lines across the cross-section of the vessel. Multi-cell heterogeneous flow in the arterioles is geometrically similar to capillary flow because of the discontinuous core that exists for both cases.

The modeling of capillary flow has concentrated on quantifying the pressure drop contribution from the red cells. Wang and Skalak (1969) conducted a rigorous analysis of the flow of a line of rigid spherical particles in capillary flow. Series solutions of the Navier-Stokes equations were obtained for given spacings between the spheres with the ratio of particle diameter to tube diameter as a parameter. Their pressure-flow relation depended on the mean velocity, the viscosity of the carrier fluid, the radius of the tuhe and a correction factor. The correction factor depended on the

spacing and clearance of the particles. Their results indicated that the added pressure drop due to the spherical particles was a strong function of the tube to sphere radius ratio and that spacing effects were only important for spacings less than one tube diameter.

Sutera et al. (1970) conducted experiments with flexihle models of red cells. In their work, the added pressure drop from the cells was measured directly. It was observed that the effect of spacing was important only for spacings less than one tube diameter, for larger spacing the added pressure drop was determined by the product of the number of cells and the added pressure drop for one cell. They presented a dimensionless correlation of the added pressure drop per cell which showed that the added pressure drop was a function of the mean velocity, tube diameter, cell diameter, carrier fluid viscosity and an elastic constant for the cell memhrane. For a line of widely spaced cells, additional variahles entered which included the input ratio of cells, cell velocity and volume, tube length, and the carrier fluid viscosity. They showed that the total pressure drop was the sum of the pressure drop for the carrier fluid at the mean velocity and the added pressure drop from the cells.

Lingard (1974) studied the flow of human red cells suspended in hovine serum albumin in nucleopore filters (pore sizes of 4.9 and 6.9 microns). They developed an equation which expressed the total pressure drop across a pore as the sum of the contribution from the cell free carrier fluid and the cells passing through the pore. The pressure contribution from the cells was proportional to the volumetric fraction of the cells in the pore.

Prasassarakich and Walawender (1980) developed a concentric annular flow model and applied it to the in vitro blood flow data of Barbee (1971). Their

model was capable of predicting the wall shear stress (Tw) versus pseudoshear rate (U) curves of Barbee's (1971) data for tuhe diameters between 29 and 811 microns and feed hematocrits ranging from 15.1 to 55.9. The Fahraeus effect was only qualitatively predicted by the CAF model hecause the discontinuous nature of the core was not considered.

A CAF model was also used hy Greenkorn (1974) to describe the pressure-flow data for the discontinuous two-phase flow of oil and water mixtures. His measurements of concentration and velocity profiles indicated that the concentric annular flow assumption provided a good approximation to the discontinuous flow pattern. The pressure drop for the flow of the mixture was predicted from the momentum transfer coefficient, flow rate, pipe diameter, and oil concentration.

The capsule flow concept has been proposed as a means for the large-scale transport of solids by pipe line (Aziz and Govier (1972)). The solids, sealed in rigid cylindrical capsules, are transported through the pipe with a carrier fluid. This concept was developed from the observations of Charles et al. (1961) who studied the two-phase flow of oil and water in a pipe. The pressure-flow behavior in the capsule flow system was descrihed hy the sum of the pressure drops for the carrier fluid and the capsule encased in the carrier fluid annulus.

The capsule flow pattern is similar in appearance to the discontinuous nature of flow in the microvasculature and suggests that the pressure-flow hehavior in both systems can he descrihed hy similar models. For the case of solids in a rigid capsule, the capsule has an infinite viscosity. For multi-cell discontinuous blood flow the capsules have a finite viscosity and experience the shear of the flow field.

The objective of this work was to develop a capsule flow model to quantitatively predict the pressure-flow behavior of blood flow as well as the Fahraeus effect. The model was based on a simple extension of the CAF model to include a discontinuous core. The model also investigated the influence of the end cap geometry of the capsule.

3.2 THEORY

Since the CAF model of Prasassarakich and Walawender (1980) is an integral part of the capsule flow model to be developed in this section, a review of the basic features, and the working equations for the CAF model will be presented to provide the necessary background.

3.2.1 A Review of the CAF Model

Prasassarakich and Walawender (1980) developed a CAF model for the flow of blood in vessels less than 400 microns in diameter. The basic physical features of the model are illustrated in Figure 1. In developing the model, they assumed a constant marginal plasma layer thickness (δ). The marginal plasma layer was assumed to exhibit Newtonian behavior and the core was assumed to have a uniform hematocrit and to obey the Casson equation.

Velocity profiles were determined for both the plasma layer and the core. For Tw/Ty greater than 10, it was found that the velocity profiles in the core had a negligible plug flow region (plug flow radius less than 0.1 R). Consequently the plug flow region was neglected. The resulting velocity profiles for the plasma layer and the core were integrated to yield the following expression for the volumetric rate

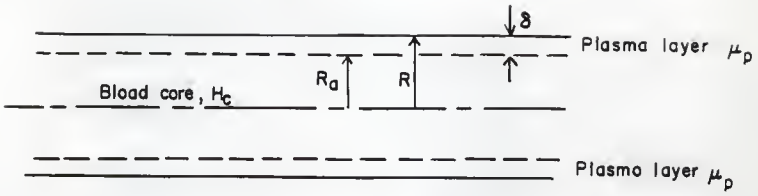

Figure 1: The Concentric Annular flow model (from Prasassarakich, 1979)

$$Q = \frac{\pi}{8\mu}\left[\frac{\Delta P}{L}\right](R^4 - Ro^4) + \frac{\pi}{8S^2}\left[\frac{\Delta P}{L}\right]Ro^4 - \frac{4\pi}{7}\frac{\sqrt{Ty}}{S^2}\sqrt{\frac{\Delta P}{2L}}\,Ro^{7/2} + \frac{\pi\, Ty}{3S^2}Ro^3 \qquad (1)$$

Order of magnitude arguments allowed equation (1) to be expressed in terms of the pressure gradient as the dependent variable as

$$\left[\frac{\Delta P}{L}\right]_{caf} = \frac{\frac{376}{147}\frac{Ty}{Ro} + \frac{64}{7}\sqrt{\frac{Ty\, S^2\, Q}{Ro^5}}\sqrt{1+E} + \frac{8\, S^2\, Q}{Ro^4}(1+E)}{(1+E)^2} \qquad (2)$$

where

$$E = \frac{S^2}{\mu p}\left(\left[\frac{R}{Ro}\right]^4 - 1\right) \qquad (3)$$

The order of magnitude arguments and neglect of the plug flow region required the following limitations on equation (2), 1) Tw greater than 20 times Ty and, 2) U greater than 3 sec^{-1}.

Prasassarakich (1979) used a constant marginal plasma layer thickness of 1.2 microns based on the work of Thomas (1962). Thomas found that in a stable suspension of spherical particles the thickness (δ) of clear suspending fluid at the tube wall was related to the particle radius (R*) by

$$\delta = 0.76\, R^* \qquad (4)$$

In the case of an erythrocyte, the value of R* may be estimated from the mean hydraulic radius (Rh), where

$$Rh = \frac{3\ \text{Volume}}{\text{Surface Area}}. \qquad (5)$$

The average human erythrocyte volume is 87 cubic microns and the average surface area is 163 square microns (Ponder, 1948). These equations and

parameters resulted in the value of 1.2 microns for the marginal layer thickness.

Equation (2) also requires the Casson parameters. Ware et al. (1974) presented the following polynomial correlations for the Casson parameters, S^2 (the Casson viscosity) and Ty (the yield stress), as a function of core hematocrit (Hc).

$$Ty = .0503 + (1.85 \times 10^{-3})\, Hc - (1.265 \times 10^{-5})\, Hc^2 + (1.65 \times 10^{-6})\, Hc^3 \quad (6a)$$

$$S = .1244 + (1.363 \times 10^{-3})\, Hc + (1.45 \times 10^{-5})\, Hc^2 \quad (6b)$$

In the CAF model, the Casson parameters depend on the core hematocrit (Hc). The value for Hc was determined by consideration of the continuity equation for the cells coupled with a trial and error procedure. The continuity equation yielded

$$Hc = (Q/Qc)Hf \quad (7)$$

where

Q = the total flow rate given in equation (1)

Qc = the flow rate in the core

Hf = feed hematocrit

Integration of the velocity profile over the core yielded the volumetric flow rate in the core as

$$Qc = \frac{\pi}{8\mu p}\left[\frac{\Delta P}{L}\right](2Ro^2R^2 - 2Ro^4) + \frac{\pi}{8S^2}\left[\frac{\Delta P}{L}\right]Ro^4 - \frac{4\pi}{7}\frac{\sqrt{Ty}}{S^2}\sqrt{\frac{\Delta P}{2L}}\,Ro^{7/2} + \frac{\pi}{3}\frac{Ty}{S^2}Ro^3 \quad (8)$$

Substitution of equations (1) and (8) into equation (7) gave

$$Hc = \frac{1 + \frac{S^2}{\mu p}\left(\left[\frac{R}{Ro}\right]^4 - 1\right) - \frac{16}{7}\sqrt{\frac{Ty\ R}{Tw\ Ro}} + \frac{4}{3}\frac{Ty\ R}{Tw\ Ro}}{1 + \frac{2S^2}{\mu p}\left(\left[\frac{R}{Ro}\right]^2 - 1\right) - \frac{16}{7}\sqrt{\frac{Ty\ R}{Tw\ Ro}} + \frac{4}{3}\frac{Ty\ R}{Tw\ Ro}} \qquad (9)$$

which was reduced, by order of magnitude considerations, to the approximate expression

$$Hc = Hf\ \frac{1 + \frac{S^2}{\mu p}\left(\left[\frac{R}{Ro}\right]^4 - 1\right)}{1 + \frac{2S^2}{\mu p}\left(\left[\frac{R}{Ro}\right]^2 - 1\right)} \qquad (10)$$

Equation (10) was found to give less tban 2% error for Tw greater than 10 times Ty. The CAF model also used the core hematocrit (Hc) to predict the in situ tube hematocrit (Ht′) from

$$Ht' = Hc\left[\frac{Ro}{R}\right]^2 \qquad (11)$$

The model developed by Prasassarakicb and Walawender (1980) was applied to a case wbere the peripheral plasma layer viscosity and thickness were specified. A trial and error procedure was used to evaluate the core bematocrit for a given feed hematocrit and tube diameter using equations (6) and (10). These parameters were tben used in equation (2) to predict the Tw versus U·behavior of Barbee′s (1971) blood flow data for feed hematocrits from 15.1 to 55.9 and tube diameters from 29 to 221 microns and to predict the in situ bematocrit from equation (11).

3.2.2 The Capsule Flow Model

The main features of the capsule flow model are illustrated in Figure 2. The model envisions a discontinuous core of cells (capsules) instead of the continuous core assumed in the CAF model. In the capsule flow model, each capsule is surrounded by a thin layer of plasma of constant thickness as in the CAF model.

The model postulates that as with rigid capsules, the pressure drop over the length Lt can be determined by summing the pressure drop contributions from the capsule segment of length Lc (as determined from the CAF model) and the plasma gap length ΔL (as determined from the Poiseuille equation). The model also assumes that the pressure gradient in the capsules is the same as in the CAF model. The resulting pressure drop is given by

$$\left[\frac{\Delta P}{L}\right]_{\text{capsule model}} = \frac{Lc}{(Lc+\Delta L)}\left[\frac{\Delta P}{L}\right]_{caf} + \frac{\Delta L}{(Lc+\Delta L)}\left[\frac{\Delta P}{L}\right]_{plasma} \tag{12}$$

To facilitate comparison with the CAF model, equation (12) was divided by the pressure gradient for the CAF model to give a relationship for the pressure gradient ratio, $\bar{R}$, as

$$\bar{R} = \frac{\left[\frac{\Delta P}{L}\right]_{\text{capsule model}}}{\left[\frac{\Delta P}{L}\right]_{\text{caf model}}} \tag{13}$$

Substituting equation (12) into equation (13) followed by rearrangement yields

$$\bar{R} = \frac{Lc}{(Lc+\Delta L)} + \frac{\frac{\Delta L}{(Lc+\Delta L)}}{\left[\frac{\Delta P}{L}\right]_{caf} \Big/ \left[\frac{\Delta P}{L}\right]_{plasma}} \tag{14}$$

Defining the spacing parameter (X) as

$$X = \Delta L / Lc$$

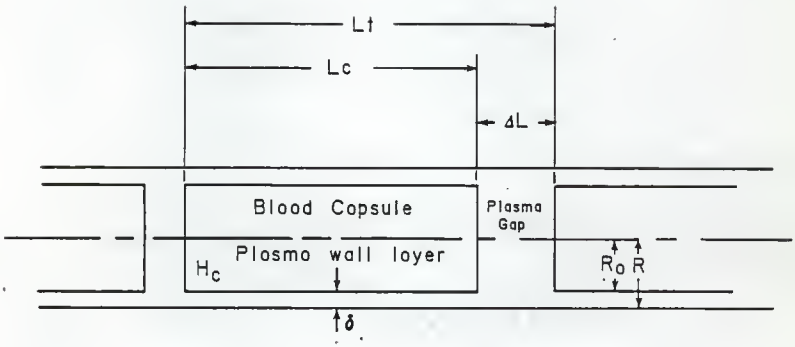

Figure 2: The Capsule flow model

and the CAF model pressure gradient to the Poiseuille pressure gradient ratio as

$$Pr = \left[\frac{\Delta P}{L}\right]_{caf} \Big/ \left[\frac{\Delta P}{L}\right]_{plasma}, \tag{15}$$

allows equation (14) to be simplified to

$$\bar{R} = \frac{1}{1+X} + \frac{X}{1+X}\left[\frac{1}{Pr}\right] \tag{16}$$

For the gaps, Newtonian flow is assumed and the pressure gradient is given by

$$\left[\frac{\Delta P}{L}\right]_{plasma} = \frac{8\,\mu p\, Q}{\pi R^4} \tag{17}$$

The ratio Pr, is determined by dividing equation (2) by equation (17) to obtain

$$Pr = \left[\frac{47}{147}\frac{\pi\, Ty\, R^3}{Q\, S^2}\frac{R}{Ro}\frac{S}{\mu p} + \frac{8}{7}\sqrt{\frac{Ty\, R}{Q\, S^2}^3}\sqrt{\frac{S}{\mu p}^4}\sqrt{\frac{R}{Ro}^5}\sqrt{(1+E)}\right.$$

$$\left. + \frac{S}{\mu p}^2 \frac{R}{Ro}^4 (1+E)\right] \frac{1}{(1+E)^2} \tag{18}$$

The following dimensionless variables are defined:

$$Bm = \frac{\pi\, Ty\, R^3}{Q\, S^2} = \text{modified Bingham number} \tag{19}$$

$$N = \frac{R}{Ro} = \text{the tube to core radius ratio} \tag{20}$$

$$K = \frac{S^2}{\mu p} = \text{the Casson core to plasma viscosity ratio} \tag{21}$$

These dimensionless groups can be introduced into equation (18) to obtain

$$Pr = \frac{N\,K}{(1+E)^2}\left[\frac{47}{147}\,Bm + \frac{8}{7}\,Bm\,N^{1/2}\,(1+E)^{3/2} + N^{1/2}\,(1+E)^{3}\right] \tag{22}$$

Substitution of equation (22) into equation (16) yields

$$\bar{R} = \frac{1}{(1+X)}\left[1 + \frac{X(1+E)^2}{N\,K}\left\{\frac{1}{\frac{47}{147}\,Bm + \frac{8}{7}\,Bm\,N^{1/2}\,(1+E)^{3/2} + N^{1/2}\,(1+E)^{3}}\right\}\right] \tag{23}$$

where E is a function of N and K. Expressing equation (3) in terms of the dimensionless numbers gives

$$E = K\,(N^4 - 1) \tag{3a}$$

Equation (23) shows that the pressure ratio $\bar{R}$ is a function of four dimensionless variables, X, N, K, and Bm.

Figure 2 indicates that the capsules (containing the red blood cells) are right circular cylinders. Consequently the in situ volume fraction of cells, Ht", can be defined as

$$Ht'' = \frac{\text{Volume of Cells}}{\text{Total Volume}} = \frac{(\text{Volume Cylinder})(Hc)}{\text{Total Volume}} = Hc\left[\frac{Ro}{R}\right]^2 \frac{Lc}{(Lc+\Delta L)} \tag{24}$$

Substituting Equation (11) into equation (24) and introducing X gives

$$Ht'' = Ht'\left(\frac{1}{1+X}\right) \tag{25}$$

Equation (25) can be used to evaluate X from Ht' and Ht" if it is rearranged to

$$X = \left(\frac{Ht'}{Ht''}\right) - 1 \tag{26}$$

It has been assumed that Hc is as predicted by the CAF model in the development of equation (26).

3.3 CAPSULE GEOMETRY VARIATION

As an alternate to the blunt end capsule, a cylinder with hemispherical ends was also considered. It was assumed that the radius of a hemispherical end was equal to the radius of the core (Ro). For the geometry shown in Figure 3, an alternative expression for the spacing parameter, X, was derived. For the modified capsule geometry

$$Ht'' = \frac{(\text{Volume Cylinder} + \text{Volume Sphere})(Hc)}{\text{Total Volume}} \tag{27}$$

Substituting for the respective volumes and simplifying gives

$$Ht'' = \frac{(Ro^2 Lc - 2/3\ Ro^3)\ Hc}{R^2\ (Lc+\Delta L)} \tag{28}$$

Equation (28) can be rearranged to

$$\Delta L/Lc = \frac{1}{Ht''}\left(Hc\left[\frac{Ro}{R}\right]^2 - \frac{2}{3} Hc \left[\frac{Ro^2}{R^2}\frac{Ro}{Lc}\right]\right) - 1 \tag{29}$$

Substituting equation (3) gives

$$X = \Delta L/Lc = \left(\frac{Ht'}{Ht''} - 1\right) - \frac{2}{3}\left[\frac{Ht'}{Ht''}\right]\left[\frac{Ro}{Lc}\right] \tag{30}$$

Equation (30) is similar to equation (26), however it contains a correction term for the hemispherical end caps.

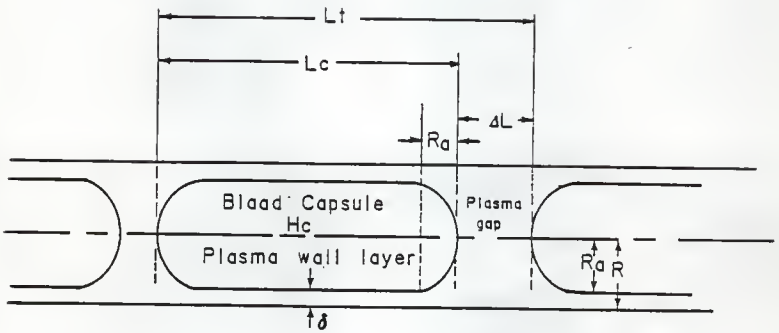

Figure 3: The Capsule flow model with hemispherical end caps

3.4 COMPUTATIONS

The comparison between the capsule flow model and the CAF model has been conveniently expressed in dimensionless form by equation (24). For the blunt end cylindrical capsules, the model was tested by using the experimental in situ hematocrit data of Barbee (1971) and the corresponding predicted in situ hematocrits of Prasassarakich and Walawender (1980). For the capsules with hemispherical end caps, the physiological observations of several investigators were used in addition. The use of both equation (26) and equation (30) force the Fahraeus effect to be satisfied through the ratio Ht"/Ht´. For the evaluation of equation (23) it is necessary to determine suitable values for the dimensionless numbers X, N, K, E and Bm.

3.4.1 Computations for the Blunt End Capsules

The value of N is determined when the tube radius is chosen because of the assumption of a constant marginal layer thickness of 1.2 microns. Equation (20) gives a unique value of N because Ro = R - δ. For the blunt cylindical capsule, the value of X is determined from equation (26) which is function of Ht´ and Ht". The data of Barbee (1971) and the predictions of the CAF model (Prasassarakich and Walawender (1979)) for observed Ht" and predicted Ht´ were used. These data are presented in Table 1 as a function of vessel diameter. The ratio of Ht" to Ht´ is independent of feed hematocrit and U and is only a function of tube diameter (Prasassarakich and Walawender (1980)). Consequently the selection of tube diameter also permits specification of X. Note that the use of the data for Ht" and Ht´ forces the Fahraeus effect to be satisfied.

The value of the dimensionless viscosity, K, depends on the Casson viscosity (s^2) and the plasma viscosity (μp). The plasma viscosity was taken

TABLE 1

The ratio of (Ht") to (Ht′) for the blood data of Barbee (1971) (from Prasassarakich and Walawender, 1980)

Tube diameter, D (microns)	$\frac{Ht''}{Ht'}$
29	0.70
59	0.81
75	0.84
99	0.87
128	0.91
154	0.93
221	0.98
811	1.00

to be 1.54 centipoise, the value in Barbee's (1971) experiments. The Casson viscosity depends on the core hematocrit which is a function of the feed hematocrit and the tube radius. In order to avoid the trial and error calculation of the Casson parameters, an average core hematocrit of 42% was assumed for preliminary evaluations. This assumption is reasonable, since for a given feed hematocrit, the variation in the core hematocrit will be small with respect to variations in tube diameter. For this average core hematocrit the value of S is 0.2072 which gives a value of K of 2.8. The value of Ty, the other Casson parameter, was lumped into the Bingham number. For direct comparison with Barbee's (1971) data, the trial and error procedure mentioned previously was used to determine the Casson parameters.

The Bingham number is dependent on the yield stress, the Casson viscosity, the tube radius, and the flow rate as indicated by equation (19). For a specified tube radius Bm is then dependent on the pseudoshear rate (U) (since $Q = 2\ \pi\ R^3\ U$) and the Casson parameters which depend on core hematocrit. The pseudoshear rates for Barbee's (1971) data varied between 2 and 100 sec^{-1}. For typical conditions (a core hematocrit of 42%), the Bingham number for Barbee's data varied between 0.005 and 0.3. This range of Bm was used for the preliminary tests of the model. The pressure ratio $\bar{R}$ was calculated as a function of Bm for different vessel diameters. Specific calculations for tube diameters of 29 and 99 microns were made for direct comparison with the Tw versus U data of Barbee (1971).

3.4.2 Computations for the Capsules with Hemispherical End Caps

Again, the values of N, K, and Bm are determined as for the blunt capsules. However, determination of the spacing parameter (X) depends on the additional variable, Lc (the length of the capsule) which makes a different computational approach necessary. For this case the specification of X (the spacing parameter) depends on Ht′, Ht", Ro, and Lc as indicated by equation (30). The values of Ht′/Ht" are given in Table 1 as a function of vessel diameter. The end cap radius, Ro is equal to the radius of the core, and is determined once the tube radius is specified. Unfortunately, lengths of the blood capsules (Lc) are not available from Barbee′s (1971) data. Consequently an approach based on the ratio of Ro to Lc was developed.

The values of Ro/Lc were intuitively assumed to be less than 0.5 for all tube diameters (i.e. the capsules are larger than spheres). For each tube diameter a range of Ro/Lc ratios were used to compute X. Values of Ro/Lc which gave negative values of X (not physically possible) were discarded. Acceptable values of X were used in equation (23) to compute $\bar{R}$ over a Bingham number range of $.005 < Bm < 0.3$. For each tube diameter, Ro/Lc was adjusted until all $\bar{R}$ values calculated for the range of Bingham numbers were 0.95 or higher. As with the blunt cylindrical capsules, this method also forced the Fahraeus effect to be satisfied.

3.5 RESULTS AND DISCUSSION

The preliminary calculations for the blunt capsules over the range of Bm of Barbee′s (1971) data indicated that the pressure drop ratio was less than unity for all cases with deviations as high as 20%. Further the deviation increased as the tube diameter decreased and Bm increased. For the 29 micron

tube the deviation was about 20% at a Bm of 0.3 (U = 2). For the 221 micron tube the deviation was less than 2% for all Bm. Because of the assumptions made in tbe model, the pressure drop ratio was expected to be less than unity. However, the validity of the model can only be determined by direct comparison with Barbee's (1971) data.

The blunt end capsule flow model was used to predict the Tw versus U behavior for the 29 and 99 micron tubes at the specific feed hematocrits of Barbee's data (1971). The results of these predictions, and the predictions of the CAF model are compared in Figure 4. Altbough, the differences were negligible for the 99 micron diameter tube, they were significant for the 29 micron diameter tube. Consequently the model witb blunt end capsules is not suitable for small diameter tubes.

In the second approach, numerical values of Ro/Lc were determined for different tube diameters whicb predicted the pressure drop within 5% as well as satisfying the Fahraeus effect. Tbe literature and other sources were searched to find Ro/Lc data as a function of vessel radius. The publisbed data of Jeffords and Knisely (1956), Bloch (1962), and Branemark (1968) and films of Bloch (High Speed Cinematography of the Microvascular System) and Berman (Blood Flow in Small Vessels) were examined and provided this information. Their microphotographs, anatomical drawings, and films yielded Ro/Lc data for comparison with the calculations. The Ro/Lc versus $\bar{R}$ curve that forced the capsule model to predict the pressure-flow data to within 5% is sbown in Figure 5. The points on Figure 5 present the limited physiological observations. The comparisons suggest that the second approach is a reasonable approximation.

Tbe bemispherical end capsule flow model was also used to predict the Tw versus U behavior for the 29 and 99 micron tubes for specific feed hematocrits

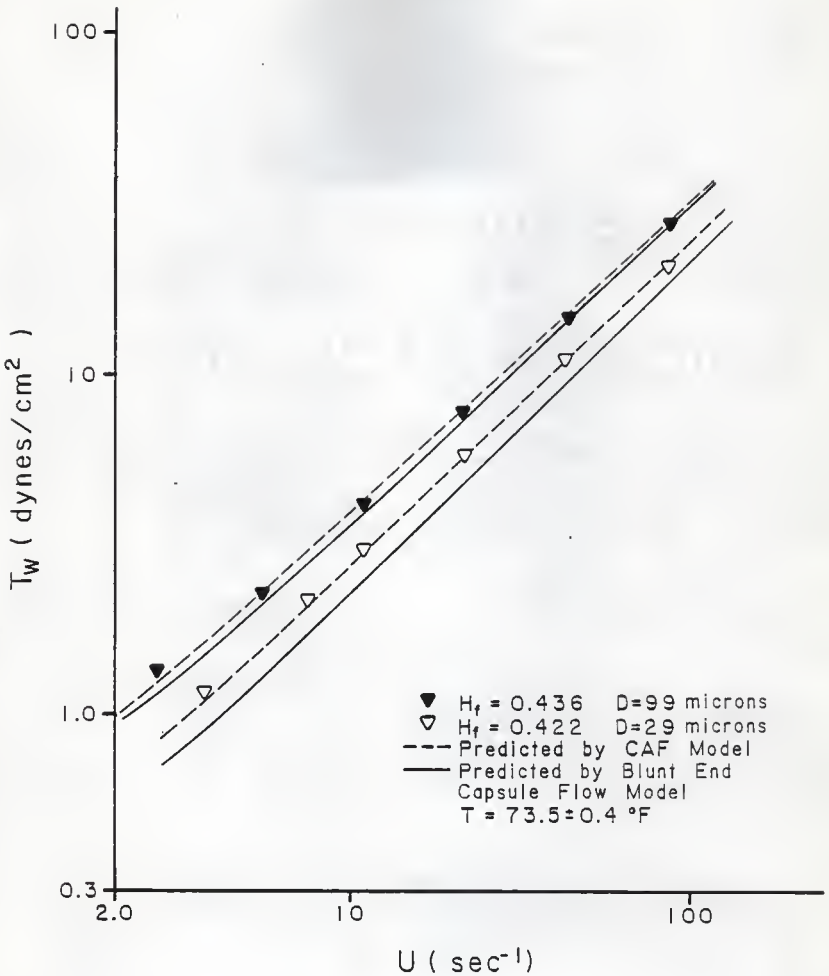

Figure 4: The comparison of Barbee's (1971) data and the behavior predicted by the CAF and blunt end Capsule flow models

of Barbee's data (1971). Tbe results of tbese predictions are compared with his data in Figure 6. As indicated by the figure, the agreement hetween the predictions and the data is good.

The literature data for Ro/Lc agrees reasonably well with Figure 5 considering the difficulties in securing complete data. In most cases the feed hematocrits were not availahle. The vessel walls were not always clearly distinguisbahle and the cell diameters were sometimes difficult to discern. The clusters of cells were sometimes irregular in shape and determination of the exact radius and length was difficult. Considering the difficulties, the agreement in Figure 5 is most encouraging.

Tbe present model bas not attempted to consider interactions between closely spaced capsules. In capillary flow modeling, it has been ohserved tbat interaction effects are important for cell spacings less than one tube diameter (e.g. Lew and Fung (1969), Wang and Skalak (1969), and Sutera et al. (1970)). The inclusion of interaction effects results in an increase in the predicted pressure drop. Estimates hased on the second capsule flow model and Barbee's (1971) data, indicate that hoth the capsule length and the spacing decrease with decreasing tuhe diameter. These estimates coupled witb tbe observations in capillary flow modeling suggest that tbe inclusion of a correction factor for spacing, can improve tbe model that has been developed.

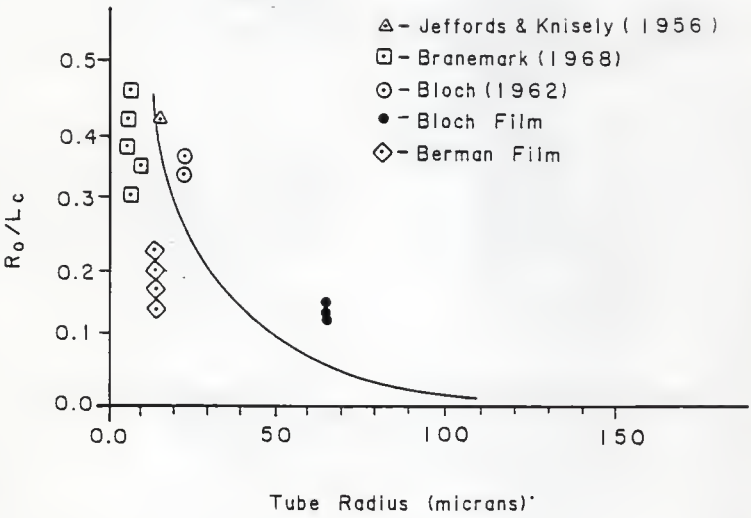

Figure 5: The Ro/Lc vs R curve that adjusts $\bar{R}$ so that it lies between 0.95 and 1.0

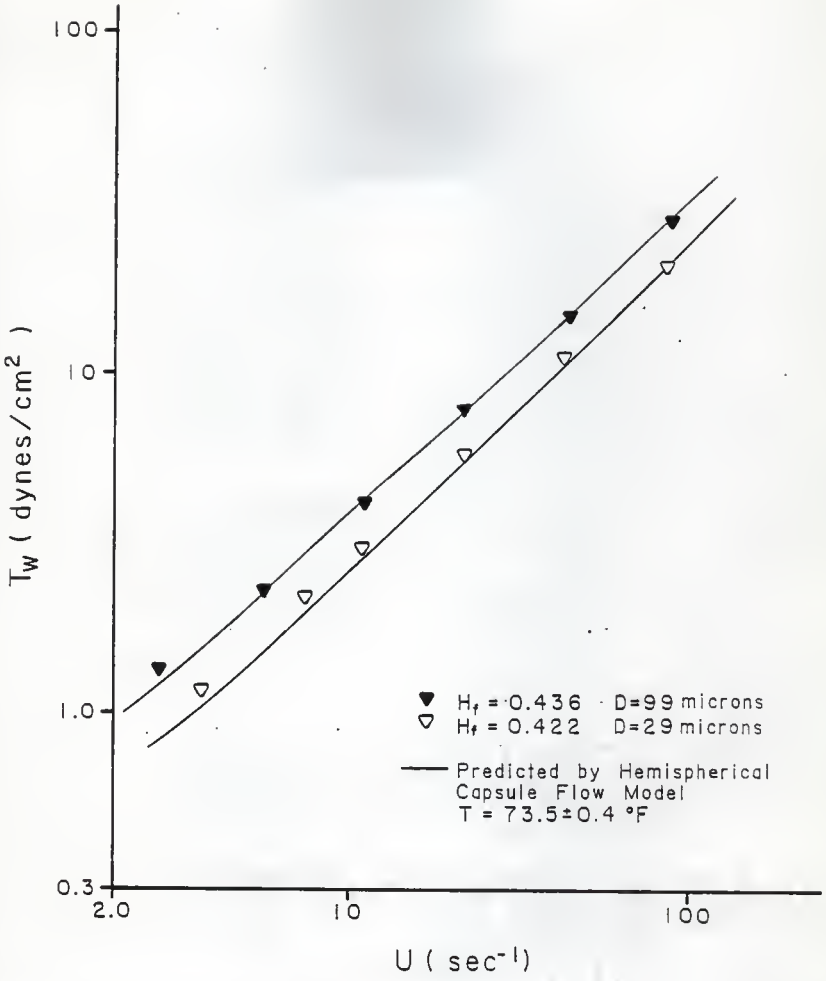

Figure 6: The comparison of Barbee's (1971) data to the behavior predicted by the hemispherical Capsule flow model

3.6 SUMMARY

The capsule flow model with hemispherical end caps predicted the Tw versus U behavior of Barbee's (1971) in vitro data within 5%. The model used the experimental in tube hematocrit data and an Ro/Lc versus $\bar{R}$ curve, substantiated by measurements from the literature, to predict pressure-flow behavior. The agreement with the in vitro data of Barbee (1971) is most encouraging. Considering the difficulty in obtaining measurements of Ro/Lc from the literature, the agreement of the data points with the Ro/Lc versus $\bar{R}$ curve is also encouraging. Future quantitative measurements of the geometric details of capsule flow in the microvasculature have the potential to improve the predictive capabilities of the capsule flow model.

3.7 NOMENCLATURE

Bm	:	dimensionless Bingham number
D	:	tube diameter (cm)
Hc	:	core hematocrit (%)
Hf	:	feed hematocrit (%)
Hr	:	dimensionless tube relative hematocrit
Ht	:	tube hematocrit (%)
Ht'	:	predicted in tube hematocrit (%)
Ht"	:	observed in tube hematocrit (%)
K	:	dimensionless viscosity ratio
Lc	:	total capsule length (cm)
Lt	:	total length from capsule to capsule (cm)
ΔL	:	length of gap between capsules (cm)
N	:	dimensionless radius ratio

Pr	:	dimensionless pressure gradient ratio
$\Delta P/L$	:	pressure gradient (dynes/cm^3)
Q	:	total flow rate (cm^3/sec)
Qc	:	flow rate of core region (cm^3/sec)
$\bar{R}$	:	dimensionless pressure ratio for the capsule flow model
R	:	tube radius (cm)
Ro	:	radius of core region (cm)
Rp	:	radius of plug region (cm)
Rh	:	hydraulic radius of the red cell (cm)
R*	:	radius of the particle (cm)
S	:	Casson constant ($dyne^{1/2}sec^{1/2}$/cm)
T	:	shear stress (dynes/cm^2)
Tw	:	wall shear stress (dynes/cm^2)
Ty	:	yield stress (dynes/cm^2)
U	:	pseudoshear rate (sec^{-1})
X	:	dimensionless spacing parameter
δ	:	plasma layer thickness (cm)
μa	:	apparent viscosity (poise)
μp	:	plasma viscosity (poise)

Cbapter IV

ANALOGY BETWEEN BLOOD FLOW IN SMALL VESSELS AND THE FLOW OF OIL AND WATER IN GLASS TUBES

4.1 INTRODUCTION

In the microcirculation blood flow is heterogeneous in nature when the vessel to red cell diameter ratio ranges from 4-50. Tbe flow pattern can be described as clusters of red cells and entrapped plasma surrounded by an annulus of plasma, with plasma filling tbe gaps between the clusters. Tbis flow behavior bas been observed in vivo by Krogh (1922), Jeffords and Knisely (1956), Palmer (1959), Bloch (1962), Monro (1963), and Branemark (1968) and in vitro by Barbee (1971). If tbe shear rate is high enougb, the plasma gaps can disappear and tbe flow can be described as a continuous core of cells surrounded by an annulus of plasma.

Microcirculatory flow is also characterized by the fact that the Fahraeus and Fabraeus-Lindqvist effects occur. The Fahraeus (1929) effect refers to the decrease in tbe tube relative hematocrit witb decreasing tube diameter down to diameters of about 20 microns. This phenomena haa been confirmed by Hocbmuth and Davis (1969), Barbee and Cokelet (1971), Azelvandre and Oiknine (1976), and Gaehtgens et al. (1978). An inversion of the Fabraeus effect, in which the tube relative hematocrit increases with decreasing tube diameter, occurs for diameters below 20 microns (e.g. Cokelet (1976), Albrecht (1979), Gaebtgens (1980), and Oda et al. (1983)). Tbe Fahraeus-Lindqvist (1931) effect (e.g. Azelvandre and Oiknine (1976), and Gaebtgens (1980)) refers to the decrease in

apparent viscosity with decreasing tube diameter. At a vessel diameter of about 10 microns an inversion occurs where the apparent viscosity increases with decreasing tube diameter (e.g. Dintenfass (1967), Lingard (1977), and Gaehtgens (1980)).

The phenomenon of multi-cell heterogeneous (capsule) flow in the arterioles (diameters greater than 30 microns) is paralleled by single cell heterogeneous flow in the capillaries (diameters less than 30 microns) where plasma gaps exist between the cells. Heterogeneous flow in the capillaries has been observed in vivo by Palmer (1959), Bloch (1962), Monro (1963), and Branemark (1968) and in vitro by Hochmuth et al. (1970), Albrecht (1979), and Gaehtgens (1980). Multi-cell heterogeneous flow in the arterioles has a geometric similarity to capillary flow because of the discontinuous core that exist for both cases.

Charles et al. (1961) studied the flow of neutrally buoyant oils (viscosity 6.9 and 16.8 centipoises) and water in 2.64 cm diameter pipes. In the laminar flow region, they observed both bubble and capsule flow with uniform spacings. At superficial water velocities of 0.254 cm/sec, the introduction of small quantities of oil resulted in a symmetrically dispersed bubble flow pattern. With an increase in the superficial oil velocity the oil bubbles moved closer together to form capsules with diameters nearly equal to the tube diameter. A continuous central core of oil flowing inside a film was formed as the oil velocity was further increased. The observed flow patterns were defined by separate regions on a superficial oil velocity versus superficial water flow map.

The oil-water flow patterns observed by Charles et al. (1961) exhibited some structural analogies to blood flow in the microvessels. Additionally, for

tbe laminar region in whicb both bubble and capsule flow were observed, the in situ volume fraction of oil was less than the input fraction. This is analogous to tbe Fahraeus effect for blood flow in the microvessels. At high water velocities, turbulent oil droplet flow was observed and the in situ volume fraction of oil was less tban the input fraction. The oil droplet flow is similar to tbe individual cell flow that Barbee (1971) reported for his visual observations.

Prasassarakich (1979) examined the apparent analogy between the flow of oil-water mixtures and tbe flow of blood in small diameter (diameters greater than or equal to 29 microns) tubes and reported the following similarities:

1. For a given tube diameter, log-log plots of wall shear stress (Tw) versus pseudoshear rate (U) shifted downward as the feed hematocrit or input oil concentration decreased.

2. For a given feed hematocrit or input oil concentration, log-log plots of Tw versus U shifted downward as tube diameter decreased. This phenomena paralleled the Fahraeus-Lindqvist effect. For the flow of oil and water, Cbarles et al. (1961) found the in situ oil concentration to be less than the input oil concentrations. However, Prasassarakich did not measure in situ oil concentrations.

3. Both the oil-water system and blood flow in small tubes could be correlated by tbe relation, $D^{m}Tw = AU^{s}$.

The analogy was not complete and Prasassarakicb (1979) found tbat there were some differences between the two flow systems. The plot of $D^{m}Tw$ versus U shifted downward as the blood feed hematocrit decreased from 50 to 15. In Prasassarakich's (1979) oil-water system similar trends were observed for a decrease in input oil concentration from 75% to 50% and 25% to 10% but not from 50% to 25%. The discontinuity was attributed to the observation that tbe flow patterns for 75% and 50% oil were botb capsule flow and those for 25% and 10% oil were both bubble flow.

Another difference was observed in the behavior of the power law coefficient, n. For the blood flow data of Barbee (1971) the value of n was approximately 0.9 to 1.0 for all feed hematocrits from 15 to 56 and tube diameters from 29 to 221 microns. In the oil-water system of Prasassarakich, n changed strongly as a function of input oil % (from 0.6 at 75% to 0.9 at 10% for a tube diameter of 0.339 cm) and mildly as a function of tube diameter. This strong dependence on input oil concentration was due to the flow pattern shifts in the oil-water system.

The lowest Metzner-Reed Reynolds numbers obtained by Prasassarakich were 30 and ranged as high as 1000. This was much greater than the values of 0.02 to 0.03 reported (Whitmore (1968) and Lightfoot (1974)) for arterioles under basal conditions, and Barbee's (1971) data which had Reynolds numbers between 0.02 and 3.0.

The objective of the present work was to determine if the analogy of Prasassarakich (1979) could be further extended. This was investigated by examining lower Reynolds numbers and corresponding pseudoshear rates. Two flow systems were examined. System I was composed of oil and water phases and System II was composed of oil and water/glycerol phases. The Reynolds numbers for System I ranged from 1 to 250 and those for System II ranged from 0.005 to 2. At these low Reynolds numbers, both oil-water flow systems exhibited the capsule type flow that has been observed in the microcirculation.

4.2 EXPERIMENTAL EQUIPMENT

The apparatus used in this study is shown schematically in Figure 1. The components included: 1) Oil and aqueous phase reservoirs, 2) Two continuous syringe pumps (Harvard Apparatus model 972), 3) A cylindrical glass test section, 4) A pressure transducer (Statham model P 23 BB), 5) A Beckman-Offner Type R Dynograph, 6) A strain gage coupler (Beckman-Offner type 9803), and 7) A pressure calihration column. Supporting equipment consisted of: 1) A constant temperature hath, 2) A Cannon-Fenske 150 viscometer, and 3) A 25 ml pyncnometer.

The syringe pumps were used to pump each phase from their respective storage reservoirs into the entrance of the test section. In the entrance section, the oil phase and aqueous phase were comhined concentrically through a capillary having an inside diameter of 1.6 mm, with the oil being inside a water annulus. Construction details for the entrance section are presented in Figure 2.

Experiments were performed with a cylindrical glass tuhe, with a diameter of 0.339 cm. The test section for the pressure drop measurement was 45 cm, the entrance length to the test section was 37 cm and the exit length was 38 cm. The pressure drop over the test section was measured with a pressure transducer which was connected to the upstream pressure tap, the downstream tap, and the pressure calihration column hy means of a 3-way stopcock. The pressure taps were constructed from 20 guage syringe needles and were mounted through holes in the wall of the glass tube with epoxy resin. Intramedic tubing, with an inside diameter of 0.157 cm, was used to connect the pressure taps, calibration column and pressure transducer using "Luer Lok" adaptors. The pressure measurements were recorded with a Beckman-Offner type R Dynograph. A type 9803 strain gage coupler interfaced the pressure transducer and the dynograph.

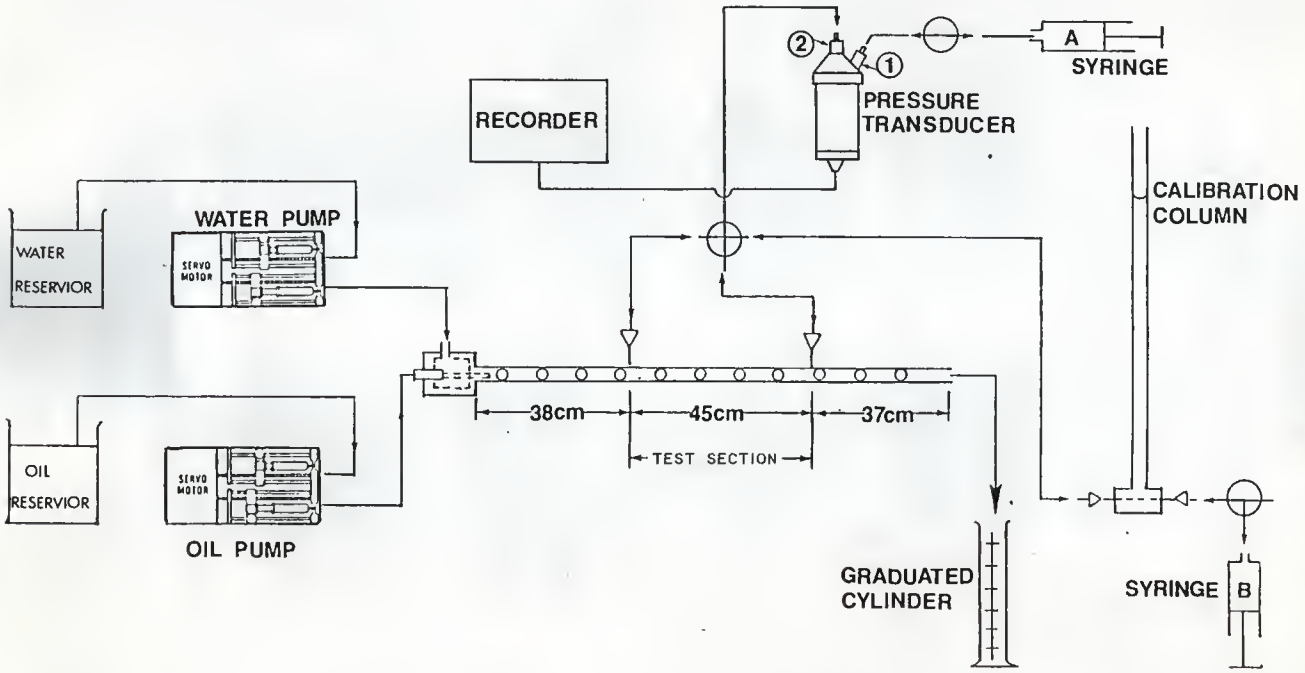

Figure 1: Schematic diagram of the experimental apparatus

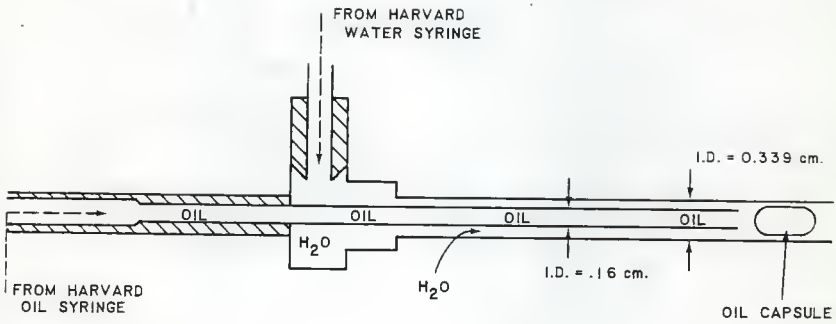

Figure 2: Entrance region of the test section

The calibration column shown in Figure 1 allowed the pressure transducer to be directly calihrated. It was constructed from a 120 cm length of 1 cm I.D. glass tuhing and inserted into a plexiglass well. Two small holes were drilled perpendicular to the well and a 16 guage syringe needle was inserted through the side of the well into one of the holes to connect the column with the pressure transducer. A second 16 guage needle was inserted in the second hole to connect the column to a syringe of water allowing the height of the water in the calibration column to he adjusted. Graph paper, graduated in 1 mm divisions, was placed in back of the column to measure the height of the water column.

A Cannon-Fenske 150 viscometer was used to verify the viscosity of the oil/CCl_4 and aqueous phases for each experiment. The 25 ml pycnometer was used to determine the density of each phase to insure that evaporation losses during storage between experiments were not significant.

4.2.1 Test Fluids

For System I a white mineral oil, Drakeol, ohtained from Imperial Oil Ltd. was used. It had a viscosity of 13.788 cp at 25°C. The density was adjusted by adding 21.8% volume carbon tetrachloride (CCl_4) so that the oil phase density approached that of water, 0.996 gm/cm^3 at 25°C. The viscosity of the Drakeol/CCl_4 phase was 5.375 cp at 25°C.

System II was prepared by adding 40% hy volume of glycerol to the water phase. The density of the water/glycerol phase was 1.11 gm/cm^3 at 22°C and was only weakly dependent on temperature. The visosity of the water/glycerol phase was 4.409 cp at 22°C. Drakeol and CCl_4 were mixed so that the density of the oil phase was 1.11 gm/cm^3. The viscosity of the oil phase was 3.737 cp at

22°C. The density of the oil phase was not very sensitive to temperature, bowever the kinematic viscosity was.

In hotb System I and System II an orange dye was added to the oil phase wbicb made it easily distinguishable from the aqueous phase. One significant difference existed between System I and System II. The water/glycerol carrier phase of System II bad a higher kinematic viscosity tban the oil phase. In System I the water phase bad a lower kinematic viscosity than the oil phase. The addition of the glycerol to the water phase in System II made it possihle to obtain Reynolds numhers less than 1.

4.3 EXPERIMENTAL PROCEDURE

Prior to the start of each experiment it was necessary to purge air bubbles from the pressure measuring system. To do tbis tbe pressure transducer (sbown in Figure 1) was first flushed with water hy applying gentle pressure to syringe A. Water entered tbrough port 1 and displaced air bubhles from the chamber through port 2. When the air was displaced, intramedic tubing with "Luer-Lok" fittings was connected between port 2 and tbe 3-way stopcock. The lines for each pressure tap and the calibration column were then purged with water. The heigbt of the pressure transducer diaphragm was adjusted so tbat it was level with the centerline of the test section and the zero point of the calibration column.

The syringe pumps were filled witb oil and water (water/glycerol for system II) so that an experimental run could he started. The flow rates of oil and water were selected from tbe available pump settings. Flow rates of each pbase were selected to give a range of total flow rate and approximate input oil percentages of 10, 25, 50, and 70 or 75. The oil and water pumps were then

started and effluent was collected in an Erlenmeyer flask until a steady state flow pattern was observed visually throughout the tube.

At this point, a recorder sensitivity level was selected that produced a near maximum possible deflection for the measured pressure drop. The upstream and downstream pressures were determined by switching the pressure transducer to the calibration column and duplicating the response lines at each pressure tap. The pressure drop was measured in this manner at least twice for each steady state flow experiment.

Occasionally, the oil phase would move into the pressure tap needles and cause gradual decreases in the pressure readings. The movement of the oil phase occurred as the 3-way stopcock was positioned alternately between pressure taps and the calibration column. As a preventive measure, turning of the stopcock was done as slowly as possible, but this did not always prevent the problem. When necessary, small quantities of water were gently pushed through the pressure taps to force the small bubble of oil from the needle. When the pressure drop measurements were completed, the Erlenmeyer collecting flask was replaced with a graduated cylinder, and the flow rate was measured with a stopwatch.

During the flow rate measurement, which varied from 150 seconds to 7,700 seconds, the pressure drop was monitored to insure the maintainance of a steady value. The quantities of effluent collected varied with the flow rate range under investigation. A minimum of 10 ml was collected for the low flow rates and a maximum of 200 ml was collected for the high flow rates. All experiments were conducted at room temperature which ranged from 23.5°C to 28.0°C. The temperature in the vicinity of the test section was recorded.

When the flow rate measurement was completed, the phases were allowed to separate by gravity. Any oil that adhered to the side of the graduate was gently pulled to the surface with a stainless steel wire or glass rod. The volumes for each phase and total volume were recorded and the phases were separated and returned to storage.

The range of variables covered for each system are shown in Tables 1 and 2.

TABLE 1

Summary of experimental conditions for System I

% oil	Reynolds Number	Flow rste (cc/min)	Pressure drop (cm H_2O)
10 ± 2	4.7 - 251.7	3.1 - 42.6	0.3 - 1.7
25 ± 3	1.9 - 30.7	2.8 - 18.8	0.3 - 1.8
50 ± 3	1.1 - 18.9	2.5 - 19.2	1.2 - 3.2
75 ± 3	1.1 - 9.8	3.9 - 16.5	1.6 - 4.2

TABLE 2

Summary of experimental conditions for System II

% oil	Reynolds Number	Flow rate (cc/min)	Pressure drop (cm H_2O)
10 ± 2	0.02 - 1.97	0.12 - 2.46	0.1 - 0.6
25 ± 3	0.01 - 0.73	0.13 - 1.96	0.2 - 0.9
50 ± 3	0.005 - 0.91	0.13 - 3.7	0.6 - 2.6
70 ± 3	0.02 - 0.84	0.37 - 4.3	1.4 - 3.8

4.4 CALCULATIONS

The experimental pressure drop and flow rate data were converted to wall shear stress (Tw) and pseudoshear rate (U) data using the following relations

$$Tw = \frac{D\Delta P}{4L} \tag{1}$$

$$U = \frac{4Q}{\pi D^3} = \frac{\text{average velocity}}{\text{tube diameter}} \tag{2}$$

Metzner and Reed (1955) proposed a generalized Reynolds number such that the conventional friction factor correlation could be applied to a general non-Newtonian fluid. It is defined as

$$ReMR = \frac{D^n v^{2-n} \rho}{q} \tag{3}$$

where

$$q = K' 8^{n-1}$$

$$K' = \frac{K}{8^n}$$

For a general non-Newtonian fluid the values of K and n can change continuously for the log-log plots of the wall shear stress versus pseudoshear rate data. Their values can be defined on a point by point basis, with n being the slope of the tangent to the curve of log Tw versus log U, and log K equal to the extrapolation of that tangent to U=0. For fluids that obey the power law model, log-log plots of Tw versus U are linear and have a slope of n and an intercept equal to the log of K. In the present work values of n and K were determined by linear regression of the log-log plots of the Tw versus U data. These parameters coupled with the measured flow rates and known tube diameter permitted calculation of the Reynolds number from equation (3).

Metzner and Reed also showed that in the laminar flow region where ReMR < 2100, the following relationship for the friction factor was obeyed.

$$f = 16/ReMR \tag{4}$$

where

$$f = \frac{D\Delta P}{4L} \Big/ \frac{\rho V^2}{2} = \frac{2Tw}{\rho V^2} \tag{5}$$

Equation (5) was used to evaluate the friction factor for comparison with the correlation given hy equation (4). In addition, values of the apparent viscosity, μa, were calculated for the data using the Hagen-Poiseuille relationship:

$$\mu a = \frac{\pi \Delta P \, R^4}{8 \, Q \, L} \tag{6}$$

Lord, Hulhey and Melton (1967) developed a generalized empirical approach for the correlation of turhulent flow data in smooth pipes for any time-independent fluid. They used a general form of the Blasius equation for turbulent flow

$$f = B \left[\frac{D \, V \, \rho}{\mu} \right]^a \tag{7}$$

and combined it with the fanning friction factor of equation (5) to formulate a relationship hetween the pressure drop and the independent variables, tuhe diameter and average velocity. Their result was expressed as

$$\frac{D^{m'_1} \Delta P}{4 \, L} = A'_1 \, (8V)^{s'_1} \tag{8}$$

where m'_1, A'_1, and s'_1 are parameters. This correlation permitted the superposition of data ohtained with a given fluid and a range of pipe diameters.

Prasassarakich (1979) proposed a variation of equation (8) for laminar flow and suggested that it would be useful for predicting the pressure-flow behavior of both oil-water mixtures and blood. Her expression wss

$$D^m Tw = A\ U^s \tag{9}$$

Equation (9) may be rearranged to give the power law model

$$Tw = \left(\frac{A}{D^m}\right) U^s = K'' U = K\ U^S \tag{10}$$

Equation (9) was also used to correlate the experimental data.

4.5 RESULTS AND DISCUSSION

4.5.1 System I

The experiments with System I resulted in the flow patterns shown in Figure 3. Reynolds numbers ranged from 1.13 to 251.7 and pseudoshear rates ranged between 1 and 10 sec^{-1}. Figure 4 presents log-log plots of the wall shear stress versus the pseudoshear rate for each of the four input oil percentages investigated with System I. The linear form of the plots in Figure 4 suggests that the power law model

$$Tw = KU^n \tag{11}$$

may be suitable to describe the behavior of System I. The values of K and n for each oil percentage, determined by linear regression, are presented in Table 3. Included in the table are the statistical parameters R^2 and the standard error (S.E.) of K and n. The data are well described by the power law model since all R^2 values are greater than 0.95.

The power law coefficient n characterizes the degree of non-Newtonian behavior for time-independent fluids. The greater the deviation of n from unity, the more non-Newtonian the fluid. The coefficient K characterizes the consistency of the fluid and increases as the viscosity of the fluid increases.

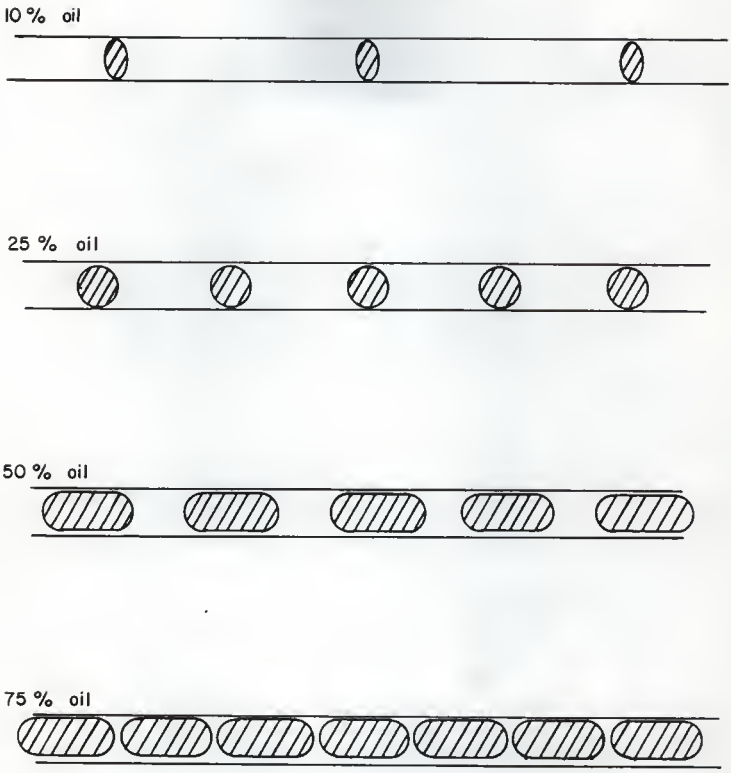

Figure 3: Flow patterns of System I and System II

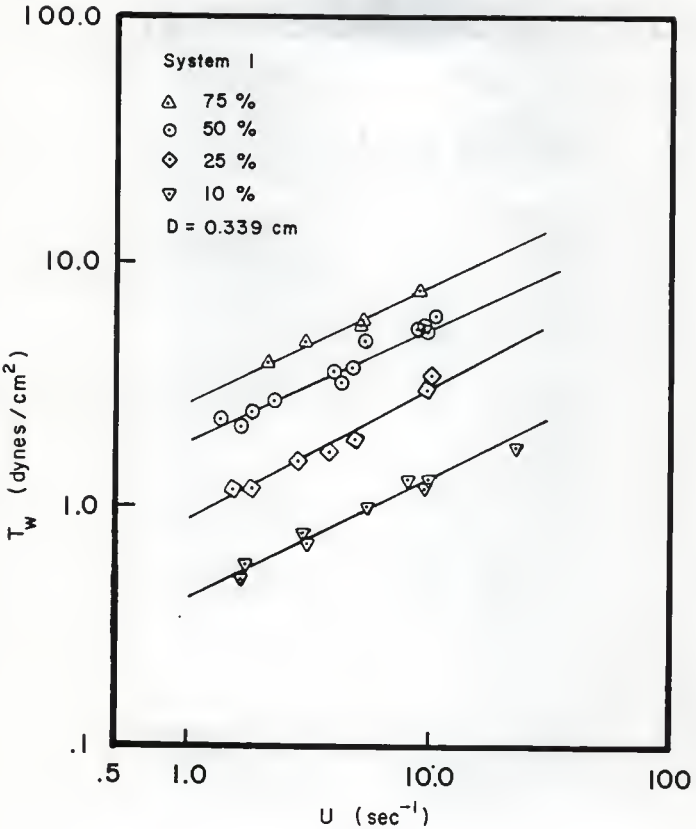

Figure 4: Effect of the input oil % on the flow curves of System I in a 0.339 cm I.D. glass tube

TABLE 3

Rheological constants for System I ($Tw = KU^n$)

% oil	Model R^2	K	S.E. of K	n	S.E. of n
10	0.9683	0.431	0.057	0.479	0.035
25	0.9726	0.899	0.060	0.533	0.040
50	0.9725	1.847	0.041	0.448	0.026
75	0.9817	2.664	0.058	0.471	0.037

In the laminar flow region where ReMR < 2100, the Metzner Reed friction factor correlation as given by equations (4) and (5) may be applied to the data of System I. Figure 5 shows good agreement of the oil-water data with this correlation. System I yielded Metzner Reed Reynolds numhers as low as 1.0 while Prasassarakich's (1979) data were only as low as 30.

Comparison of the System I power law parameters (Tahle 3) with those of Prasassarakich (1979) (Table 4) for a tube diameter of 0.339 cm reveals a significant difference in the flow behavior of the two flow systems. The value of n for System I was approximately constant for all oil percentages (average 0.48) whereas it decreased with increasing oil percentage in Prasassarakich's study. Figure 4, which shows nearly parallel lines for all oil percentages, also implies that n is approximately constant for System I. In this respect System I parallels the behavior of the blood flow data of Barbee (1971) which indicate nearly parallel Tw versus U plots as a function of hematocrit. Thus the results of the System I experiments further extend the analogy between two phase oil-water flow and the flow of hlood in the microcirculation . However, it should he noted that the value of n with System I was about one half of that for Barbee's data for blood flow.

Prasassarakich (1979) also reported that the pattern of flow, for U between 20 and 40 sec^{-1}, changed progressively from spherically shaped bubbles at 10% and 25% oil to capsules (progressively elongated bubbles) at 50% and 75%. At higher U values (70 to 110 sec^{-1}) she ohserved that spherical huhbles for 10% and 25% oil travelled in groups (from 2-4 bubhles) instead of singly and that spherical hubhles often followed the oil capsules for 50% and 75% oil. No such groupings were observed in the present work. This observation offers a possihle explanation for the increasing non-Newtonian hehavior observed in Prasassarakich's study.

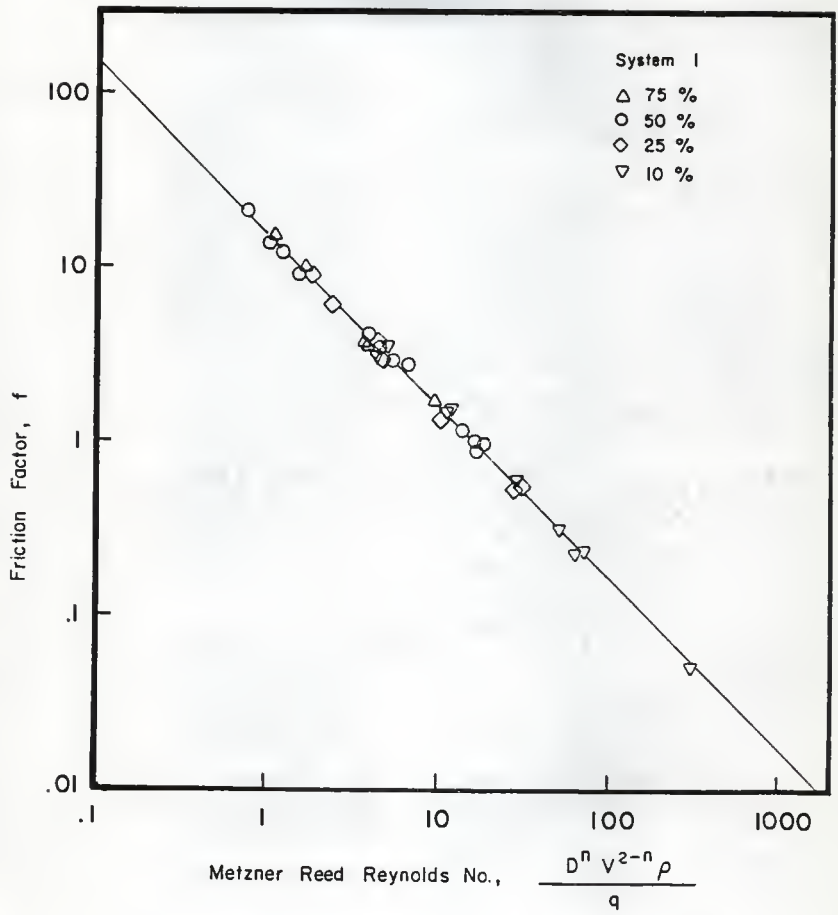

Figure 5: Friction factor versus the generalized Metzner Reed Reynolds number for System I data

TABLE 4

Rheological constants for the oil-water system ($Tw = KU^n$) of Prasassarakich (1979)

% oil	K			n		
	D=0.26 cm	D=0.339 cm	D=0.5 cm	D=0.26 cm	D=0.339 cm	D=0.5 cm
10 + 2	0.209	0.199	-	0.831	0.906	-
25 + 2	0.304	0.328	0.354	0.843	0.876	0.960
50 + 3	0.747	0.949	1.731	0.725	0.687	0.613
75 + 3	2.186	2.134	-	0.503	0.596	-

In System I, for pseudoshear rates from 1-10 sec^{-1} (Reynolds numbers from 1 - 250) and all oil input percentages, the oil phase flowed as single entities without group formations. Tbe shapes of tbe oil bubhles and capsules for System I are illustrated in Figure 3. Notice that at 10% oil, the bubbles as ohserved (by eye) were not perfectly spherical and tbat tbose at 25% oil produced bubbles tbat were more nearly spherically in shape. At 50% and 75%, oil the system produced capsules but they were not of the elongated type described by Prasassarakicb.

The apparent viscosity as defined hy equation (6) was calculated for eacb oil concentration on a point by point basis. Tbe results of the calculations are shown in Figure 6. Lines were fit to the data by regression analysis. As shown in tbe figure, tbe apparent viscosity increased as U decreased for each oil percentage. The results were similar to ohservations of the behavior of the apparent viscosity of blood reported hy Merrill et al. (1963), Dintenfass (1963), Goldstone et al. (1970), Brooks et al. (1970), Schmid-Schonbein et al. (1973), and Bate (1977). The analogy of the flow of oil and water to the flow of blood is further extended by this similarity.

Prasassarakich (1979) fitted equation (9) to tbe in vitro blood flow data of Barhee (1971) and her own oil-water data. She used Bard´s (1967) nonlinear parameter estimation method to determine A, m, and s in equation (9). Her plots of $D^{m}Tw$ versus U showed that Barbee´s data could be correlated by equation (9) with tbe feed hematocrit as a parameter. The correlation lines for blood shifted downward with decreasing feed bematocrit.

The parameters determined for Barbee´s (1971) data are shown in Figure 7. The value of A (an indicator of the viscosity) increased with increasing feed hematocrit. The parameter m removed the dependence on tube diameter. It also

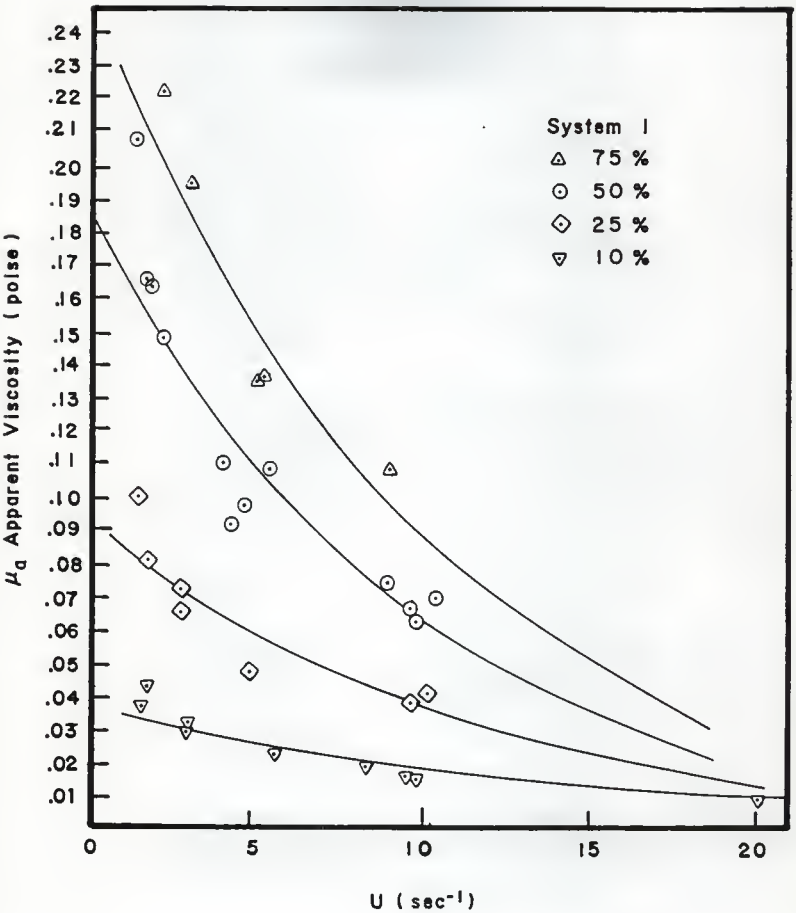

Figure 6: Effect of U and input oil % on the apparent viscosity of System I

accounted for the Fahraeus-Lindqvist effect. The parameter s (an indicator of non-Newtonian behavior) showed that while Barbee's data was non-Newtonian its non-Newtonian nature was not a strong function of feed hematocrit.

Prasassarakich (1979) also correlated her oil-water data using equation (9). The plots of $D^m Tw$ versus U did not continuously shift downward with a decrease in input oil concentration. They did decrease from 75% to 50% and 25% to 10% but not from 50% to 25%. This occurred because of a shift in the type of flow pattern.

The data for System I were fitted to the correlation of equation (9) using Bard's (1967) nonlinear parameter estimation method. The results of the correlation are shown in Figure 8. The correlation lines for $D^m Tw$ versus U for System I shifted downward with decreasing oil % for 75% and 50% oil as was observed for the blood flow data of Barbee (1971) for tubes with diameters from 29 to 221 microns. However, the correlation lines shifted upward with decreasing oil % for 25% and 10% oil. This trend was opposite of that for the blood flow data.

Since System I included data for only a 0.339 cm glass tube the diameter term in equation (9) was incorporated with A to yield a constant, K", as shown in equation (10). The consistency of the nonlinear parameter estimation was checked for each oil % by the comparison of K" and s from equation (10) with the power law parameters. The comparison was favorable for all input oil % for System I.

The values of the parameters A, m, and s for System I are presented in Table 5. The similarity of the behavior of the parameters for 75% and 50% oil to the blood flow results is illustrated in Figure 7. The trends in all three parameters paralleled those for blood flow. The parameter A increased with

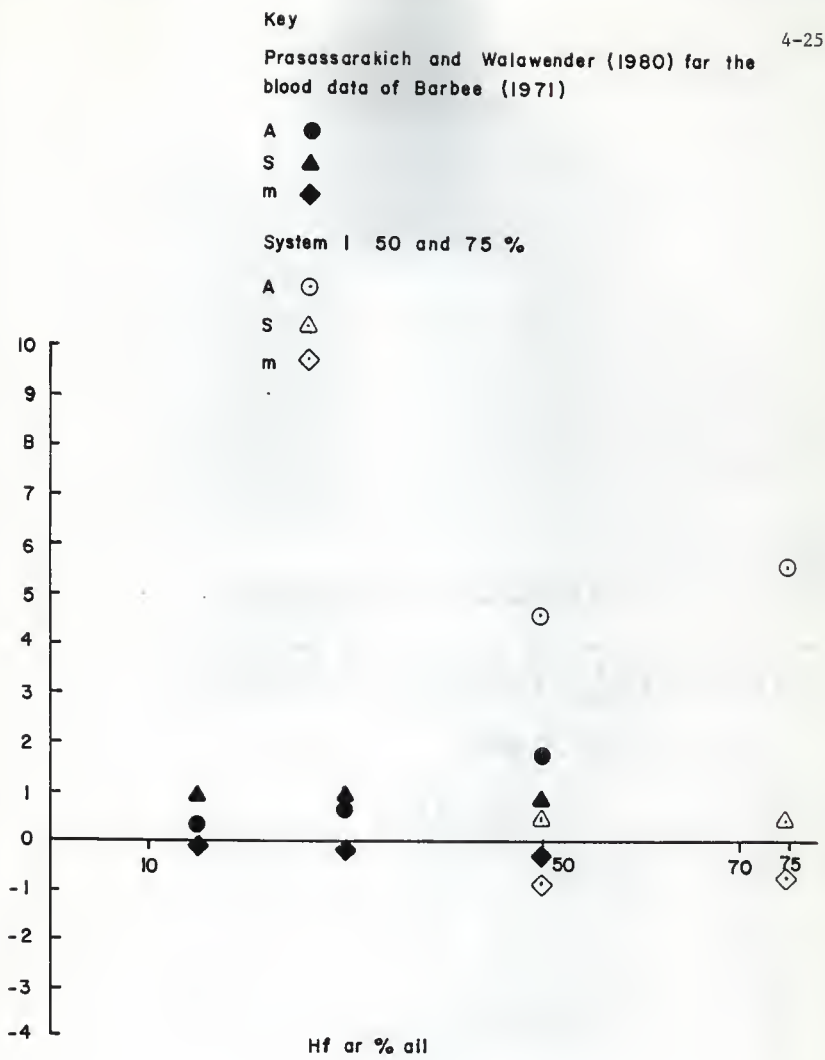

Figure 7: Plots of A vs Hf, a vs Hf, and m vs Hf for Barbee's blood flow data (from Prasassarakich, 1979) and System I

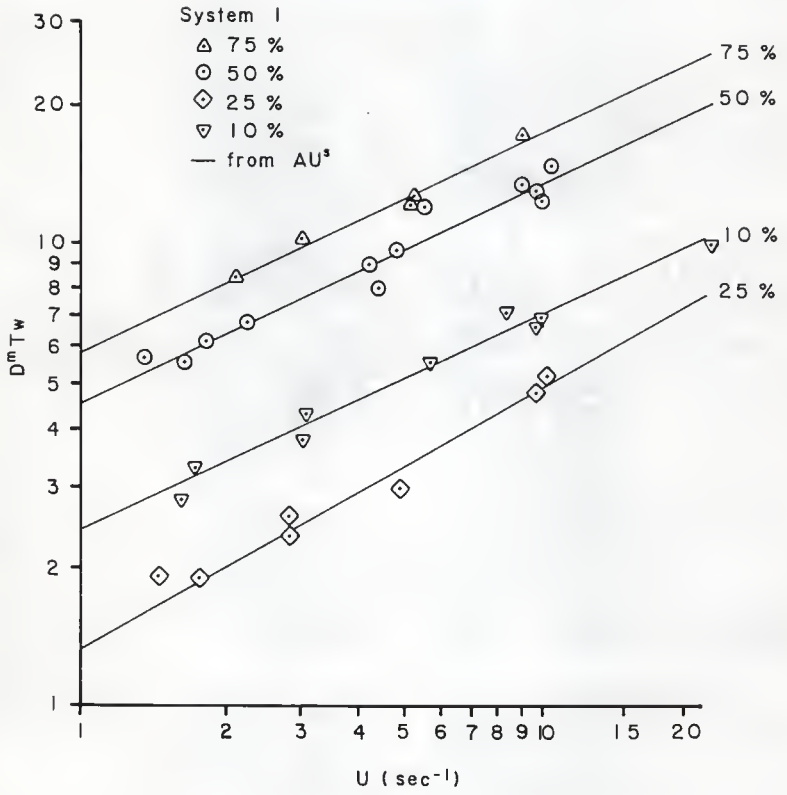

Figure 8: The plots of $D^m Tw$ versus U for System I

increasing oil %, the value of m extrapolates to zero, and the value of s extrapolates to unity. These observations indicate that the capsule flow of the 50% and 75% input oil for System I is physically analogous to the multi-cell heterogeneous flow of blood. The trends of the parameters for 10% and 25% oil were opposite of those for 50% and 75% oil. Since their behavior was similar to the trends of System II, they will be discussed further in the next section.

The System I experiments indicated that the capsule flow of oil-water was similar to that of blood in that n was approximately constant for all oil percentages. A complete analogy was maintained with 50% and 75% oil. Since one of the objectives was to obtain Reynolds numbers less than 1, and System I would not support stable flow at these low Reynolds numbers, it was modified by the addition of glycerol to the water phase to form a second system. System II yielded capsule flow at Reynolds numbers less than 1.

TABLE 5

The nonlinear parameters A, m, and s for System I oil-water flow

% input oil	A	m	s
10	2.45	-1.573	0.461
25	1.34	-0.416	0.564
50	4.57	-0.844	0.472
70	5.63	-0.731	0.491

4.5.2 System II

Experiments with System II produced flow patterns that were similar in appearance to those in System I. Figure 3 represents the shapes of the bubbles and capsules which passed through the 0.339 cm diameter tube with both System I and System II. The Reynolds numbers ranged from 0.005 for 50% oil to 1.97 for 10% oil and the pseudoshear rates ranged hetween 0.06 and 2.0 sec^{-1}. For the U and Reynolds numhers of System II, oil bubbles existed for 10% and 25% oil and oil capsules for 50% and 70% oil. The oil bubbles and capsules travelled individually without group formations, over the entire range of Reynolds numbers.

The wall shear stress (Tw) versus pseudoshear rate (U) data are plotted with oil percentages as a parameter in Figure 9. The power law model was again appropriate for description of the data. The lines in Figure 9 were obtained hy linear regression and the power law coefficients and the corresponding statistical measures are presented in Table 6. As with System I the data of System II were well represented by the power law equation. The R^2 values for the model were greater than 0.95 for oil inputs of 25, 50, and 70 percent and greater than 0.93 for the 10% experiments. As with System I, the value of n was approximately constant (average 0.48). The value of K for a given input oil % increased from System I to System II indicating an increase in the overall viscosity of System II. This was expected since glycerol was added to the water phase of System II.

The Metzner-Reed correlation was used to examine the data of System II and the results are presented in Figure 10. The data were descrihed well by the correlation. The apparent viscosity was also calculated for each trial for System II. The results are presented in Figure 11. The lines shown in Figure

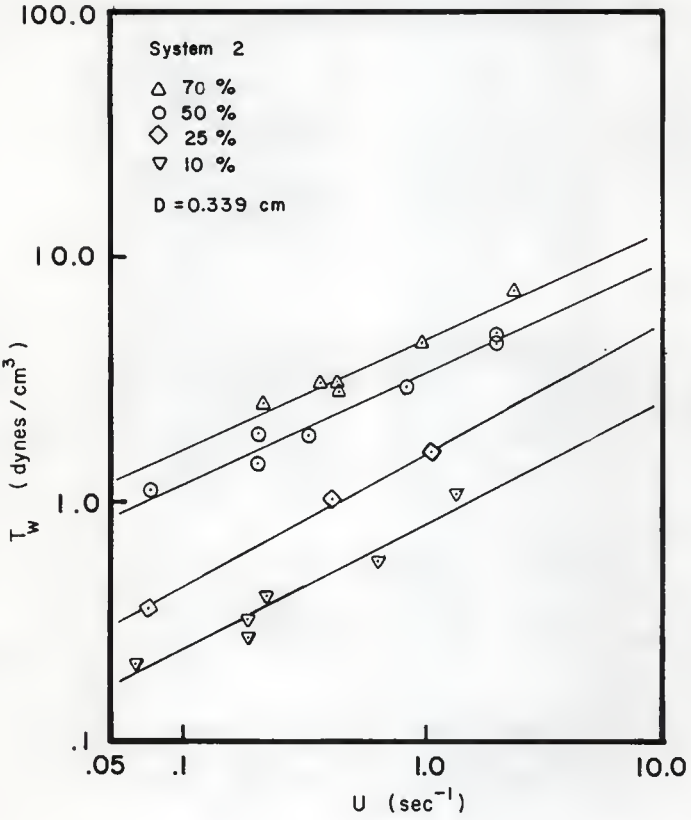

Figure 9: Effect of the input oil % on the flow curves of System II in a 0.339 cm I.D. glass tube

TABLE 6

Rheological constants of System II ($Tw = KU^n$)

% oil	Model R^2	K	S.E. of K	n	S.E. of n
10	0.930	0.803	0.112	0.507	0.069
25	0.999	1.543	0.029	0.541	0.018
50	0.974	3.309	0.046	0.451	0.033
70	0.971	4.548	0.037	0.448	0.038

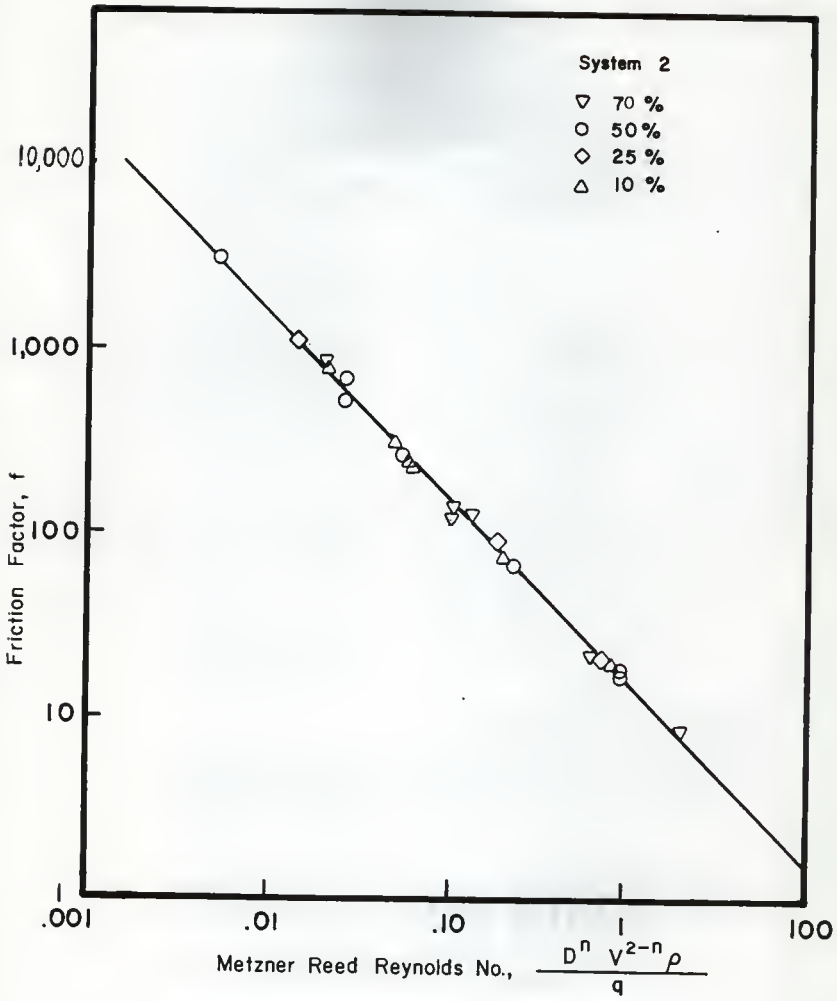

Figure 10: Friction factor versus the generalized Metzner Reed Reynolds number for System II data

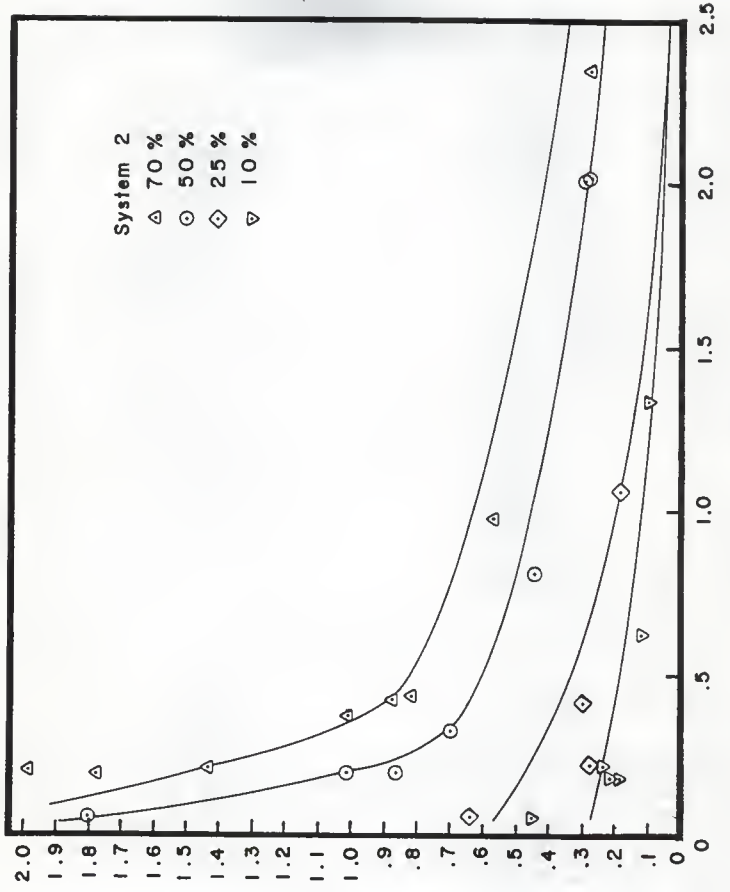

Figure 11: Effect of U and input oil % on the apparent viscosity of System II

11 were fit to the apparent viscosity data by regression analysis. The apparent viscosity increased sharply as U decreased for each input oil %. As in System I, an analogy to the flow behavior of blood was indicated.

The correlation of equation (9) was fitted to the System II data using Bard's (1967) nonlinear parameter estimation method. The results of the correlation are shown in Figure 12. As with the 10% and 25% oil of System I, the plots of $D^{m}Tw$ versus U of System II shifted downward with increasing input oil. This trend was opposite of that for the blood data of Barbee (1971) for tube diameters from 29 to 221 microns.

Since System II included data for only a 0.339 cm glass tube, the diameter term of equation (9) was incorporated with A to give a constant, K". The consistency of the nonlinear parameter estimation was checked by the comparison of K" and s from equation (10) with the power law parameters. The comparison was favorable for all input oil % for System II. The values of the parameters for System II are presented in Table 7. The plots of A, m, and s, as shown in Figure 13, indicate a reversal in the trends for A and m, in comparison to those shown in Figure 7 for blood flow in vessels with diameters of 29 microns and above.

Barbee (1971) also obtained a limited amount of blood flow data for tube diameters of 8.7, 15.3 and 23.0 microns. The behavior of the plots of the wall shear stress versus pseudoshear rate for the small diameter tubes was the same as for the larger diameter tubes discussed earlier. For constant feed hematocrit the Tw versus U curves shifted downward with decreasing tube diameter, and for constant tube diameter the Tw versus U curves shifted downward with decreasing feed hematocrit. Equation (9) correlated Barbee's data for small tube diameters as a function of feed hematocrit as it did for

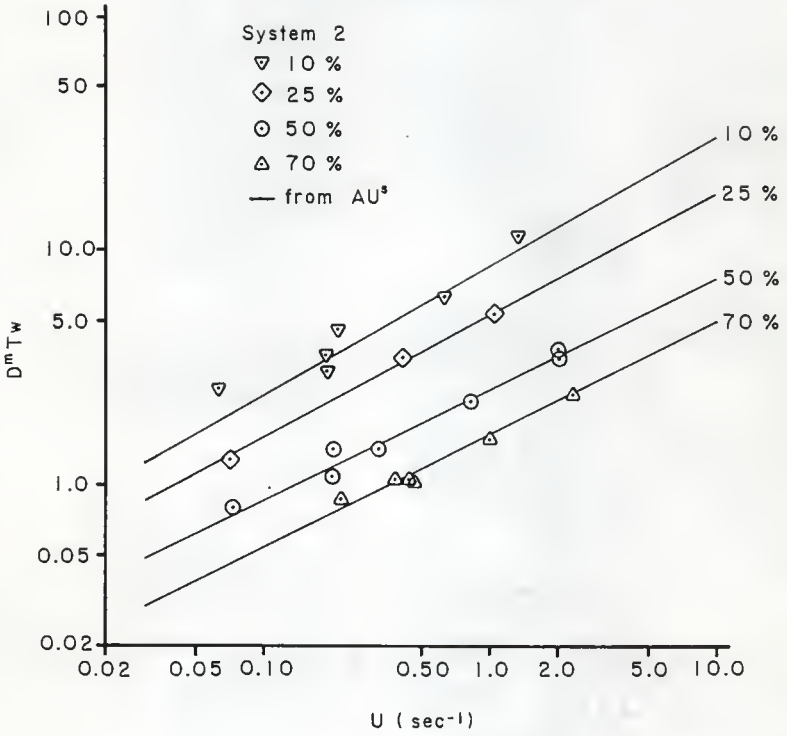

Figure 12: The plots of $D^{m}Tw$ versus U for System II

his data for tbe larger diameter tubes. Equation (9) was also applied to Barbee's data for tbe 8.7 micron tube witb feed hematocrits of 24.8%, 35.9%, 47.2% and 54.6%. The parameters K" and s, based on the correlation of equation (9) compared favorably with tbe power law parameters K and n for all feed hematocrits. Tbis result indicates tbat the application of the correlation of equation (9) to a single tube diameter yields valid results.

The plots of $D^{m}Tw$ versus U, for the 8.7 micron tube, shifted downward witb decreasing feed hematocrit as did the data for System I (10% and 25%) and System II. For Barbee's small tube blood flow data, the behavior of A and m, as a function of hematocrit, exhibited the same trends as shown in Figure 13 for System II and Figure 7 for tbe 10% and 25% oil of System I. The observations indicate an analogy of the oil-water flow for System I (10% and 25%) and System II (all %) to the single cell flow of blood in capillaries.

System I (10% and 25%) and System II are analogous to the observations for single cell flow in vessels less than 11 microns in diameter. The 10% and 25% input oil observations in Systems I and II are analogous to the flow of mildly deformed single cells observed in vessels of 8 to 11 microns (e.g. Gaebtgens (1980)). For both cases, the ratio of the length of the mildly deformed cell or oil bubble (10% and 25% oil) to the vessel diameter was less than 1. The flow for 50% and 70% input oil is analogous to the flow of deformed single cells which occur in vessels less than 8 microns in diameter. In this case, tbe cells deform extensively and tbeir length to vessel diameter ratio increases to values greater than 1 such that they are capsule shaped (e.g. Hochmuth et al. (1970) and Gaehtgens (1980)). The oil capsules for 50% and 70% oil had length to vessel diameter ratios greater than 1, making their flow analogous to the flow of deformed cells in vessels less than 8 microns in diameter.

TABLE 7

The nonlinear parameters A, m, and s for System II oil-water flow

% input oil	A	m	s
10	9.48	-2.215	0.589
25	5.33	-1.156	0.521
50	2.54	-0.249	0.469
70	1.61	0.968	0.476

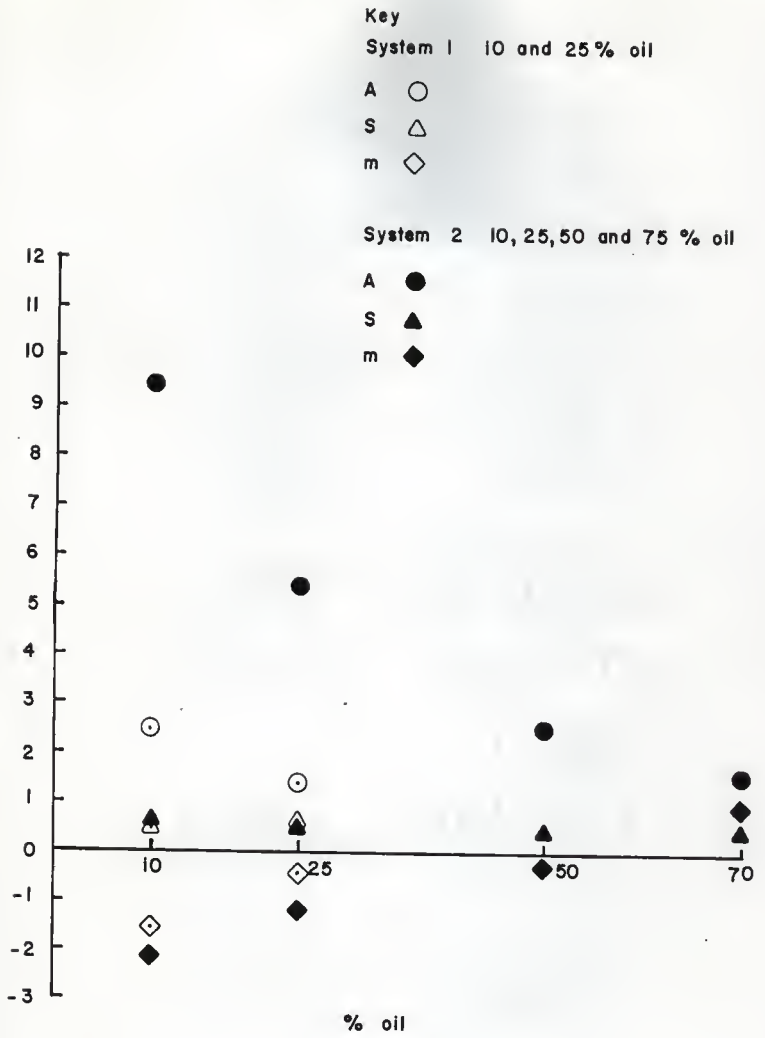

Figure 13: Plots of A vs %, s vs %, and m vs % for 10% and 25% oil in System I and all input oil % in System II

Tbe analogy of tbe 50% snd 70% oil flow to the deformed single cell flow in vessels smaller than 8 microns is also supported by the observations on the bebavior of the apparent viscosity. In tbe work of Lingard (1977), the apparent relative resistance for the flow of red cells in 4.9 and 6.9 micron diameter pore filters was measured. Tbey found tbat tbe relative resistance decreased sharply with increasing mean velocity. Figure 11 also sbows a strong decrease in apparent viscosity witb increasing U for the 50% and 70% oil flow of System II.

4.6 CONCLUSIONS

The results of the experiments performed with System I and System II lead to tbe conclusion that the laminar flow of oil-water mixtures at low Reynolds numbers (ReMR between 0.005 and 30) sbow a variety of analogies to the flow of blood in tbe microcirculation and in small glass tubes.

1. Tbe flow of tbe oil-water of Systems I and II were physically analogous to tbat of blood flow in that tbey exhibited capsule flow having a discontinuous phase and continuous phase. The analogy was applicable to both tbe multi-cell capsule flow observed in arteriole sized vessels and tbe single cell flow in capillaries.
2. For a given tube diameter plots of Tw versus U shifted downward as input oil % decreased. This was also observed in tbe blood flow data of Barhee (1971) for both large and small tubes.
3. The value of n was a constant for all input oil % investigated, i.e. the Tw versus U curves were parallel for all input oil %. The sverage slope for these plots was 0.48 for both System I and System II. Tbis type of behavior was also observed for Barhee's (1971) data, however tbe slope

of the Tw versus U curves was between 0.9 and 1.0 for both large and small tubes.

4. The apparent viscosity decreased with increasing pseudoshear rate for both System I and System II for all U values between 0.05 and 10 sec^{-1}. For blood, the apparent viscosity has also been observed to decrease with increasing pseudoshear rate for flow in both arteriole and capillary sized vessels.

5. System I data were described by the correlation of Prasassarakich (1979). The trends for A, m, and s for 50% and 75% input oil were analogous to those observed for the blood data of Barbee (1971) for arteriole sized vessels.

6. System II data were also described by the correlation of Prasassarakich (1979). The trends for the parameters A and m for System I (10% and 25%) and System II were opposite of the trends for arteriole sized vessels and paralleled the trends for capillary sized vessels. The oil-water data for these cases showed an analogy to the observations of blood flow in capillaries smaller than 11 microns in diameter.

The results of this work suggest that the oil-water flow of Systems I and II at low Reynolds numbers can be used to simulate blood flow in arterioles and capillaries because of a) the similarity of the flow patterns of oil-water mixtures to blood flow (discontinuous flow) and b) the similarity of the various measures of the flow. The parallel for both arteriole and capillary blood flow to the flow of oil-water mixtures is identical for points 1 through 4. However, the identical trends are not present in the plots of $D^{m}Tw$ versus U. This is the only flow feature which distinguishes a difference between arteriole and capillary blood flow.

4.7 NOMENCLATURE

A, A′	:	nonlinear parameters that characterize viscosity
D	:	diameter of the vessel (cm)
f	:	friction factor
K, K′	:	parameters of the power law equation
L	:	length of the test section (cm)
m, m′	:	nonlinear parameters that give dependence on diameter
n	:	a parameter of the power law equation
ΔP	:	pressure drop across the test section (dynes/cm^2)
$\Delta P/L$	:	pressure gradient (dynes/cm^3)
Q	:	total flow rate (cc/min)
ReMR	:	Metzner Reed Reynolds number
R^2	:	statistical measure of goodness of fit
s, s′	:	nonlinear parameters that give dependence on U or V
Tw	:	wall shear stress (dynes/cm^2)
U	:	pseudoshear rate (sec^{-1})
V	:	mean velocity (cm/sec)
μ	:	viscosity (poise)
μa	:	apparent viscosity (poise)
ρ	:	density (gm/cm^3)

Chapter V

CAPSULE VELOCITY AND GEOMETRIC FEATURES FOR OIL-WATER FLOW ANALOGS TO BLOOD FLOW

1.1 INTRODUCTION

In the microcirculation blood flow is beterogeneous in nature, with two distinguisbable pbases, tbe cells and tbe plasma. In tbe arterioles, flow may he described as clusters of red cells separated by gaps of plasma. Multi-cell heterogeneous (capsule) flow of this type has heen observed in vivo by Krogh (1922), Jeffords and Knisely (1956), Palmer (1959), Bloch (1962), Monro (1963), and Branemark (1968). It bas also been observed in vitro by Hochmuth et al. (1970), Barhee (1971), and Gaehtgens (1980). Multi-cell heterogeneous flow in tbe arterioles appears to he geometrically similar to tbe flow of individual red cells in the capillaries. The similarity can be observed in vivo hy comparing the film of Bloch (High Speed Cinepbotograpby of the Microvascular System) with the film of Berman (Blood Flow in Small Vessels) and the work of Monro (1963), and in vitro by comparing tbe works of Hochmuth et al. (1970) and Gaebtgens (1980).

For arteriole sized vessels (i.e. vessels greater than 25 microns in diameter) both in vivo and in vitro studies have observed the flow patterns and measured velocities of individual red cells, velocity profiles, and in situ hematocrits. In vivo studies include those of Gaehtgens et al. (1970), Ricbardson et al. (1971), Rosenblum (1972), Schmid-Scbonbein and Zweifach (1975), Einav et al. (1975), and Fronek and Zweifacb (1977). In vitro studies

include those of Bugliarello and Hayden (1963), Gaehtgens et al. (1970), Bugliarello and Sevilla (1970), Barbee (1971), Jendrucko and Lee (1973), Gupta and Seshadri (1977), and Gaehtgens et al. (1978). The flow pattern observations of these researchers have identified capsule type flow in arterioles. The velocity profiles in vessels greater than 20 microns in diameter have been found to be blunted parabolas (with blunting increasing with decreasing vessel diameter) for both in vivo and in vitro studies. For pseudoshear rates less than 1 sec^{-1}, Barbee (1971) observed total blunting of the velocity profiles for flow in glass tubes ranging from from 29 to 221 microns in diameter. The velocities of the individual red cells in arterioles have been found to range from 1 mm/sec to as high 24 mm/sec for both in vivo and in vitro investigations. In situ hematocrits have been found to be less than the feed hematocrit (the Fahraeus effect) for in vitro studies in vessels greater than 20 microns in diameter. In vivo studies have not produced measurements of the in situ hematocrit.

For precapillaries (10-25 microns in diameter) and capillaries (less than 10 microns in diameter) both in vivo and in vitro studies have observed the flow patterns and measured velocities of individual red cells, velocity profiles, and in situ hematocrits. In vivo studies include those of Krogh (1922), Palmer (1959), Monro (1963), Greenwald (1969), Gaehtgens et al. (1970), Rosenblum (1972), Johnson et al. (1973), Fronek and Zweifach (1977), and Butti et al. (1978). In vitro studies include those of Dintenfass (1967), Hochmuth et al. (1970), Barbee (1971), Lingard (1977), Gaehtgens et al. (1978), Albrecht et al. (1979), and Gaehtgens (1980). Observations of flow in capillary sized vessels (less than 10 microns in diameter) have indicated that deformation of the cells can occur such that the cells become capsule shaped. The in vitro

work of Hochmuth et al. (1970) found that the lengths of capsule shaped cells ranged from 8.5-9.0 microns in a 4.5 micron diameter capillary to 6.5 microns for capillaries with diameters greater 7.6 microns. Monro's (1963) in vivo study in the rahhit ear chamher determined hlood capsule lengths and plasma gap lengths for precapillaries with diameters of 11 and 12 microns. The capsule lengths averaged 13.8 and 25.3 microns for the respective vessel diameters. The ratio of the plasma gap length to the capsule length was 0.98 for the 11 micron vessel and 0.38 for the 12 micron vessel.

The velocities of red cells flowing in precapillaries and capillaries have heen ohserved to he as high as 2.5 mm/sec but usually average 1 mm/sec. The velocity profiles, measured for precapillaries, are hlunted paraholas with centerline velocities ranging from 1.3 to 1.6 times the mean velocity. For true capillaries, the velocity profiles hecome totally hlunted and the cell velocity equals the mean velocity. An inversion of the Fahraeus effect hegins in precapillaries with diameters less than 20 microns. For capillary diameters less than 10 microns, the in situ hematocrit has heen ohserved to increase from 0.7 times the feed hematocrit in a 10 micron vessel to 0.94 times the feed hematocrit in a 3.3 micron vessel (Alhrecht, 1979).

Red cell velocities and velocity profiles have heen determined hy analysis of photographic (Wayland and Johnson, 1967), video (Butti et al., 1975), and anemometric (Einav et al., 1975) measurements for flow in hoth arterioles and capillaries. Phase contrast microscopes and non-invasive television microscopy have heen used to produce images of the flow that can he analyzed hy frame hy frame or cross-correlation techniques. Laser Doppler anemometry has also heen used to determine velocities and velocity profiles.

Although numerous data are available in the literature on individual cell velocities and velocity profiles in different parts of the microcirculation, data on the geometric features of the flow, namely the lengths and spacings of the capsules or cells are limited. In chapter 4, oil-water flow analogs to blood flow in the microcirculation were presented. These flow analogs showed a number of similarities to microcirculatory blood flow such as the flow curve behavior and the variation in apparent viscosity with pseudoshear rate. In view of the success of the oil-water analogs in simulating various flow features, the flow analogs were further investigated to determine their ability to simulate capsule velocities and geometric features.

The objective of this study was to obtain quantitative data on the oil capsule velocities and geometric features of the capsules, namely the lengths and spacings. A fiber optic system was used to obtain the necessary data. Two oil-water flow systems were examined for low pseudoshear rate (U) flow. System I was composed of oil and water phases and System II was composed of oil and water/glycerol phases. The U ranges investigated for System I ranged from 1 to 10 sec^{-1} (Reynolds numbers ranging 1 to 250) and those for System II ranged from 0.06 to 2 sec^{-1} (Reynolds numbers ranging from 0.005 to 2). Over this range of U, both oil-water flow systems exhibited the capsule and bubble types of flow that have been observed in arterioles and capillaries in the microcirculation.

1.2 EXPERIMENTAL EQUIPMENT

The apparatus used in this study is shown schematically in Figure 1. The components included: 1) oil and aqueous phase reservoirs, 2) two continuous syringe pumps, 3) a cylindrical glass test section, 4) a pressure transducer, 5) a strain gage coupler, and 6) a Beckman-Offner Dynograph, and 7) a fiber optic system with its supporting equipment. Steady flow of oil and water was established in the test section and pressure drop and flow rate data were ohtained. Details of the experimental apparatus are presented in chapter 4.

Information on the capsule velocity, length, and spacing was obtained with the fiber optic system after steady huhble or capsule flow was established for a given trial. The fiber optic system and its supporting components included: 1) a laser (Spectra-Physics model 136), 2) an enclosed double point light detector box, 3) two fiber optic probes, 4) two silicon phototransistors (Radio Shack model FPT 100), 5) a fifteen volt D.C. power supply, 6) an amplifier, 7) a reel to reel four channel tape recorder (Hewlett Packard model 3960), 8) two oscilloscopes (Tektronix Type 531 A and Fairchild model Du Mont 766), 9) a correlator and probability analyzer (Honeywell model SAI - 43 A), and 10) a strip chart recorder (Bausch & Lomb 10 mv VOMS),

The light detector box shown in Figure 2 was constructed of plexiglass. It provided a supporting structure for the fiber optic probes, the phototransistors, and the test section. Its dimension were 2.3 cm X 3.5 cm X 4.6 cm and it was wrapped with black construction paper to screen the 60 cycle noise produced by the fluorescent lighting in the laboratory. The fiber optic prohes were inserted through two holes so that light from the laser could be projected perpendicularly through the flow test section at two axial points along the center of the tuhe. The diameter of a fiber optic probe was 1.0 mm

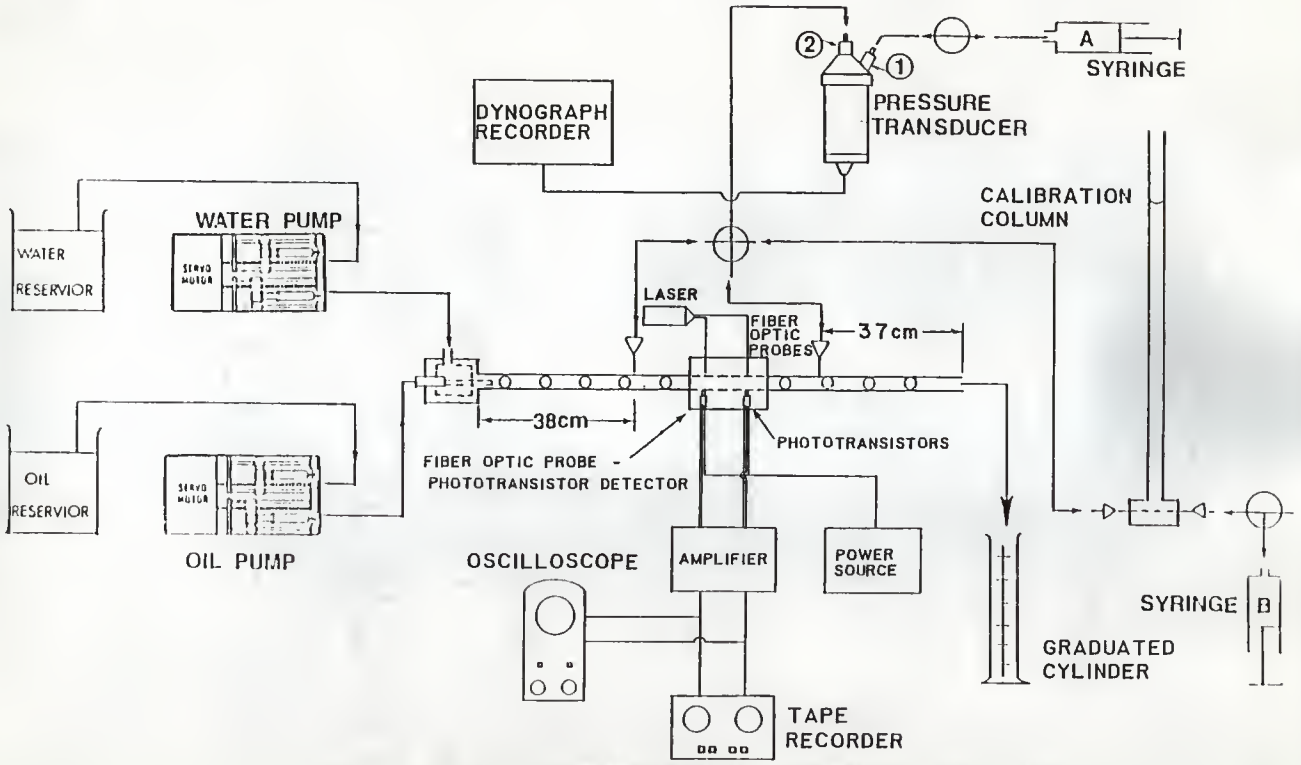

Figure 1: The experimental apparatus used for measuring capsule velocity and geometry and the in situ oil %

and the distance hetween the fiher optic prohes was 2.3 cm. Directly across from the fiber optic probes, two larger holes were drilled in the hox to position two silicon phototransistors to detect the light transmitted through the test section.

The phototransistors were driven hy a 15 volt D.C. power supply. The outputs from the phototransistors were channeled through amplifiers with variahle resistive control which allowed the magnitude of the signals from them to he adjusted. The amplified signals were ohserved on a two channel oscilloscope during each trial to insure their integrity and were then recorded hy a four channel tape recorder for future analysis.

The correlator and prohahility analyzer were used for cross-correlation of the phototransistor signals which were first recorded and then replayed for later analyses. The strip chart recorder was used to produce hard copies of the phototransistor signals so that the oil capsule geometry could be examined. A recording chart speed of 0.846 cm/sec was appropriate for all experimental runs.

In hoth System I and System II an orange dye was added to the oil phase which made it easily distinguishahle from the aqueous phase. Flow rates of each phase were selected to give a range of total flow rate and approximate input oil percentages of 10, 25, 50, and 70 or 75.

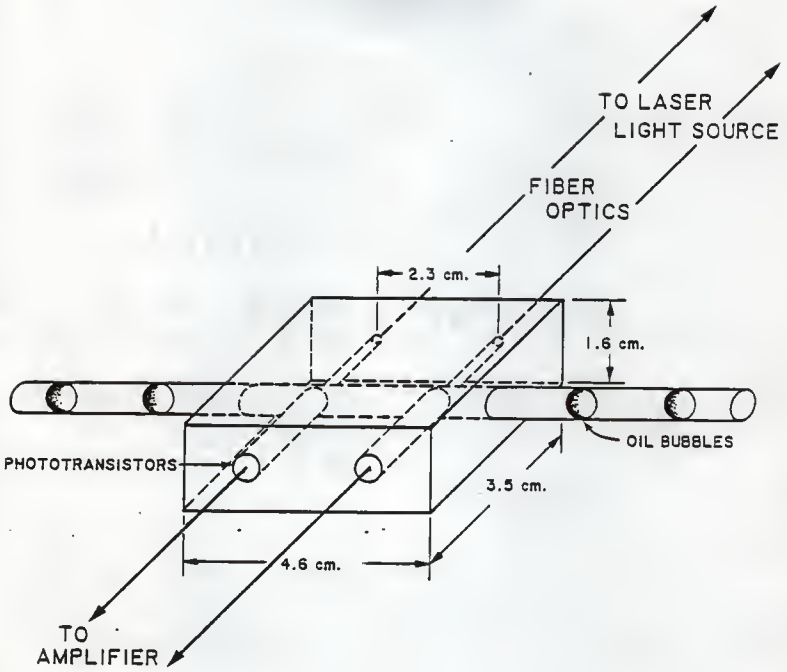

Figure 2: The fiber optic probe - phototransistor detection device

1.3 EXPERIMENTAL PROCEDURE

Initially, the establishment of a steady flow for the input oil % of interest was necessary. The observation of steady upstream and downstream pressures and consistent bubble or capsule flow patterns indicated that steady flow existed. Flow rates were then measured by collecting effluent with graduated cylinders and measuring the collection time with a stopwatch. Details of these procedures have been included in chapter 4.

With steady flow established, the laser, the power supply, the amplifier, the oscilloscope, and the tape recorder were turned on. The signals from each of the phototransistors were observed simultaneously on a two channel oscilloscope. For System II, an approximate square wave response was obtained. The amplitudes of the approximate square waves were adjusted with the variable resistors to insure a 1 to 5 volt response. The shape of the square waves were also observed to insure their consistency with respect to one another. Adjustments with the variable resistors permitted the response of both phototransistors to closely approximate each other. The amplitudes of each signal were not usually identical, but the shapes were always similar. When this was accomplished the amplified signals were recorded on tape for post experiment analysis.

Over the course of these measurements, pressures were monitored to insure steady state conditions and the input response needle on the tape recorder was observed to insure the recording of the data. The minimum number of capsules monitored and recorded was 6 for 10% input oil and a pseudoshear rate of 0.065 sec^{-1}. For the low flow rates, the bubbles passed by so infrequently that only a few could be recorded. The maximum number of oil capsules monitored and recorded was 461 for 25 % input oil and a pseudoshear rate of 2.57 sec^{-1}. Tape

footages were noted so that the phototransistor data for each trial could be identified for post experiment analysis.

The ranges of variables covered for each system are shown in Tables 1 and 2. Over the range of flow rates examined, bubble flow existed for 10% and 25% input oil and capsule flow existed for 50% and 70% or 75% input oil in both oil-water systems.

TABLE 1

Summary of experimental conditions for System I

% oil	U (sec^{-1})	Flow rate (cc/min)	Pressure drop (cm H_2O)
10 ± 2	1.69 - 23.2	3.1 - 42.6	0.3 - 1.7
25 ± 3	1.54 - 10.24	2.8 - 18.8	0.3 - 1.8
50 ± 3	1.36 - 10.45	2.5 - 19.2	1.2 - 3.2
75 ± 3	2.12 - 5.34	3.9 - 16.5	1.6 - 4.2

TABLE 2

Summary of experimental conditions for System II

% oil	U (sec^{-1})	Flow rate (cc/min)	Pressure drop (cm H_2O)
10 ± 2	0.065 - 1.34	0.12 - 2.46	0.1 - 0.6
25 ± 3	0.07 - 1.07	0.13 - 1.96	0.2 - 0.9
50 ± 3	0.07 - 2.015	0.13 - 3.7	0.6 - 2.6
70 ± 3	0.20 - 2.34	0.37 - 4.3	1.4 - 3.8

1.4 CALCULATIONS

The capsule centerline velocity and the mean flow velocity were determined from the data for both systems. Geometric features of the bubbles and capsules, namely the lengths and spacings were also determined for the System II data.

1.4.1 Velocities

The oil capsule centerline velocities were calculated using the time (Z) necessary for a capsule to pass between the two fiber optic probes and their corresponding phototransistors and the distance between the probes (2.3 cm). The time (Z) was determined by the cross-correlation of the recorded phototransistor signals using the Honeywell correlator and probability analyzer. The cross-correlation function for the two similar waveforms is defined as

$$Rxy(Z) = \frac{1}{T} \int_0^T x(t)\, y(t + Z)\, dZ \qquad (1)$$

where

x(t) = sample voltage time history record from the upstream detector

y(t) = sample voltage time history record from the downstream detector

Z = the time displacement between similar waveforms

t = time

T = the sampling time

The cross-correlation function was estimated by the following operations.

1. Delaying the signal x(t) relative to the signal y(t) by a time displacement equal to Z seconds, called the lag time.

2. Multiplying the value of y(t) at any instant hy the value of x(t) that had occurred Z seconds hefore.

3. Averaging the instantaneous product over the sampling time.

As the lag time was changed, a plot of the cross-correlation function Rxy(Z) versus lag time (Z) was ohtained which had a maximum. The value of Z at which the maximum occurred was the time delay required for an oil capsule to traverse the distance between the two prohes.

The centerline velocity of the oil capsules was calculated from

$$Vcc = \frac{2.3 \text{ cm}}{Z} \tag{1}$$

The mean velocity of flow was determined from the flow rate hy

$$Vm = \frac{4\,Q}{\pi\, D^2} \tag{2}$$

where

Q = the total volumetric flow rate

D = the tuhe diameter

The pseudoshear rate was calculated from

$$U = \frac{4\,Q}{\pi\, D^3} \tag{3}$$

1.4.2 Geometry, Length, and Spacing

A typical oil capsule and an enlarged square wave from a single phototransistor are shown for System II in Figure 3. The capsule spacing and geometric features are illustrated by the representative square waves shown in Figure 4. In hoth Figures 3 and 4 the flow direction is from right to left. The definitions of sLc, Lc, ΔL, ΔR, and Lt with respect to the oil capsule are;

sLc = the length of the cylindrical section of the oil capsule,

Lc = the total length of an oil capsule,

ΔL = the length of the aqueous phase between oil capsules,

ΔR = the length of the capsule end cap,

Lt = the characteristic average length from the leading edge of one capsule to the leading edge of the next capsule.

These lengths are proportional to the distances shown in Figure 3. The baseline of the phototransistor signal occurred when the water phase passed the detection point. As the leading edge of an oil capsule crossed the laser beam the slope of the signal became positive. The leading end cap region is represented by the positively sloping section of the approximate square wave. When the cylindrical section of the oil capsule crossed the path of the laser beam the slope of the signal became zero and the signal maintained its maximum magnitude as long as the cylindrical section of the capsule was detected. When the trailing end cap reached the detector the slope of the signal became negative and moved towards the baseline. At this time the significance of the overshoot in both the leading and trailing end caps is not understood. The dashed lines shown in Figure 3 were used as the basis for estimation of each of the characteristic dimensions; sLc, Lc, ΔL, ΔR, and Lt.

For any absolute length (al) in the oil-water system the phototransistor trace exhibits a corresponding length (al′). The corresponding length of the phototransistor trace does not normally equal the absolute length because of the varying capsule velocity and the speed of the strip chart recorder (0.846 cm/sec). The value of any absolute length is calculated from the corresponding length by

$$al = \left[\frac{al'}{0.846 \text{ cm/sec}}\right] \times Vcc \qquad (4)$$

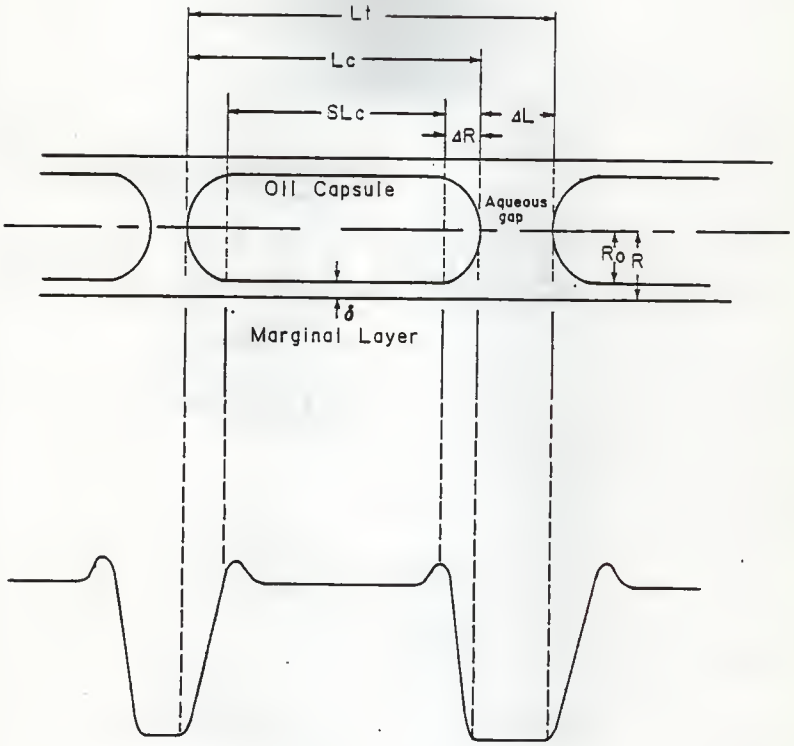

Figure 3: A sample oil capsule with its respective dimensions and an enlarged phototransistor square wave

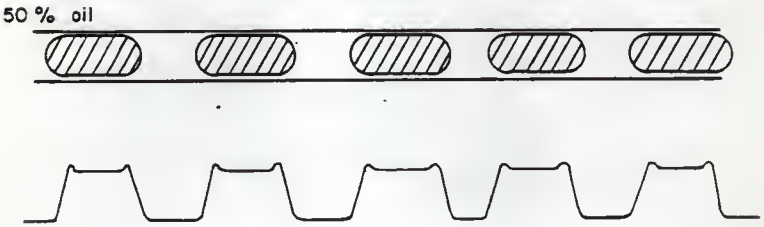

Figure 4: The photo-transistor traces which represent the geometry and spacing of the oil capsules

Values of sLc'_i, Lc'_i, and Lt'_i were determined for each bubble and capsule in a given trial by measuring the corresponding lengths from the phototransistor trace. Average values of sLc'_i, Lc'_i, and Lt'_i were determined and then converted to sLc, Lc, and Lt using equation (4).

The spacing (ΔL), end cap length (ΔR), and the spacing parameter (X) were calculated from

$$\Delta L = Lt - Lc \tag{5a}$$

$$\Delta R = 0.5\ X\ (Lc - sLc) \tag{5b}$$

$$X = \Delta L/Lc \tag{5c}$$

1.5 RESULTS

Figures 5a, 5b, 6a, and 6b present plots of the capsule centerline velocity versus the mean flow velocity. The capsule velocity is approximately equal to the mean flow velocity for both System I and System II for all pseudoshear rates and oil % investigated.

For the higher shear rates for system I, the frequency of the oil bubbles (10% and 25%) and capsules (50% and 75%) was sufficiently high that determination of the geometric features from the strip chart recorder trace was impossible. A typical recorder trace for System I is shown in Figure 7. The data for System II, which had pseudoshear rates less than 1 sec^{-1}, had well defined traces (as shown in Figures 3 and 4) and permitted the evaluation of sLc, Lc, and Lt.

The geometric characteristics of the oil capsules for System II were determined for the entire range of pseudoshear rate and input oil %. The results for the length of the cylindrical segment of a capsule (sLc) and total capsule length (Lc), each expressed as a fraction of the distance between

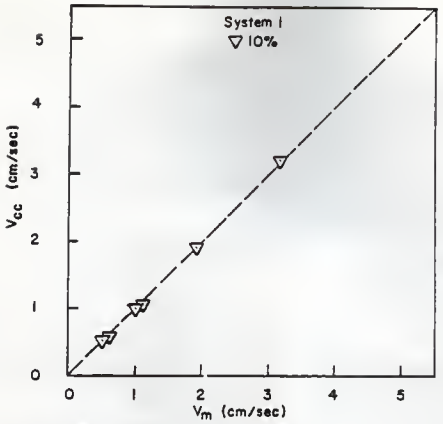

Figure 5a: Capsule velocity versus mean velocity, 10%, System I

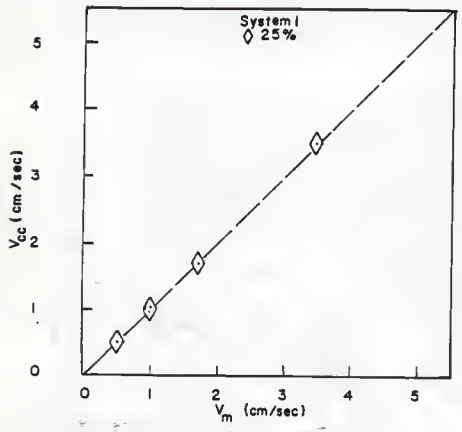

Figure 5b: Capsule velocity versus mean velocity, 25%, System I

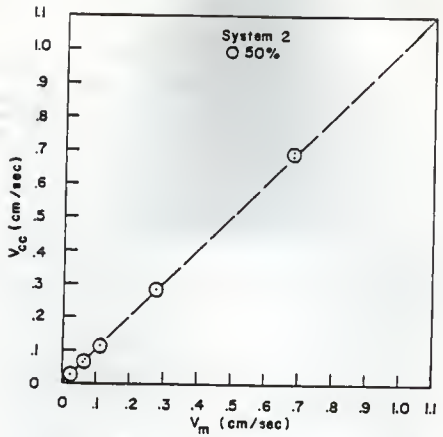

Figure 6a: Capsule velocity versus mean velocity, 50%, System II

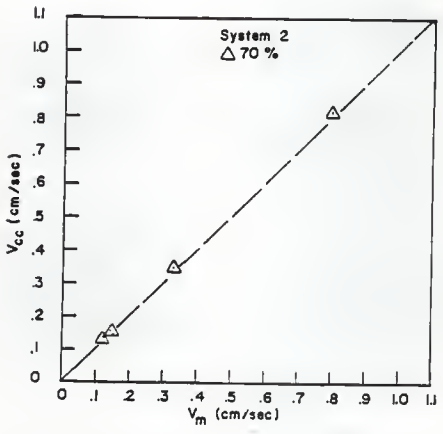

Figure 6b: Capsule velocity versus mean velocity, 70%, System II

Figure 7: The phototransistor signals for System I

capsules (Lt) are plotted as functions of input oil % in Figure 8. The line of unit slope represents the points at which either of these fractions (expressed as %) would equal the input %. The values of sLc/Lt and Lc/Lt are estimates of the in situ oil fraction. The fraction sLc/Lt underestimates the in situ oil % because it does not include the leading and trailing end caps. The ratio of Lc/Lt overestimates the actual in situ oil % because it treats both end caps as blunt ended cylinders.

Figure 9 shows that the ratio of the length of an oil capsule (Lc) to the total length (Lt) between capsules increases with increasing input oil %. The ratio does not show a dependence on pseudoshear rate for the range investigated. At 10% oil, the ratio is 0.15 and it increased to 0.85 for 70% oil.

Figure 10 presents the ratio of the aqueous phase gap length (ΔL) between capsules to the total length of a capsule (Lc). This ratio (X, the spacing parameter) increases with decreasing input oil % but shows no dependence on pseudoshear rate. It ranges from 0.2 at 70% oil to 5.9 at 10% oil.

Figure 11 shows the variation in total length (Lc) of the oil capsules as a function of pseudoshear rate for different input oil %. The capsule length increases with increasing input oil % from 0.4 cm at 10% oil to 0.75 cm at 70% oil. It does not show a dependence on pseudoshear rate.

Figure 12 illustrates the increase in the average gap length (ΔL) between capsules as the input oil % decreases. The average gap spacing is not a function of the pseudoshear rate. It increases from 0.1 cm at 70% oil to 2.3 cm at 10% oil.

Figure 13 illustrates the variation in total length (Lt) as a function of pseudoshear rate for different input oil %. It increases with decreasing input

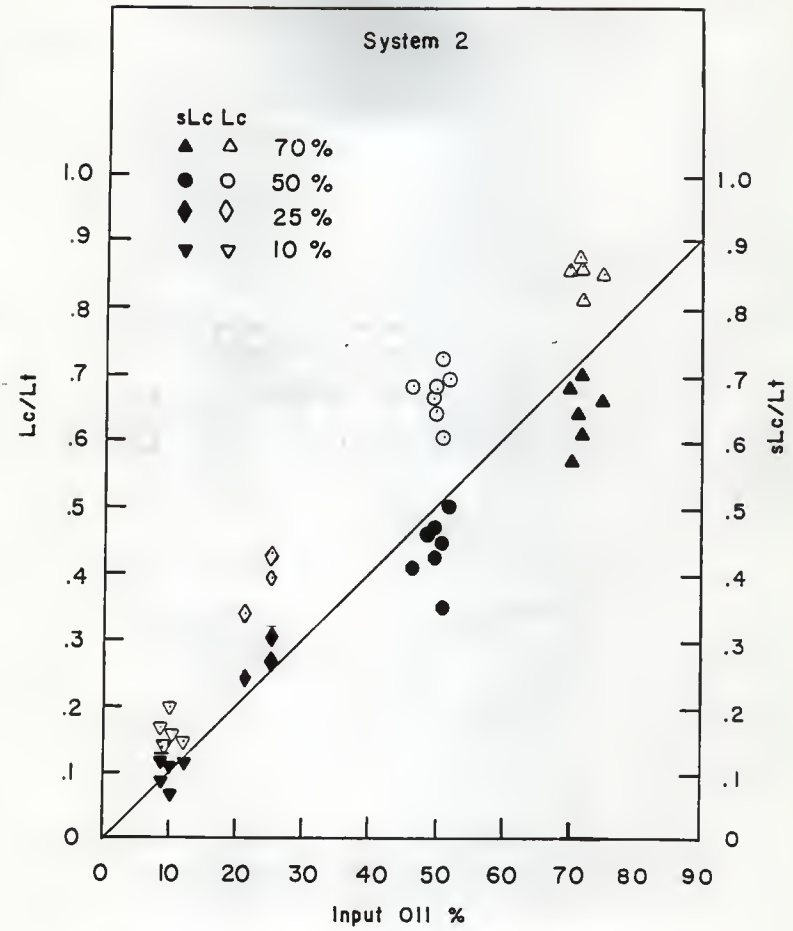

Figure 8: In situ versus discharge oil % for System II.

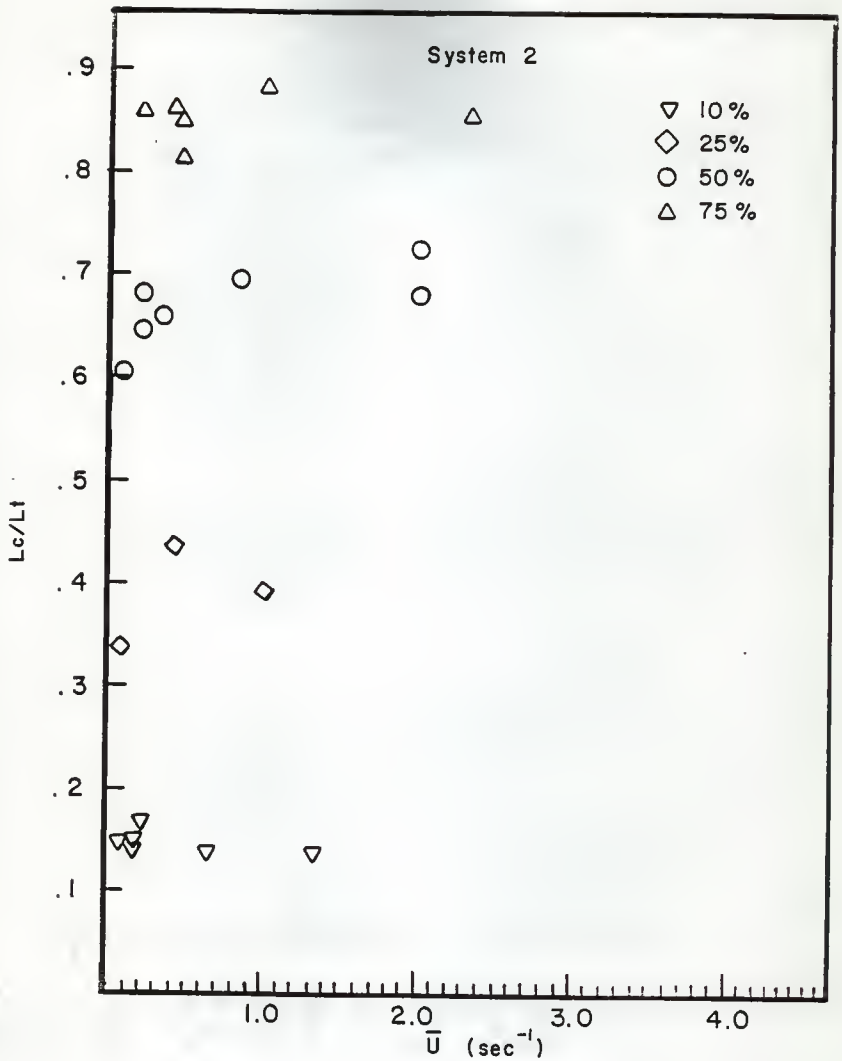

Figure 9: Lc/Lt versus U for System II.

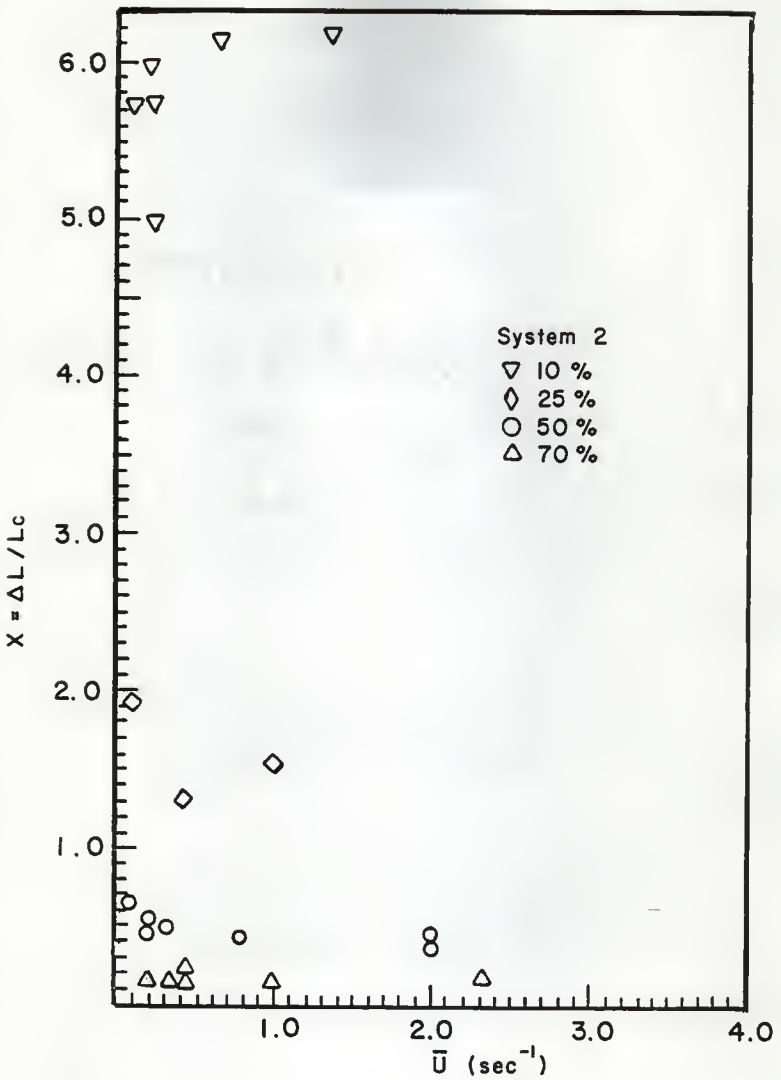

Figure 10: Spacing parameter, X, versus U for System II.

oil % but shows no dependence on pseudoshear rate. The total length exhibits a minimum of about 0.85 cm for 50 % oil. The maximum characteristic total length is about 2.7 cm for 10 % oil.

Figure 14 illustrates the dependence of the end cap length (ΔR) on the pseudoshear rate. For 10% and 70% input oil the end cap length appears to increase with increasing pseudoshear rate. The increasing trend is not exhibited by the data of the 25% and 50% input oil. The magnitude of the 10% data is greater than the magnitude of the 70% data. The data for 10% and 70% exhibit less scatter than the data for 25% and 50% input oil. The general trend of the data as a composite is one of increasing ΔR with increasing U. The end cap length ranges from 0.045 cm to 0.09 cm for pseudoshear rates less than 1 sec^{-1}. For a value of U of 2.0 sec^{-1} the end cap length is about 0.12 cm. From these measurements it is apparent that the end caps become more blunted as the pseudoshear rate decreases.

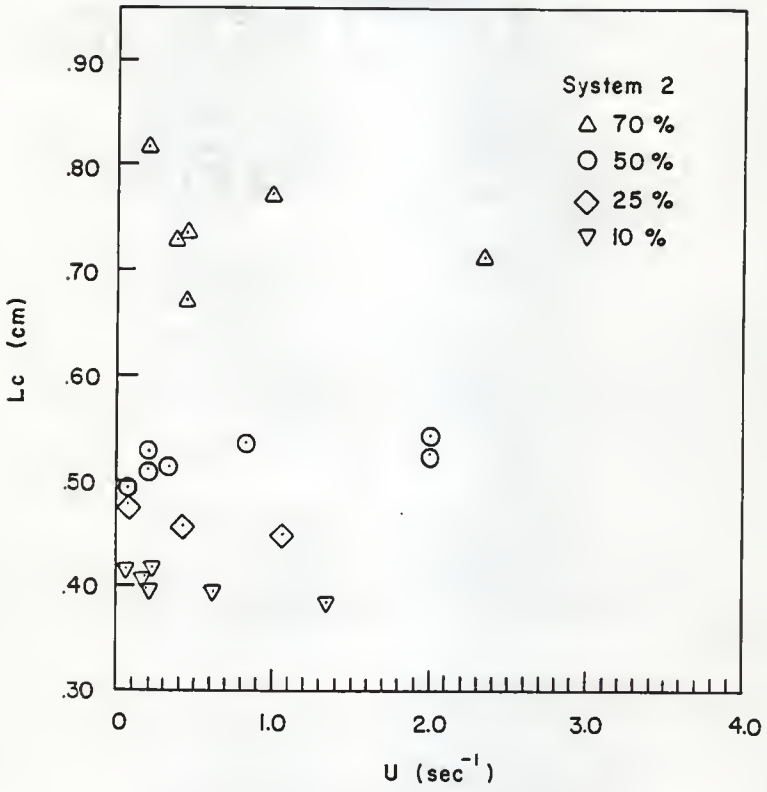

Figure 11: Capsule length versus U for System II.

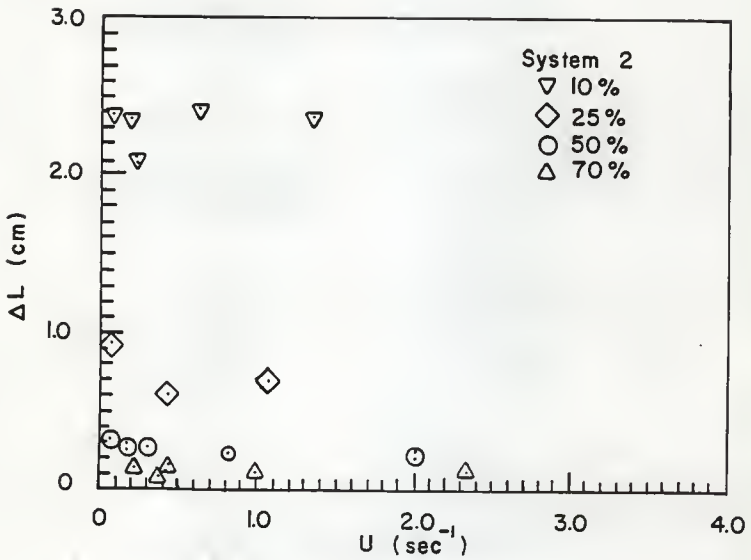

Figure 12: Gap length versus U for System II.

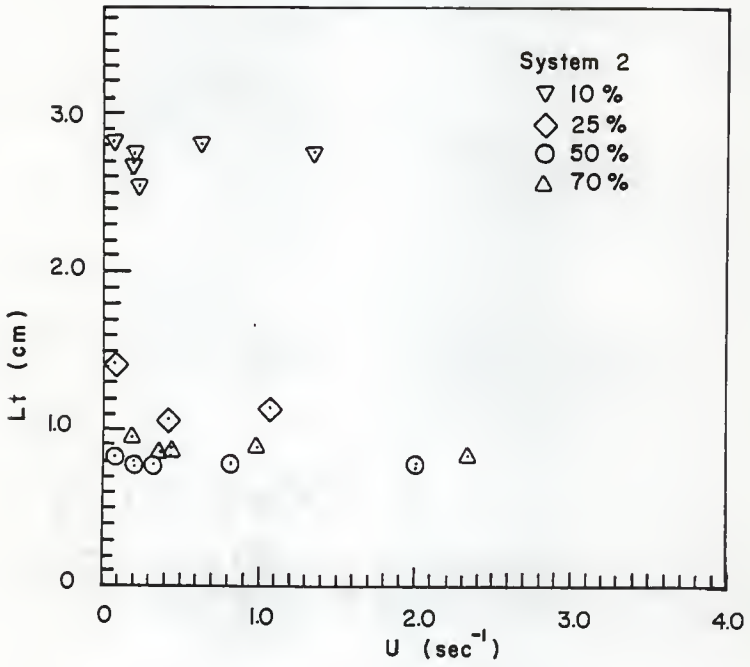

Figure 13: Total length from capsule to capsule versus U for System II.

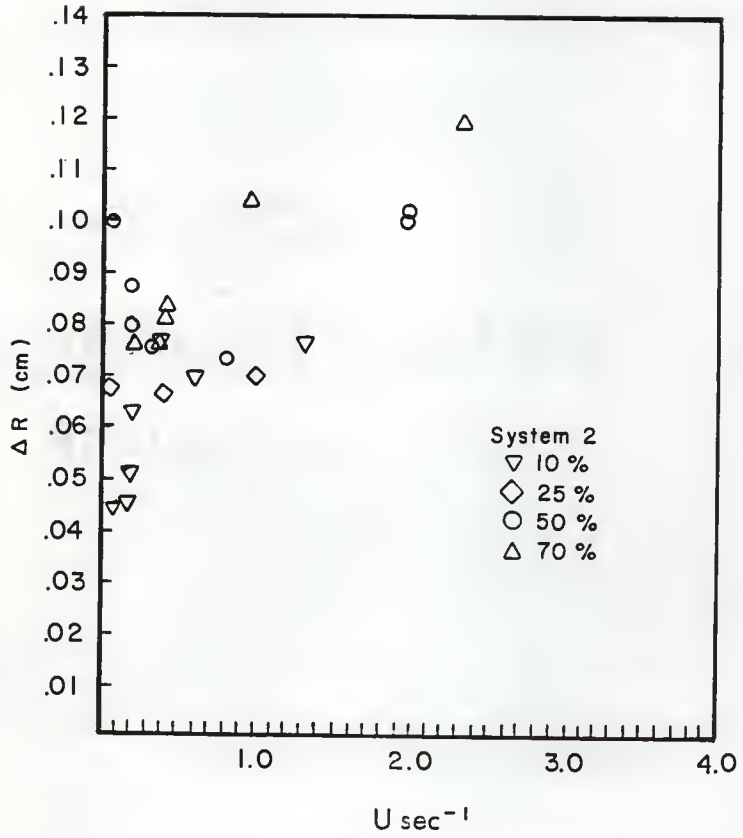

Figure 14: End cap length versus U for System II.

1.6 DISCUSSION

The similarity of the oil-water flow of System I to arteriole flow and System II to capillary flow is further extended by the results presented in this chapter. The additional similarities involve capsule velocity, the velocity profile, the Fahraeus effect, and capsule spacing and length.

The centerline velocities for System I ranged from 5 to 35 mm/sec and corresponded to the velocity ranges reported in the literature for arterioles with diameters greater than 25 microns (e.g. Gaehtgens et al. (1970), Richardson (1971), Einav et al. (1975), and Fronek and Zweifach (1977)). The blunt velocity profiles (capsule velocity equal to mean velocity) for System I parallel the observations of Barbee (1971) who found that plug flow occurred in arteriole sized vessels for U values less than 1 sec^{-1}. For System I plug flow was present for all pseudoshear rates investigated.

The centerline capsule velocities for System II ranged from 0.1 to 8 mm/sec with most of the data below 3 mm/sec. This range of centerline velocity corresponds to the ranges reported in the literature for flow in capillaries (average of about 1 mm/sec) as noted by Greenwald (1969), Gaehtgens et al. (1970), and Butti et al. (1978). The blunt velocity profiles (capsule velocity equal to the mean flow velocity) of System II correspond to the results for single cell capillary flow in the literature reported for both in vivo and in vitro flow.

Studies of in vivo and in vitro blood flow have shown that velocity profiles become increasingly blunted as the vessel diameter decreases toward the red cell diameter (Bugliarello and Hayden (1963), Gaehtgens et al. (1970), Schmid-Schonbein (1975), and Einav et al. (1975)). Cohen and Marsh (1980) measured cell velocities in glass tubes between 16 and 28 microns in diameter

and found that the ratio of cell to mean velocity decreased from 1.6 to 1.3 as the tube diameter decreased from 28 to 16 microns. For capillaries with diameters equal to or less than the cell diameter the cell velocity is equal to the mean velocity. Alhrecht et al. (1979) investigated the development of plug flow in tubes ranging in diameter from 3.3 to 11.0 microns and found that the ratio of cell velocity to plasma velocity decreased from 1.6 for the 11.0 micron tuhe to 1.0 for the 3.3 micron tuhe. The ahove discussion shows that the velocities in System I are similar to the velocities reported for flow in arterioles and that the velocities in System II are similar to those reported for flow in capillaries. The results for hoth systems show completely hlunted velocity profiles that have heen ohserved in hoth arteriole and capillary flow.

For vessels greater than 25 microns in diameter (arteriole sized vessels) the Fahraeus (1929) effect (the decrease in tuhe relative hematocrit with decreasing tuhe diameter) occurs. An inversion of the Fahraeus effect, in which the tuhe relative hematocrit increases with decreasing tuhe diameter, has heen observed for capillary sized vessels with diameters helow 25 microns (e.g. the in vitro studies of Cokelet (1976), Alhrecht (1979), Gaehtgens (1980), and Oda et al. (1983)). The study of Cokelet (1976) found that the tuhe relative hematocrit ohtained a minimum value of 0.47 in a 15 micron diameter tuhe and increased to 1 in an 8.1 micron diameter tuhe. Alhrecht's study also demonstrated the inversion in tuhes ranging in diameter from 3.3 to 11 microns. He found that the tube relative hematocrit increased from 0.7 in an 11 micron diameter tube to 0.94 in a 3.3 micron diameter tuhe.

The line in Figure 8 represents the case where the in situ oil % equals the input oil %, which is equivalent to a total inversion of the Fahraeus effect. The ratio sLc/Lt is an underestimate of the in situ oil % and the

ratio Lc/Lt is an overestimate. The actual in situ oil % will be between these estimates. The actual in situ oil % should be near the line because of the plug flow condition for the flow. This is another similarity that System II shows to single cell capillary flow.

The spacing parameter ($X = \Delta L/Lc$) for System II has approximate values of 0.15, 0.50, 1.55, and 5.80 for 70, 50, 25, and 10 % input oil respectively. For the in vivo work of Monro (1963), the spacing parameter for two capillaries, 11 and 12 microns in diameter, was estimated to be 0.38 and 0.98 respectively. The magnitudes of the spacing parameter for both System II and Monro's data are similar. The trends in the spacing parameter with respect to in situ oil % and hematocrit are also similar; as the in situ oil % or hematocrit decreases, the spacing parameter increases. The analogy between System II and capillary flow is further extended by this evidence.

The ratio of the radius (R) of the vessel to the length of a capsule (Lc) is another geometric ratio that was examined. The values of R/Lc for System II were 0.24, 0.32, 0.38, and 0.43 for 70, 50, 25, and 10 % oil respectively. Hochmuth et al. (1970) measured cell lengths as they traversed capillaries between 4.5 and 10.7 microns in diameter and found R/Lc ratios of 0.26, 0.41, and 0.47 for capillaries with diameters of 4.5, 6.2, and 6.7 microns. The ratio increased to 0.58 and above for capillaries with diameters of 7.6, 8.5, 9.7, and 10.7 microns. The values of this ratio are similar for both flow systems. For flow in capillaries with diameters less than the cell diameter the ratio R/Lc decreases with decreasing vessel diameter because the cell is transformed from its undeformed biconcave disc shape to a capsule shape (Hochmuth et al. (1970)). For the data of Hochmuth et al. (1970), it has been observed that the red cell shape changes from an elongated parachute shape in a

4.5 micron diameter tube to a nearly spherical shape in a 9.7 micron diameter tube. This behavior is similar to the elongated capsules observed with 50% and 70% oil and the nearly spherical bubbles with 10% and 25% oil. The capsule length (Lc) did not change significantly with increasing velocity (from 0.1 to 3 mm/sec) for all input oil % of System II. Hochmuth et al. (1970) showed that the red cell lengths were constant over a similar range of velocities (0 to 2 mm/sec). The above discussion provides additional analogies between the oil-water flow of System II and single cell capillary flow.

The ratio of R/Lc for arteriole sized vessels ranges from 0.10 to 0.45 as was calculated from the data of Jeffords and Knisely (1956), Branemark (1968), and Bloch (1962), and the films of Bloch and Berman. The ratio of R/Lc for System II is similar, ranging from 0.24 to 0.43. This geometric feature shows that the flow of System II is similar to flow in arteriole sized vessels as well as capillary sized vessels.

1.7 SUMMARY

The analogy of the bubble and capsule flow of oil and water at low pseudoshear rates (from 0.06 to 10) to single cell capillary flow and very low shear rate arteriole flow is further extended by the findings of this study. A variety of similarities are indicated and they include:

1. The range of velocities for System I coincide with those reported in the literature for flow in arteriole sized vessels.
2. The plug flow in System I which occurred for all oil % and all pseudoshear rates between 1 and 10 sec^{-1} is similar to the plug flow observed by Barbee (1971) in arteriole sized vessels greater than 29 microns in diameter for pseudoshear rates of 1 sec^{-1} or less.

3. The range of velocities for System II coincide with those reported in the literature for flow in capillary sized vessels.
4. The velocity results indicate the existence of plug flow. Albrecht's (1979) study of single cell blood flow in capillaries equal to or less than the size of the cell have also indicated plug flow.
5. The magnitudes and trends of the spacing parameter for System II were found to be similar to those obtained by Monro (1963).
6. The values of R/Lc for System II were similar to those reported by Hochmuth et al. (1970) for single cell capillary flow. The values of R/Lc calculated from other studies and films on arteriole flow extended this analogy of System II to arteriole sized vessels as well.
7. The capsules for the 50% and 70% oil of System II were similar to the elongated parachute shapes observed by Hochmuth et al. (1970) in capillaries.
8. The bubbles for the 10% and 25% oil of System II were similar to the nearly spherical red cells observed by Hochmuth et al. (1970) in precapillaries.
9. Neither the oil capsule lengths for System II nor the red cell lengths reported in the literature depended on velocity.

The results of this work suggest that the oil-water flow of System II simulates single cell capillary flow. Some elements of the analogy hold for both arteriole and capillary flow.

1.8 NOMENCLATURE

al	:	absolute length in the oil-water flow system (cm)
al'_i	:	corresponding length on the phototransistor trace (cm)
D	:	tube or vessel diameter (cm or microns)
ΔL	:	aqueous gap length in a flow system (cm or microns)
ΔR	:	end cap length of an oil bubble or capsule (cm)
Lc	:	oil, blood, or red cell capsule length (cm or microns)
Lc'_i	:	corresponding oil capsule length on phototransistor trace (cm)
Lt	:	average total length from one oil capsule to the next (cm)
Lt'_i	:	corresponding total length on the phototransistor trace (cm)
Q	:	total volumetric flow rate (cm^3/sec)
R	:	radius of tube or vessel (cm or microns)
Rxy	:	cross-correlation function
slc	:	cylindrical length of oil capsule (cm)
slc'_i	:	corresponding cylindrical length on phototransistor (cm)
t	:	time (sec)
T	:	sampling time (sec)
U	:	pseudoshear rate (sec^{-1})
Vcc	:	centerline oil capsule velocity (cm/sec)
Vm	:	mean flow velocity (cm/sec)
x	:	sample upstream voltage (volts)
y	:	sample downstream voltage (volts)
Z	:	lag time (sec)

Chapter VI

CONCLUSIONS AND RECOMMENDATIONS

The major conclusions from this work are summarized below:

1). The capsule flow model described the wall shear stress (Tw) versus pseudoshear rate (U) behavior of the blood flow data of Barbee (1971) to within 5%. It considered both the discontinuity of the blood core and the Fahraeus effect through the spacing parameter. Capsules with hemispherically shaped end caps were assumed in the model, which was used to determine geometric features of the capsule flow in the form of a relationship between Ro/Lc and R from experimental blood flow data. The relationship between Ro/Lc and R was verified by comparison with physiological observations.

2). In the comparative study of the low Reynolds number flow of oil and water (System I and System II) and the flow of blood in the microcirculation (arterioles and capillaries) it was found that a number of analogies exist for both types of flow. In both oil-water systems for a given tube diameter, the flow curves shifted downward with decreasing input concentration and, for a given input concentration the Tw versus U flow curves shifted downward with decreasing tube diameter. This behavior has been observed for blood flow in arteriole and capillary sized vessels. The apparent viscosity decreased with increasing U for a given input oil % for both oil-water systems. This was also the case for both arteriole and capillary flow. The correlation of Prasassarakich and Walawender (1980) provided the only method by which the two oil-water systems and arteriole and capillary flow could be distinguished from

one another. The 50% and 75% oil of System I was analogous to the multi-cell capsule flow in arteriole sized vessels. The flow of the 10% and 25% oil of System I and System II were analogous to single cell flow in capillaries.

3). Further study of the similarity of oil and water mixtures and blood flow in the microcirculation extended the analogy to include velocity and geometric features. Capsule velocities, velocity profiles, and geometric features, namely length and spacing were determined for the oil-water flow systems. The velocities of System I corresponded to those reported in the literature for arterioles and the velocities of System II corresponded to those reported in the literature for capillaries. In addition, key geometric ratios for oil-water flow were similar to physiological values in arterioles and capillaries. The geometric features for oil-water flow were found to be independent of flow velocity as is the case in microcirculatory flow.

The following recommendations are offered for extensions of the present work:

1). The analogy of oil-water flow was found to apply to capillaries for Reynolds numbers less than 1. In capillary flow U is larger by an order of magnitude relative to the present oil-water flow systems. Flow in the capillaries has been observed in which U ranged between 100 and 200 sec^{-1}. It is therefore suggested that the same oil-water/glycerol system (System II) be studied at pseudoshear rates greater 10 sec^{-1} in an attempt to match the pseudoshear rate range observed for capillaries.

2). The analogy was also found to apply to arterioles for U values less than 1 sec^{-1}. At these low U values the velocity profiles were totally blunted. Normal arteriole flow shows only partial blunting. Therefore, a study of the same oil-water system (System I) with U values greater than 10

sec^{-1} can potentially give flow with only partial blunting and a tube relative percentage less than 1 (the occurrence of the Fahraeus effect).

3). At the higher pseudoshear rates applicable to future experimentation the chart recorder frequency response will be insufficient. The phototransistor traces will be poorly defined for both flow systems. It is suggested that the phototransistor traces be analyzed using computer techniques for greater speed and accuracy.

4). It is suggested that the in situ oil % be measured after stopping flow.

5). It is suggested that an adjustable fiber optic system be constructed so that the distance between the phototransistor detecting points may be adjusted to match the distance between bubbles or capsules. This will allow only a single bubble or capsule to exist between the detecting points at a time instead of multiple bubbles or capsules. This will make determination of the lag time by cross-correlation easier.

BIBLIOGRAPHY

Albrecht, K. H., Gaehtgens, P., Pries, A. and Heuser, M. (1979). The Fahraeus effect in narrow capillaries (i.d. 3.3 to 11 microns). Microvascular Res. 18, 33.

Azelvandre, F. and Oiknine, C. (1976). Effet Fahraeus et Effet Fahraeus-Lindqvist: Resultats Experimentaux et Modeles Theoriques. Biorheology 13, 325.

Aziz, K. and Govier. G. W. (1972). The Flow of Complex Mixtures in Pipes. Van Nostrand Reinhold Publishing Co., New York.

Baker. M. (1972). Double-slit photometric measurement of velocity profiles for blood in microvessels and capillary tubes. Doctoral thesis, California Institute of Technology, Pasadena.

Barbee, J. (1971). The flow of human blood through capillary tubes with inside diameters between 8.4 and 221 microns. Doctoral thesis, California Institute of Technology, Pasadena.

Barbee, J. H. and Cokelet, G. R. (1971). The Fahraeus effect. Microvascular Res. 3, 6.

Barbee, J. H. and Cokelet, G. R. (1971). Prediction of Blood Flow in Tubes with Diameters as Small as 29 microns. Microvascular Res. 3, 17.

Barnard, A. C. L., Lopez, L. and Hellums J. D. (1968). Basic theory of blood flow in capillaries. Microvascular Res. 1, 23.

Bard, Y. (1967). Non-linear Parameter Estimation and Programming. IBM New York Scientific Center.

Bate, H. (1977). Blood viscosity at different shear rates in capilllsry tubes. Biorheology 14, 267.

Bayliss, L. E. (1960). Flow properties of blood and other biological systems, Copley, A. L. and Stainsby, G. (Editors). Pergamon Press, London.

Berman, H. J. A film: Blood Flow in Small Vessels. Dpt. of Biology, Boston University. Boston, Ma.

Bloch, E. H. (1962). A quantitative study of the hemodynamics in the living microvascular system. Amer. J. Anat. 110, 125.

Bloch, E. H. A film: High Speed Cinephotography of the Microvascular System. Dpt. of Anatomy, Western Reserve University. Cleveland, Ohio.

Branemark, P. I. and Johnson, I. (1963). J. Roy. Microscop. Soc. Serial 3, 82, 245-249.

Branemark, P. I. and Lindstrom, J. (1963). Biorheology 1, 139.

Branemark, P. I. (1968). Rheological aspects of low flow states. In: Microcirculation as Related to Shock. Shepro, D. and Fulton G. P. (Editors). Academic Press. New York, 1968, pp. 161-180.

Brooks, D. E., Goodwin, J. W., and Seaman, G.V.F. (1970). Interactions among erythrocytes under shear. J. Appl. Physiol. 28, 174.

Bruck, S.D. (1974). Blood compatible synthetic polymers. Springfield, Ill., Charles C. Thomas, Publisher.

Brundage, J. T. (1934). Blood and plasma viscosity determined by the method of concentric cylinders. Amer. J. Physiol. 110, 659.

Bugliarello, G. and Hayden, J. W. (1963). Detailed characteristics of the flow of blood in vitro. Trans. Soc. Rheol. VII, 209.

Bugliarello, G. and Hsiao, G. C. (1969). A mathematical model of the flow in the axial plasmatic gaps of the smaller vessels. Biorheology 7, 5.

Bugliarello, G. and Sevilla, J. (1970). Velocity distribution and other characteristics of steady and pulsatile blood flow in fine glass tubes. Biorheology 7, 85.

Burton, A. C. (1972). Physiology and biophysics of the circulation. Year Book, Medical Publishers, Chicago. Chicago, Year Book, Medical Publishers.

Butti, P., Intaglietta, M., Reimann, H., Holliger, Ch., Bollinger, A. and Anliker, M. (1975). Capillary red blood cell velocity measurements in human nailfold by videodensitometric method. Microvascular Res. 10, 220.

Casson, N. (1959). Rheology of dispersed systems. Mill, D. C. (Editor). Pergamon Press, Oxford.

Cerny, L.C., Cook, F. B. and Walker, C. C. (1962). Rheology of blood. Amer. J. Physiol. 202, 1188.

Cerny, L. C. (1963). A region of Newtonian flow for whole blood. Biorheology 1, 159.

Charles, M. E., Govier, G. W. and Hodgson, G. W. (1961). The horizontal pipeline flow of equal density oil-water mixtures. Can. J. Chem. Eng. 39, 27.

Charm, S. E. and Kurland, G. S. (1962). Tube flow behavior and shear stress-shear rate characteristic of canine blood. Amer. J. Physiol. 203, 417.

Charm, S. E. and Kurland, G. S. (1965). Viscometry of human blood for shear rates of 0-100,000 sec . Nature 206, 617.

Charm. S. E., Kurland, G. S. and Brown, S. L. (1968). The influence of radial distribution and marginal plasma layer on the flow of red cell suspensions. Biorheology 5, 15.

Charm, S. E., Kurland, G. S. (1974). Blood flow and microcirculation. Wiley and Sons, New York.

Chien, S., Usami. S., Dellenback, R. J., and Bryant, C. (1971). Comparative hemorheology-Hematological implications of species differences in blood viscosity. Biorheology 8, 35.

Cohen, H. J. and Marsh, D. J. (1980). In vitro calibration of a video based method for measuring blood velocity in kidney medulla and other tissues subject to respiratory motion. Microvascular Res. 19, 277.

Cokelet, G. R., Merrill, E. W., Gilliland, E. R., Shin, H., Britten, A. and Wells, R. E. (1963). Rheology of human blood: Measurement near and at zero shear rate. Trans. Soc. Rheol. 7, 303.

Cokelet, G. R. (1976). Blood rheology interpreted through the flow properties of the red cell. In: Microcirculation. J. Grayson and W. Zingg (Editors). New York: Plenum, Vol. I., pp. 9-32.

Coulter, N. A., Jr. and Pappenheimer, J. R. (1949). Turbulence in flowing blood. Amer. J. Physiol. 159, 401.

Dintenfass L. (1963). Biorheology 1, 91.

Dintenfass L. (1967). Inversion of the Fahraeus-Lindqvist phenomenon in blood flow through capillaries of diminishing radius. Nature 215, 1099.

Dintenfass, L. (1976). Rheology of the blood in diagnostic and preventive medicine. Boston, Butterworths.

Ehrly A. M., Lange, B., (1971). Reduction in blood viscosity and disaggregation of erythrocyte aggregates by streptokinase. In: Theoretical and clinical hemorheology (Edited by Hartert, H. H. and Copley, A. L.).

Ehrly, A. M. (1973). Influence of arwin on the flow properties of blood. Biorheology 10, 453.

Einav, S., Berman, H. J., Fuhro, R. L., DiGiovanni, P. R., Fine, S. and Fridman, J. D. (1975). Measurement of velocity profiles of red blood cells in the microcirculation by laser doppler anemometry (LDA). Biorheology 12, 207.

Fahraeus, R. (1929). The suspension stability of blood. Physiol. Rev. 9, 241.

Fahraeus, R. and Lindqvist, T. (1931). The viscosity of the blood in narrow capillary tubes. Amer. J. Physiol. 96, 562.

Fronek, K. and Zweifach, B. (1977). Microvascular blood flow in cat tenuissimus muscle. Microvascular Res. 14, 181.

Gaehtgens P. (1980). Flow of Blood Through Narrow Capillaries: Rheological Mechanisms Determining Capillary Hematocrit and Apparent Viscosity. Biorheology 17, 183.

Gaehtgens, P., Meiselman, H. J. and Wayland, H. (1970). Velocity profiles of human hlood at normal and reduced hematocrit in glass tuhes up to 130 microns diameter. Microvascular Res. 2, 13.

Gaehtgens, P., Meiselman, H. J. and Wayland, H. (1970). Erythrocyte flow velocities in mesenteric microvessels of the cat. Microvascular Res. 2, 151.

Gaehtgens, P., Benner. K. U. and Schichendantz, S. (1976). Flow velocities of RBC and their suspending medium measured in a glass capillary (i.d. 11 microns) using the photometric dual slit method. In: Microcirculation. J. Grayson and W. Zingg (Editors). Vol. I, pp. 105-106. Plenum Press, New York.

Gaehtgens, P., Alhrecht, K. H. and Kreutz, F. (1978). Fahraeus effect and cell screening during tuhe flow of human blood. I. Effect of variation of flow rate. II. Effect of dextran-induced cell aggregation. Biorheology 15, 147.

Gauthier. F. J., Goldsmith, H. L., and Mason, S. G. (1972). Flow of Suspensions Through Tuhes-X Liquids Drops as Models of Erythrocytes. Biorheology 9, 205.

Gazley, C. (1972). Small-scale phenomena in the flow of dispersions. Report p-4796, The Rand Corporation, Santa Monica, California.

Goldstone, J., Schmid-Schonhein, H. and Wells, R. (1970). The rheology of red blood cell aggregates. Microvascular Res. 2, 273.

Green, H. D. (1944). Circulation: Physical principles. Medical Physics Vol. I, The Year Book Puhlishers Inc., Chicago.

Greenkorn, R. A., Kessler. D. P. and Garten, W. P. (1974). Correlation of two phase liquid annular flow in pipes. Paper presented at Pittsburgh AIChE Meeting, June.

Greenwald, E. K. (1969). Quantification of the erythrocyte flux in individual capillaries. Microvascular Res. 1, 410.

Guest, M. M., Bond, T. P., Cooper. R. G. and Derrick, J. R. (1963). Science 142, 1319.

Guest, M. M., Derrick, J. and Bond, T. P. (1971). Altered rheology in human microcirculation resulting from abnormal erythrocytes.

Gupta, B. B. and Seshadri, V. (1977). Flow of red hlood cell suspensions through narrow tuhes. Biorheology 14, 133.

Hartert, H. (1975). In: Letter to the editors, A primitive practical model of the erythrocytes for demonstration. Biorheology 12, 327.

Haynes, R. H. and Burton, A. C. (1959). Role of the non-Newtonian behavior of blood in hemodynamics. Am. J. Physiol. 197, 943.

Hershey, D. and Cho, S. J. (1966). Blood flow in rigid tubes: thickness and slip velocity of plasma film at the wall. J. Appl. Physiol. 21, 27.

Hochmuth, R. M. and Davis, D. O. (1968). Changes in hematocrit for blood flow in narrow tubes. Bibl. Anat. 10, 59.

Hochmuth, R. M., Marple, R. N. and Sutera, S. P. (1970). Capillary blood flow. I. Erythrocyte deformation in glass capillaries. Microvascular Res. 2, 409.

Jeffords, J. V. and Knisely. M. H. (1956). Concerning the geometric shapes of arteries and arterioles. Angiology 7, 105.

Jendrucko, R. J. and Lee, S. J. (1973). The measurement of hematocrit of blood flowing in glass capillaries by microphotometry. Microvascular Res. 6, 316.

Johnson, P. C., Hudnall. D. L. and Dial. J. H. (1973). Measurement of capillary hematocrit by photometric techniques. Microvascular Res. 5, 351.

Krogh, A. (1922). The anatomy and physiology of capillaries. New Haven, Conn. Yale University Press.

Kumin, K. (1949). Bestimmung de zahigkeitskowffizienten fur rinderblut bei Newtonscher stromung in verschiden weiten rohren und capillaren bei physiologischer temperatur. Dissertation, Universitat Bern.

Landis, E. M. (1926). Am. J. Physiol. 75, 548.

Landis, E. M. (1930). Heart 15, 209.

Lee, J. S. and Fung, Y. C. (1969). Modeling experiments of a single red blood cell moving in a capillary blood vessel. Microvascular Res. 1, 221.

Lew, H. S. and Fung, Y. C. (1969). The motion of the plasma between the red cells in the bolus flow. Biorheology 6, 109.

Lih, M. M. (1969). A mathematic model for the axial migration of suspended particles in tube flow. Bull. Math. Biophys. 31, 143.

Lin, K. L., Lopez, L. and Hellums, J. D. (1973). Blood flow in capillaries. Microvascular Res. 5, 7.

Lingard, P. S. (1974). Capillary pore rheology of erythrocytes. I. Hydroelastic behavior of human erythrocytes. Microvascular Res. 8, 53.

Lingard, P. S. (1977). Capillary pore rheology of erythrocytes. II. On the interpretation of human erythrocyte behaviour in narrow capillary pores. Microvascular Res. 13, 29.

Lingard, P. S. (1977). Capillary pore Rheology of erythrocytes. IV. Effect of Pore Diameter and Haematocrit. Microvascular Res. 13, 59.

Lipowsky, H. H., Shunichi, U. and Chien, S. (1980). In vivo measurements of "apparent viscosity" and microvessel hematocrit in the mesentery of the cat. Microvascular Res. 19, 297.

Lord, D.L., Hulsey, B. W. and Melton, L. L. (1967). General turbulent pipe flow scale-up correlation for rheologically complex fluids. Soc. Petrol. Engrs. J. 7, 252.

Merrill, E. W. and Wells, R. E. (1961). Flow properties of biological fluids. Appl. Mech. Rev. 14, 663.

Merrill, E. W., Cokelet, G. R., Britten, A. and Wells, R. E. (1963). Circulation Research 13, 48.

Merrill, E. W., Benis, A. M., Gilliland, A. R., Sherwood, T. K. and Salzman, E. W. (1965). Pressure-flow relations of human blood in hollow fibers at low flow rates. J. Appl. Physiol. 20, 449.

Merrill, E. W. (1969). Rheology of Blood. Physiol. Rev. 49, 863-888.

Metzner, A. B. and Reed, J. C. (1955). Flow of non-Newtonian fluids - Correlation of the laminar. transition and turbulent flow regions. A.I.Ch.E. Journal 1, 434.

Monro, P. A. G. (1963). The appearance of cell free plasma and grouping of red blood cells in normal circulation in small blood vessels observed in vivo. Biorheology 1, 239.

Muller, A. (1948). Uber das Druckgefalle im Blutgefaszen, insbesondere in den kapillaren. Helv. Physiol. Acta. 6, 181.

Noodergraaf. A. (1978). Circulatory system dynamics. New York, Academic Press.

Oda, N., Sato, M., and Ohshima N. (1983). Microhemodynamics of blood flow in glass capillaries. Microvascular Re. 26, 367.

Palmer. A. A. (1959). Quarterly J. Exp. Physiology 44, 149.

Ponder, E. (1948). Hemolysis and related phenomena. Grune & Stratton, Inc., New York.

Prasassarakich, P. (1979). Modeling of blood flow in vessels of the microcirculation. Doctoral thesis. Kansas State University.

Prasassarakich, P. and Walawender W. P. (1980). On Application of the Concentric Annular Flow Model to the Flow of Blood in Small-Diameter Tubes. Microvascular Res. 20, 165.

Pries, A. R., Albrecht, K. H. and Gaehtgens, P. (1981). Model studies on phase separation at a capillary orifice. Biorheology, 18, 355.

Prothero, J. and Burton, A. C. (1961). The physics of hlood flow in capillaries. I. The nature of the motion.

Prothero, J. and Burton, A. C. (1962). The physics of blood flow in capillaries II. The capillary resistance to flow. Biophys. J. 2, 199.

Reiner, M. and Scott-Blair, G. (1959). The flow of blood through narrow tubes. Nature 184, 354.

Richardson, D. R., Intaglietta, M. and Zweifach, B. W. (1971). Simultaneous pressure and flow velocity measurements in the microcirculation. Microvascular Res. 3, 69.

Rosenblum, W. I. (1972). Ratio of red cell velocities near the vessel wall to velocities at the vessel center in cerebral microcirculation, and an apparent effect of hlood viscosity on this ratio. Microvascular Res. 4, 98.

Sarton,G. (1927) Introduction to the history of science, V.I. From Homer to Omar Khayyam. Baltimore, Williams and Wilkins.

Sarton, G. (1952) A History of Science, I. Ancient science through the golden age of greece. Cambridge, Mass., Harvard University Press.

Seshadri, V., Hochmuth, R. M., Croce, P. A. and Sutera, S. P. (1970). Capillary blood flow. III. Deformable model cells compared erythrocytes in vitro. Microvascular Res. 2, 434.

Schmid-Schonhein, H. and Wells, R. (1969). Fluid drop-like transition of erythrocytes. Science 165, 288.

Schmid-Schonbein, H. Gosen, J. V. and Klose, H. J. (1973). Comparative microrheology of hlood: effect of desaggregation and cell fluidity on shear thinning of human and bovine blood. Biorheology 10, 545.

Schmid-Schonbein, G. W. and Zweifach, B. W. (1975). RBC velocity profiles in arterioles and venules of the rabhit omentum. Microvascular Res. 10, 153.

Scott-Blair, G. W. (1959). An equation for the flow of blood plasma and serum through glass capillaries. Nature 183, 613.

Skalak, R., Chen, P. H. and Chien, S. (1972). Effect of hematocrit and rouleaux on apparent viscosity in capillaries. Biorheology 9, 67.

Skalak, R. and Chien, S. (1981). Capillary flow: History, experiments and theory. Biorheology 18, 307.

Sutera, S. P. and Hochmuth, R. M. (1968). Large scale modeling of hlood flow in the capillaries. Biorheology 5, 45.

Sutera, S. P., Seshadri, V., Croce, P. A. and Hochmuth, R. M. (1970). Capillary blood flow. II. Deformable model cells in tube flow. Microvascular Res. 2, 420.

Thomas, H. W. (1962). The wall effect in capillary instruments: An improved analysis suitable for application to blood and other particulate suspensions. Biorheology 1, 41.

Walawender, W. P., Chen, T. Y. and Cala, D. F. (1975a). An approximate Casson fluid model for tube flow of blood. Biorheology 12, 111.

Wang, H. and Skalak, R. (1969). Viscous flow in a cylindrical tube containing a line of spherical particles. J. Fluid Mech. 38, 75.

Ware, J. H., Sorrell, F. Y. and Felder, R. M. (1974). A model of steady blood flow. Biorheology 11, 97.

Waugh, R. and Evans, E. A. (1976). Viscoelastic properties of erythrocyte membranes of different vertebrate animals. Microvascular Res. 12, 291.

Wayland, H. (1973). Photosensor methods of flow measurement in the microcirculation. Microvascular Res. 5, 336.

Wayland, H. and Johnson, P. C. (1967). Erythrocyte velocity measurement in microvessels by a two-slit photometric method. J. Appl. Physiol. 22, 333.

Whitmore, R. L. (1963). Hemorheology and hemodynamics. Biorheology 1, 201.

Whitmore, R. L. (1967). A theory of blood flow in small vessels. J. Appl. Physiol. 22, 767.

Whitmore, R. L. (1968). Rheology of the circulation. New York, Pergamon Press.

Wiberg, J. (1937). The medical science of ancient Greece: The doctrine of the heart. Janus 41:225.

Zweifach, B. W. and Intaglietta, M. (1968). Microvascular Res. 1, 83.

MODELING OF BLOOD FLOW IN THE MICROCIRCULATION

by

Steven D. Tessendorf

B.S., Washington University, St. Louis, 1978

AN ABSTRACT OF A MASTER'S THESIS

submitted in partial fulfillment of the

requirements for the degree

MASTER OF SCIENCE

Department of Chemical Engineering

KANSAS STATE UNIVERSITY
Manhattan, Kansas

1985

Tbe discontinuous nature of blood flow has been observed in both the arterioles and capillaries of the microcirculation. In the arterioles and capillaries tbe flow patterns can be described as being multi-cell heterogeneous and single cell heterogeneous, respectively. The major objectives of this work are, 1) to develop a preliminary model for multi-cell heterogenous flow in arterioles, and 2) to determine the analogies between the laminar flow of oil-water systems in cylindrical glass tubes and flow in arterioles and capillaries of the microcirculation.

A model based on modification of the Concentric Annular Flow model is proposed to describe the wall sbear stress (Tw) versus pseudoshear rate (U) behavior for blood flow in arteriole sized vessels. The model offers additional physical realism because it considers tbe discontinuous nature of the core as well as tbe Fahraeus effect. An initial attempt with blunt end capsules underestimates tbe Tw versus U bebavior of the blood flow data. A refined model was developed, based on hemispherical end caps that improved the predictions. A relationship between the core radius and the blood capsule length was developed that forced tbe model to fit tbe Tw versus U blood flow data. This relationship was verified witb physiological data from tbe literature and films.

The similarity between blood flow in arteriole and capillary sized vessels and tbe laminar flow of two oil-water systems at low pseudoshear rates (Reynolds numbers) was experimentally investigated. Pressure drop versus flow rate data were obtained as a function of input oil concentration. Tbe flow curves (Tw versus U) for oil-water mixtures and arteriole blood flow were botb described by tbe power law model. Several analogies were found between the oil-water systems and tbe flow of blood in arterioles and capillaries. These

analogies were based on 1) the dependence of the flow curves on the input concentration and tube diameter, 2) the variation of the apparent viscosity with shear rate, and 3) the similarity of flow patterns. A correlation, describing the flow curve dependence on tube diameter and pseudoshear rate, was found capable of distinguishing the differences between the flow of blood in arteriole and capillary sized vessels.

The data on capsule velocities, velocity profiles, and geometric features, namely length and spacing were also obtained for the oil-water flow systems and provided additional analogies. The velocities determined with the flow analog corresponded with those observed in arterioles and capillaries. In addition, key geometric ratios for oil-water flow were similar to physiological obvservations. The geometric features for oil-water flow were found to be independent of flow velocity as is the case in microcirculatory flow.